



University  
of Glasgow

Smith, Christopher Bruce (1975) *The mineral constituent of compact bone: its relation to mechanical properties.*

PhD thesis

<http://theses.gla.ac.uk/4358/>

Copyright and moral rights for this thesis are retained by the author

A copy can be downloaded for personal non-commercial research or study, without prior permission or charge

This thesis cannot be reproduced or quoted extensively from without first obtaining permission in writing from the Author

The content must not be changed in any way or sold commercially in any format or medium without the formal permission of the Author

When referring to this work, full bibliographic details including the author, title, awarding institution and date of the thesis must be given

**THE MINERAL CONSTITUENT OF COMPACT BONE :  
ITS RELATION TO MECHANICAL PROPERTIES**

by

**CHRISTOPHER BRUCE SMITH, B.Sc.,**  
West of Scotland Health Boards,  
Department of Clinical Physics and Bioengineering,  
11 West Graham Street,  
Glasgow, G4 9LF.

**A Thesis submitted for the Degree of Doctor  
of Philosophy of the University of Glasgow.**

**Glasgow, July, 1975.**

## TABLE OF CONTENTS

Page No.

LIST OF TABLES	
LIST OF ILLUSTRATIONS	
ACKNOWLEDGEMENTS	
SUMMARY	
LIST OF SYMBOLS AND ABBREVIATED TERMS	

CHAPTER 1	<u>GENERAL INTRODUCTION</u>	1
CHAPTER 2	<u>X-RAY DIFFRACTION ANALYSIS OF THE INORGANIC CRYSTALLINE COMPONENT OF BONE TISSUE</u>	
	Introduction	8
	The Crystalline State	10
	X-ray diffraction: theoretical considerations	12
	Materials and methods of sample preparation	16
	Method of recording x-ray diffraction patterns	19
	Results and calculations	24
CHAPTER 3	<u>DETERMINATION OF BONE APATITE CRYSTALLITE LENGTH BY X-RAY DIFFRACTION AND ELECTRON MICROSCOPY</u>	
	Introduction	34
	X-ray diffraction measurement of crystallite size: theoretical considerations	35
	Numerical correction of experimentally observed line breadth	39
	Graphical correction of experimentally observed line breadth	40
	Materials and methods: X-ray diffraction	43
	Results and calculations: X-ray diffraction	45
	Materials and methods: electron microscopy	50
	Results : electron microscopy	52
CHAPTER 4	<u>EVALUATION OF PREFERRED ORIENTATION OF APATITE CRYSTALLITES IN COMPACT BONE BY X-RAY DIFFRACTION</u>	
	Introduction	55

	<u>Page No.</u>
Theoretical considerations	56
Method of sample preparation	59
Method of recording x-ray diffraction patterns	60
Results	64
 <b>CHAPTER 5</b>	
<b><u>MECHANICAL TESTING OF BONE : THE STATE OF THE ART</u></b>	
Introduction	67
Bone tissue : review of published work	72
Whole bones : review of published work	74
Effect of storage and methods of sample preparation	75
 <b>CHAPTER 6</b>	
<b><u>TENSILE PROPERTIES OF COMPACT BONE : THEIR RELATION TO AGE AND MINERAL CONTENT</u></b>	
Introduction	78
Preparation of tensile test pieces	80
Measurement of the mineral content of tensile test pieces	83
Attachment of strain gauges to tensile test pieces	86
Method of tensile testing	87
Results and calculations	92
 <b>CHAPTER 7</b>	
<b><u>COMPRESSIVE PROPERTIES OF COMPACT BONE : THEIR RELATION TO AGE AND MINERAL CONTENT</u></b>	
Introduction	101
Preparation of compressive test pieces	103
Measurement of mineral content of compressive test pieces	104
Method of compressive testing	105
Results and calculations	106
 <b>CHAPTER 8</b>	
<b><u>THE ESTIMATION OF BONE MINERAL CONTENT AT SELECTED SKELETAL SITES BY GAMMA RAY ABSORPTION</u></b>	
Introduction	111
Material preparation	113
Measurement of K-value by gamma ray absorption	113
Measurement of mineral content by ashing	115
Results and calculations	116

CHAPTER 9	<u>THE RELATION BETWEEN FRACTURE OF THE DISTAL END OF RADIUS AND DEGREE OF MINERALISATION OF THE THIRD METACARPAL</u>	
	Introduction	121
	Method of gamma ray absorption measurement	123
	Method of radiographic estimation of bone cross-sectional area	124
	Results and calculations	126
CHAPTER 10	<u>DISCUSSION AND CONCLUSIONS</u>	130
	LIST OF REFERENCES	135
APPENDIX 1	Derivation of expression yielding the angular separation $\delta\theta$ between Bragg angles for wavelengths differing by $\delta\lambda$	148
APPENDIX 2	Diffraction line broadening due to crystallites damaged during grinding	149
APPENDIX 3	Reduction of Von Laue line profile equations to linear form	150
APPENDIX 4	Correction of observed bone apatite (002) reflection intensity for background variation	151
APPENDIX 5	Strain gauge installation procedure	153
APPENDIX 6	Derivation of expressions relating to recorder response	154
APPENDIX 7	Elastic instability (buckling) in compressive test pieces	156

LIST OF TABLES

		<u>Page no.</u>
TABLE 1	X-ray diffraction data of the eleven main reflections of bone powder.	30
TABLE 2	Angular position of the principal reflection of bone powder.	31
TABLE 3	Bone apatite unit cell parameters.	32
TABLE 4	Measured d-spacings of sodium chloride (111) and (220) reflections.	33
TABLE 5	Line breadth of the (111) reflection of sodium chloride standards.	53
TABLE 6	The relation between observed breadth $B_{obs}$ , $K\alpha$ - corrected breadth $B_c$ , and pure breadth $\beta_c$ of bone apatite (002) diffraction lines.	54
TABLE 7	Ratio of maximum to minimum photographic density of bone apatite (002) reflection recorded by a flat plate camera.	66
TABLE 8	Tensile stress relaxation data of femoral compact bone.	96
TABLE 9	Results of tests to evaluate sensitivity of ultimate tensile stress to variation in strain rate.	97
TABLE 10	Exponential relations between mechanical properties and mineralisation.	98

		<u>Page no.</u>
TABLE 11	Mineralisation and tensile properties of samples of compact bone tissue of differing age	99
TABLE 12	Linear relations between mineralisation, tensile properties and age.	100
TABLE 13	Compressive stress relaxation data of femoral compact bone.	108
TABLE 14	Exponential relations between compressive mechanical properties and mineralisation.	109
TABLE 15	Mineralisation and compressive properties of samples of compact bone tissue.	110
TABLE 16	Calibration equations for determination of mineral content from K-value.	119
TABLE 17	Relations between mineral content at mid-metacarpal site and at other selected skeletal sites.	120
TABLE 18	Metacarpal and femoral mineral density : significance of difference between groups.	129

## LIST OF ILLUSTRATIONS

		<u>Preceding numbered page</u>
FIGURE 1	Femoral portions selected to provide sample material for physical analyses	6
FIGURE 2	Reflection of x-rays by a crystalline array of atoms: condition for Bragg reflection	14
FIGURE 3	Production of bone powder by the use of a circular saw blade mounted on a milling machine	17
FIGURE 4	Goniometer powder sample holder	19
FIGURE 5	X-ray optical design of goniometer	20
FIGURE 6	(a) Spectral distribution of x-rays emitted by a copper target (b) Spectral distribution of x-rays from copper target after nickel filtration	24
FIGURE 7	Absorption versus specimen thickness for $\text{CuK}\alpha$ x-rays incident on compact bone tissue	24
FIGURE 8	Bone powder diffractogram	25
FIGURE 9	(a) Detailed recording of bone apatite (002) reflection (b) Detailed recording of bone apatite (222) reflection	27
FIGURE 10	Angular separation of diffraction angles of copper characteristic radiations, shown as a function of $2\theta$	37
FIGURE 11	Diffraction line intensity distribution $I = h(x)$ as assumed by Spencer (1949)	39
FIGURE 12	Graph for correction of geometrical line broadening	42
FIGURE 13	Relation between pure line breadth and average crystallite dimension normal to the reflecting planes	43

	<u>Preceding numbered page</u>	
FIGURE 14	Line profiles of bone apatite (002) and sodium chloride (111) reflections	45
FIGURE 15	Average bone apatite crystallite length along c-axis, versus age	49
FIGURE 16	Delineation of bone quadrants	51
FIGURE 17	Transmission electron micrograph of longitudinal bone section (x 100,000)	52
FIGURE 18	Transmission electron micrograph of longitudinal bone section (x 200,000)	52
FIGURE 19	Definition of orientation of a plane by its inclination $\theta$ and disposition $\psi$	56
FIGURE 20	Orientations of (h k l) planes capable of producing Bragg reflection	57
FIGURE 21	Flat plate camera with spring-loaded specimen holder	57
FIGURE 22	Delineation of sections for flat plate x-ray diffraction studies	59
FIGURE 23	Mounted flat plate specimens	60
FIGURE 24	Experimental arrangement for flat plate x-ray diffraction studies	60
FIGURE 25	Flat plate camera goniometer specimen holder	62
FIGURE 26	Flat plate forward diffraction pattern of transverse bone section	64
FIGURE 27	Flat plate forward diffraction pattern of longitudinal bone section	64
FIGURE 28	Observed degree of preferred orientation versus specimen angle of inclination	64
FIGURE 29	Three point bending	69
FIGURE 30	Macrotome sliding table arrangement	81

FIGURE 31	(a) Template production of tensile test piece (b) Dimensions of completed test piece	82
FIGURE 32	Miniature gamma densitometer	83
FIGURE 33	Tensile test pieces with strain gauges attached	86
FIGURE 34	Strain gauge bridge circuit	89
FIGURE 35	Experimental arrangement of tensile testing equipment	90
FIGURE 36	Tensile stress relaxation curve	92
FIGURE 37	Graphs of tensile stress and lateral strain, versus longitudinal strain	93
FIGURE 38	Ultimate tensile stress versus degree of mineralisation	93
FIGURE 39	Young's modulus versus degree of mineralisation	93
FIGURE 40	Ultimate tensile stress versus average bone apatite crystallite length	94
FIGURE 41	Experimental arrangement of compressive testing equipment	105
FIGURE 42	Compressive stress relaxation curve	106
FIGURE 43	Ultimate compressive stress versus degree of mineralisation	106
FIGURE 44	Ultimate compressive stress versus average bone apatite crystallite length	107
FIGURE 45	Schematic illustration of gamma ray absorption equipment	113
FIGURE 46	Gamma ray absorption scan profile	115
FIGURE 47	Ash value versus iodine-125 and americium-241 K-value	116

FIGURE 48	Distal radius mineral content versus mid-metacarpal mineral content	118
FIGURE 49	Mid-metacarpal mineral content versus estimated cortical area	126
FIGURE 50	Histograms showing distribution of values of mineral density of third metacarpal in male patients with Colles' fracture, and in normal male subjects	127
FIGURE 51	Histograms showing distribution of values of mineral density of third metacarpal in female patients with Colles' fracture, and in normal female subjects	127

## ACKNOWLEDGEMENTS

I wish to record my sincere thanks to each of the many colleagues and associates who have given freely of their time and skills in helping me to overcome a multitude of problems encountered during the course of my researches.

Dr. D.A. Smith (University Department of Medicine), and Dr. P.W. Horton, Dr. F.C. Gillespie (Department of Clinical Physics and Bioengineering) have provided expert advice and guidance concerning a wide variety of topics.

Mr. J. Anderson was responsible for a great deal of photographic work, conducted clinical measurement of bone mineral content, and supplied valuable assistance throughout.

I gratefully acknowledge the help provided by staff of the Department of Clinical Physics and Bioengineering, employed in the Western Infirmary mechanical workshop : viz. Mr. W. Hyslop, Mr. J. Donohoe, Mr. I.M. Thom, and Mr. J. MacFarlane. Particular credit is due to Mr. I. Thom and Mr. W. Hyslop for construction of the "miniature gamma densitometer".

I would also like to thank Dr. D. Brown (University Department of Mechanical Engineering) for advice regarding mechanical testing, Mr. S. Terras (University Department of Neuropathology) for production of transmission electron micrographs, Mr. D. Skinner (University Department of Geology) for help and advice concerning x-ray powder diffraction analysis, and Mr. W. Jones (Department of Clinical Physics and Bioengineering) for aid in preparation of tensile test pieces.

Finally, I would like to express my appreciation to Professor G.M. Wilson, and Professor J.M.A. Lenihan for their continued support.

## SUMMARY

The thesis is concerned with the role played by mineral substance in determining mechanical properties of bone. A variety of techniques have been used to study the physical nature of bone mineral and the mechanical properties of compact bone tissue. Bones obtained from male and female cadavera ranging in age from 3½ to 92 years were studied.

X-ray powder diffraction analysis has confirmed the calcium hydroxyapatite-like structure of crystalline bone mineral (chapter 2), but failed to provide evidence of the presence of any other inorganic crystalline component in bone tissue. Observed diffraction patterns each comprised a number of well-resolved reflections with comparatively little diffuse scattering, suggesting a high degree of crystallinity of bone mineral.

Average bone apatite crystallite length was determined from x-ray powder diffraction line-broadening effects (chapter 3), values being calculated using the "modified Scherrer formula". The mean of values obtained for all specimens examined was  $261 \pm 6.5$  Angstrom (2 x S.E.). This result is consistent with estimates made from transmission electron micrographs of longitudinal sections of compact bone. No

significant correlation of average bone apatite crystallite length with age, was observed.

Orientation of apatite crystallites in sections of compact bone has been investigated by recording x-ray diffraction patterns with a flat plate camera (chapter 4). Preferred orientation, parallel to the direction of propagation of haversian canals, has been demonstrated. There was no evidence of any relation between degree of preferred orientation and age, in the age range 3½ to 87 years.

Tensile and compressive mechanical properties were determined (chapters 6, 7) and considered in relation to degree of mineralisation, or mass of mineral per unit volume of compact bone, measured by a gamma ray absorption technique. Good exponential correlation was obtained, seventy-five percent of variance of ultimate tensile stress, and eighty-five percent of variance of ultimate compressive stress, being attributable to variation in mineral density.

Significant negative correlation ( $P < 0.005$ ) of average apatite crystallite length with both ultimate tensile and ultimate compressive stress, has been established. Moreover, increased crystallite length is shown to be associated with decreased mineralisation ( $P < 0.005$ ).

Bone mineral content (mass of mineral/unit length) at selected skeletal sites in human long bones, excised post mortem, has been estimated by gamma ray absorptiometry (chapter 8). The sites studied were in the central and distal portions of the right femur and right radius, the central portion of the right third metacarpal, and in the femoral neck. Calibrations to yield bone mineral content were obtained by comparing the gamma ray absorption measurements with the weights of ash residues of sections cut from the sites and maintained at 600°C. in a muffle furnace for twenty-four hours. Mineral content of the mid metacarpal site is shown to be related ( $P < 0.005$ ) to mineral content at each of the other sites in males ( $r \geq 0.54$ ), in females ( $r \geq 0.49$ ), and also in the combined group ( $r \geq 0.72$ ).

The findings referred to above provide the basis for studies described in chapter 9. A method for in vivo estimation of third metacarpal mineral density, by gamma ray absorption measurement of mineral content and radiographic evaluation of cortical bone cross-sectional area, is presented. This parameter has been measured in normal subjects and in individuals who had suffered Colles' fracture of the distal end of radius.

Male and female groups of Colles' fracture patients are shown to possess significantly lower ( $P \ll 10^{-2}$ ) metacarpal mineral density than groups of normal subjects.

It is concluded that in vivo measurement of mineral density, or degree of mineralisation, will provide a useful diagnostic indication of susceptibility to fracture.

## LIST OF SYMBOLS AND ABBREVIATED TERMS

<u>NOTE:</u>	The initial use of any abbreviated term is accompanied in the text by definition of its meaning. Therefore, the following list includes only those terms which are used on more than one occasion.
(hkl)	Miller indices of a set of atomic planes.
a, b, c	Lengths of crystal unit cell axes.
$\alpha, \beta, \infty$	Angular disposition of crystal unit cell axes.
$\lambda$	X-ray or gamma-ray wavelength.
$2\theta$	Diffraction angle.
$\theta_{hkl}$	Bragg angle for (hkl) planes.
$d_{hkl}$	Interplanar spacing of (hkl) planes.
$Cu_{K\beta}, Cu_{K\alpha}$	Denote characteristic radiations emitted by copper x-ray target.
I	Intensity of x-radiation or gamma-radiation.
$I_{\text{principal}}$	Intensity of principal Bragg reflection.
$I_{\text{Max}}$	Peak intensity of a diffraction line.
$\kappa$	Deviation from theoretical diffraction angle.
K, k	Constants used in Von Laue equations describing diffraction line profile.
$D_{hkl}$	Crystallites mean dimension in direction normal to (hkl) planes.
$\beta$	Integral pure line breadth.
$\beta_{\frac{1}{2}}$	Half maximum pure line breadth.
$B_0, B_{0\frac{1}{2}}$	Integral, and half maximum observed line breadth for small crystallites.

**CHAPTER 1**

**GENERAL INTRODUCTION**

A high proportion of bone fracture occurs in elderly subjects or people suffering from certain metabolic bone diseases (1, 2, 3, 4). For example, Knowelden, Buhr and Dunbar (1), found that the fracture rate for women over eighty-five years of age was ten times as high as the rate for women in the age range thirty-five to forty-four years. For males, the chance of sustaining a fracture more than doubled between the age of thirty-five and eighty-five. This reduced ability of the skeleton to fulfil its structural role in old age poses considerable clinical problems. These arise from the need for reliable diagnostic techniques and effective therapeutic procedures. A fuller understanding of the physical nature of skeletal degeneration is a prerequisite for the achievement of these objectives.

Now, the ability of a bone to withstand an applied force without yielding depends on its geometrical size and configuration and also on the mechanical properties of the tissue of which it is composed. A number of researchers have investigated age-related changes in the geometrical configuration of bones (5, 6, 7). Spencer and Coulombe (6) observed that the ratio of the medullary width to the total width of the shaft of the human femur

steadily decreased over the age of fifty years. Exton-Smith et al (7) measured medullary width and total width of the midshaft of the second metacarpal from hand radiographs. They calculated the cross-sectional area of cortical bone by assuming a hollow cylindrical configuration, and related the cortical area to age. Their results showed a steady increase in cortical area up to about thirty-five years, followed by a steady decrease with advancing age in both males and females.

More commonly, bone mineral content measured in vivo by either radiographic or gamma ray absorption techniques, has been used as a combined measure of bone size and bone mineralisation. Radiographic methods involve the use of standards possessing attenuation properties similar to those of bone tissue. Mineral content at a bone site is expressed as the quantity of the standard material that is required to produce the same attenuation of the x-ray beam as is produced by the bone itself. Doyle (8) used the method of Keane, Spiegler and Davis (9), to study the mineral content of the ulna in patients suffering from various metabolic bone diseases. Smith et al (10) measured the mineral content of the third right metacarpal of three hundred and twelve

male and three hundred and seventeen female volunteers, by the technique described by Anderson, Shimmins and Smith (11). Values for male and female subjects were related to age by third order polynomial equations. Percentile tables giving normal ranges of mineral content according to age and sex, were constructed from these equations. Mulligan et al (12) used revised and enlarged versions of the percentile tables to show that groups of male and female patients who had suffered sub-capital fracture of the femur, had significantly lower mineral content of the third right metacarpal than had normal subjects of the same age and sex. Other researchers have used gamma ray absorptiometry to estimate net mineral content at certain skeletal sites (13, 14, 15, 16, 17, 18). However, there are certain disadvantages in using net mineral content as a criterion of susceptibility to fracture. Firstly, it is necessary to find some means of normalising the data for varying physical size of the individual: a large person will require, and tend to possess, large bones. Mazess and Cameron (19) divided bone mineral content at sites in the shaft of long bones by total bone width, in order to normalise for varying physical size. However, such "normalised" values take no account of

differing bone geometry and the ability of certain cross-sectional configurations to withstand large externally applied forces. These problems may be avoided if, instead of studying changes in bone design, we investigate the physical properties of bone tissue. Indeed, without knowing more about the mechanical behaviour of bone tissue, it is not possible to fully evaluate the functional properties of the skeleton.

Bone tissue is a composite material comprising a collagen matrix throughout which is distributed inorganic mineral. The composite is believed to be cemented together by a ground substance containing the mucopolysaccharide "chondroitin sulphate" (20). X-ray diffraction analysis shows collagen to be arranged in helically interwoven bundles of fibres (21,22). Transmission electron micrographs indicate that, in bone tissue, these bundles of fibres display preferred orientation parallel to the long axes of haversian systems (23, 24, 25). This has been confirmed by polarized light studies of the optically active collagen (26, 27, 28). When such a fibrous composite is stressed, shear forces are established across the reinforcing inclusions. The magnitude of the shear forces depends on the elastic properties

of the component materials, and also on the sizes and orientations of the inclusions (29, 30, 31).

The major part of the work described in this thesis constitutes an investigation of the physical form of bone mineral and its relation to the mechanical properties of bone tissue. Chapter 2 describes the analysis of crystalline bone mineral by an x-ray diffraction technique, while Chapters 3 and 4 are respectively concerned with x-ray diffraction measurement of bone mineral crystallite length and orientation. Chapters 5, 6 and 7 contain details of experimental determination of the tensile and compressive properties of bone tissue and relate those properties to degree of mineralisation, mineral crystallite length, mineral crystallite orientation and age, of the specimens. The estimation of bone mineral content at selected skeletal sites by gamma ray absorption is described in Chapter 8.

The principal material for these studies consisted of one hundred and seven sets of bones removed post mortem from adult human cadavers, each set comprising the right femur, radius and third metacarpal. They included both males and females and varied in age from nineteen to ninety-two years. In addition, femora from a three and a half year old

girl and an eleven year old boy were obtained. All bones were excised within forty-eight hours of death, stripped of soft tissue and stored at minus twenty degrees centigrade in a deep freezer until required. Non-destructive gamma ray absorptiometry was first conducted. Calibrations to yield mineral content from gamma ray absorption measurements were obtained by comparing these measurements with the weights of ash residues of one centimetre long transverse sections removed from sites scanned in sixty-three sets of bones (Chapter 8). Of the bones remaining intact, thirty femora were radiographed in an anterior/posterior alignment. The radiographs were examined with the aid of an illuminated viewing box, prior to deciding which femoral sections were most suitable for the production of cortical bone specimens for the investigations described in Chapters 2 - 7. The choice was largely dictated by the requirement for uniformly shaped tensile test pieces about six centimetre in length and having the maximum possible cross-sectional area (Chapter 6). Appropriate portions of the shaft were finally selected as illustrated in figure 1, and these portions were removed with a hacksaw.

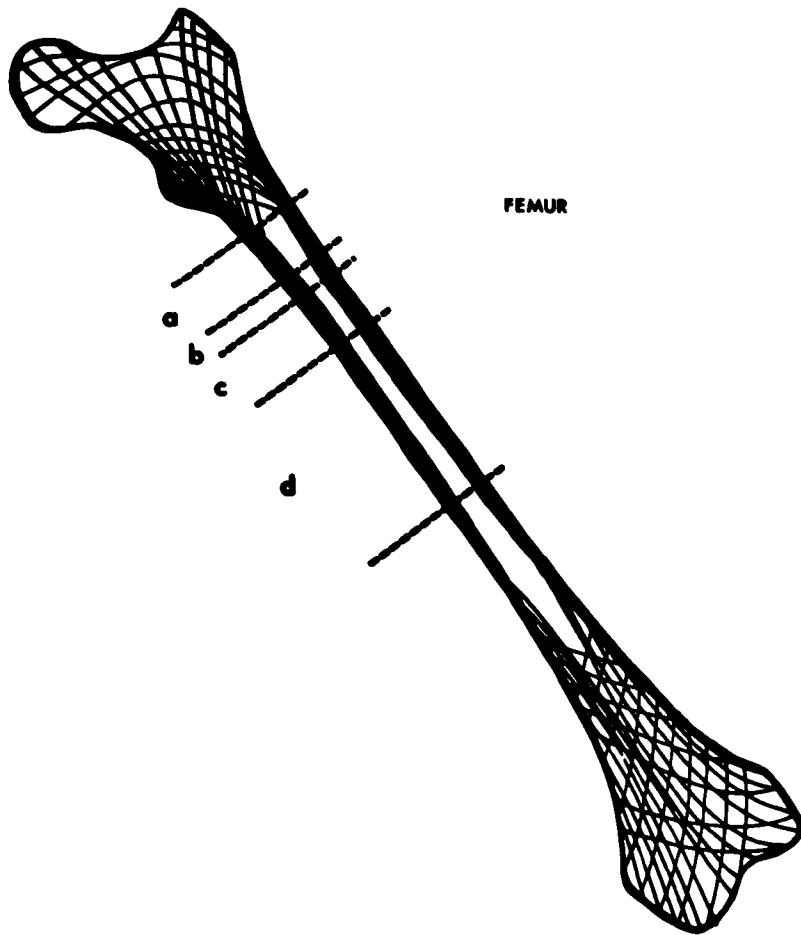


Fig. 1

- Femoral portions selected to provide sample material for physical analysis:
- (a) X-ray diffraction powder samples and electron microscopy transmission sections.
  - (b) X-ray diffraction flat plate specimens.
  - (c) Compressive test pieces.
  - (d) Tensile test pieces.

Relations between mineral content at different skeletal sites, established in Chapter 8, provide the basis of the studies described in Chapter 9. The gamma ray absorption technique was used to make in vivo measurement of the mineral content at the mid-point of the right third metacarpal. Values were divided by the corresponding cortical cross-sectional areas (estimated from radiographs) to yield the degree of mineralisation, or mass of mineral per unit volume of cortical bone tissue. Measurements of normal subjects were compared with values for subjects who had recently sustained a fracture of the distal end of radius.

The concluding chapter discusses the significance of the findings reported in this thesis, and suggests lines along which research may be usefully conducted in the future.

CHAPTER 2

X-RAY DIFFRACTION ANALYSIS OF THE INORGANIC  
CRYSTALLINE COMPONENT OF BONE TISSUE.

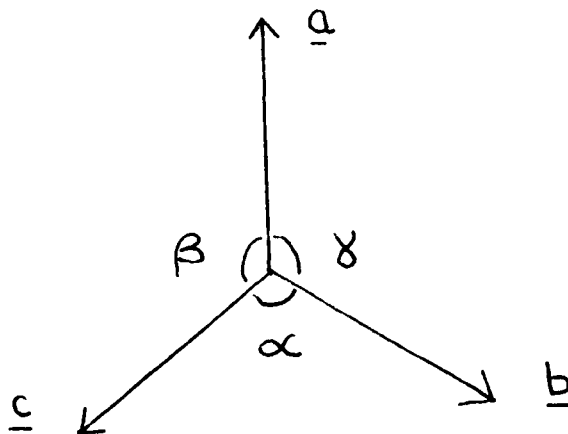
## INTRODUCTION

Using wide angle x-ray diffraction analysis De Jong (32) first reported that the mineral phase in bone has a crystal structure similar to that of calcium hydroxyapatite ( $\text{Ca}_{10}(\text{PO}_4)_6(\text{OH})_2$ ) with a hexagonal unit cell. Further evidence has been provided by chemical analysis which shows a calcium to phosphorus ratio closely corresponding to that of calcium hydroxyapatite (33, 34). A number of groups of researchers have conducted x-ray diffraction investigations of either intact bone (33, 35, 36, 37, 38, 39, 40) or powdered bone (41, 42, 43, 44, 45, 46, 47, 48, 49) obtained from various sources. Most confirm De Jong's findings and some found evidence of the presence of mineral substances other than apatite in certain specimens. Lenart, Bidlo and Pinter (48) observed diffraction lines characteristic of monetite from some bovine tibias and lines characteristic of brushite for some others. High angle x-ray diffraction studies led Posner (50) to predict the presence of substantial quantities of amorphous calcium phosphate in bone tissue. This suggestion was based on the observation of high intensity diffuse scattering like that produced by amorphous substances. Posner has attempted to estimate the "degree of

crystallinity<sup>o</sup> of bone mineral by low angle x-ray diffraction (51) and infra-red absorption spectroscopy (52, 53).

## THE CRYSTALLINE STATE

In crystalline materials, constituent atoms are arranged in a regular fashion comprising a three-dimensional repetition of a basic unit. The size and structure of this basic unit can be described by specifying the parameters of a "unit cell" which in certain cases need not be the complete unit of repetition. The structure of a crystalline substance is thus simply that of the unit cell. Unit cells are defined by the relative directions and lengths of three axes delineated as shown below:



It is found that all known types of crystal structure can be described by one of only seven systems of axes. The simplest system is "cubic", having the axes mutually perpendicular ( $\alpha = \beta = \gamma = 90^\circ$ ) and of

equal length ( $a = b = c$ ). Thus the crystal structure of a material known to belong to the cubic system can be uniquely defined by stating the length of its unit cell axes.

For reasons which will become apparent later, it is useful to describe the orientation of planes of atoms in terms of the unit cell parameters. This is accomplished by arbitrarily assigning the position of the origin of the unit cell axes on one of the planes in question, and then stating the intercepts made on the unit cell axes by an adjacent parallel plane, as multiples of the unit cell dimensions, viz.  $m.a$ ,  $n.b$ ,  $p.c$ . Thus, the orientation of that set of parallel planes can be described by these intercepts. However, in order to express more simply the fact that planes may be parallel to one or two of the unit cell axes and would therefore intercept them at infinity, we use the "Miller Indices"  $h, k, l$ , defined as the reciprocals of  $m, n, p$  respectively. The orientation of ANY set of planes is then given by its Miller indices  $(h\ k\ l)$ .

For each crystal system there is a fixed relation between the interplanar spacing ( $d$ ) of any set of parallel planes, the Miller indices of

these planes, and the parameters of the unit cell. For example, with a substance of the cubic system, the d-spacing between adjacent planes with Miller indices (h k l) is:  $d_{hkl} = a/(h^2 + k^2 + l^2)^{\frac{1}{2}}$ . More complex relations apply to other crystal systems. With the advent of x-ray diffraction techniques, it became possible to employ such relations to calculate the internal atomic structures of crystalline materials.

#### X-RAY DIFFRACTION : THEORETICAL CONSIDERATIONS

The ability of internal atomic layers within crystals to reflect x-rays so as to produce intensity maxima at certain angles of reflection, was first established in an experiment devised by Van Laue in 1912 and carried out by his assistants Friedrich and Knipping. They demonstrated that a narrow beam of x-rays, incident on a single crystal of zincblende, was scattered preferentially in certain directions. Furthermore, the pattern of these diffraction maxima, recorded on a photographic plate placed normal to the incident beam, possessed the same features of symmetry as the external faces of the crystal observed with an optical goniometer.

Van Laue and Sir Lawrence Bragg derived analogous expressions showing that for a fixed wavelength of incident radiation, each direction of preferred scattering is indicative of the presence of parallel planes of atoms with a particular interplanar separation. The Bragg law states that the angle  $\theta_{hkl}$ , termed the Bragg angle, at which radiation of wavelength  $\lambda$  must be incident on a set of planes (h k l) with interplanar separation  $d_{hkl}$ , in order to be reflected with the maximum possible intensity, is given by the expression:

$$n \cdot \lambda = 2 d_{hkl} \cdot \sin \theta_{hkl}$$

where  $n$  is an integer indicating the order of the reflection. In practice, we are usually concerned with the interpretation of first order reflections and  $n$  is set equal to unity. It can be seen from the Bragg law that the orientation of a crystal with respect to the direction of propagation of the incident x-ray beam, decides which sets of atomic planes (h k l) produce diffraction maxima.

By recording the diffraction patterns of single crystals, crystallographers have been able to determine interplanar spacings and hence deduce the internal atomic structures of many crystalline

materials. However, interplanar separations can be calculated more readily from x-ray diffraction patterns when the effects of crystal orientation are eliminated. This is achieved by producing a "powdered" sample, with particle size sufficiently small to ensure that the x-ray beam impinges on large numbers of crystallites inclined at every possible orientation. The resultant diffraction pattern then includes each intensity maximum which the sample material is capable of producing with the wavelength of x-ray employed. The complete pattern is recorded photographically, or by electronic counting equipment. In either case, the results are analysed to give the angular positions and relative intensities of the diffraction maxima, and hence yield the interplanar spacings with which they correspond. Now, according to the laws of reflection, equal angles are made with reflecting planes by both incident and reflected beams. This means that the angle BETWEEN incident and reflected beams is always twice the angle of incidence (Fig. 2), and in the case of Bragg reflection is equal to  $2 \theta_{hkl}$ , or twice the Bragg angle. Since in practice the direction of the incident beam is fixed, the angular positions of reflections are stated with

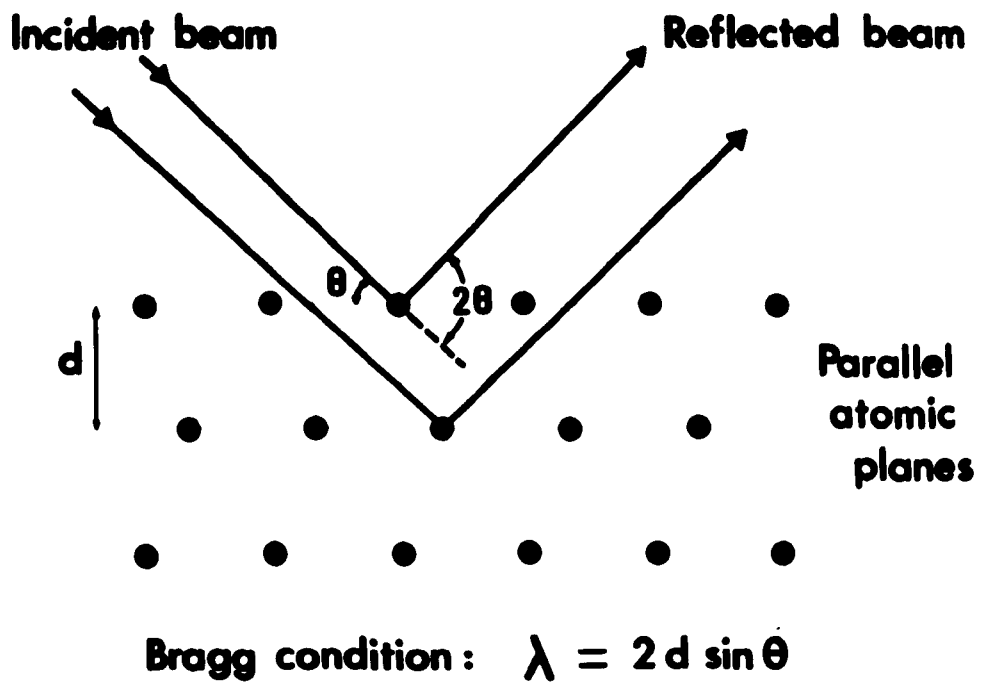


Fig. 2 "Reflection" of x-rays by a crystalline array of atoms : condition for Bragg reflection.

respect to this direction. Intensities of reflections are normally expressed as percentages of the intensity of the strongest reflection present in the diffraction pattern.

In order to identify unknown materials, reference is made to the ASTM Powder Diffraction File\* in which records of the diffraction data and structures of crystalline substances are filed according to the interplanar or d-spacing of the strongest reflection produced by the substance (referred to hereafter as the 'principle d-spacing'). The card corresponding to the material with principle d-spacing closest to that of the substance being analysed is selected, and the angular positions and relative intensities of the remaining reflections of the observed pattern are compared with the data provided on the card. Due to instrumental problems of recording widely differing intensities of reflection, the relative intensity values quoted are often not accurate. Prime importance is therefore paid to comparing the angular positions of the reflections. There may be sufficiently close agreement to positively identify the test material: otherwise, reference

\* AMERICAN SOCIETY FOR TESTING MATERIALS, POWDER DIFFRACTION FILE.

is made to the card corresponding to material with the next closest principle d-spacing. If the sample is unlike any recorded in the ASTM Powder Diffraction File, then the evaluation of its structure is more complicated. However, since for each crystal system only certain combinations of Miller indices are physically possible, detailed study of the angular distribution of reflections enables the crystal system to be deduced. Unit cell dimensions can then be calculated from d-spacings.

#### MATERIALS AND METHODS OF SAMPLE PREPARATION

Complete transverse sections, approximately one inch in length, were removed from close to the proximal end of the shaft of twenty-nine human femora as described earlier (Chapter 1). The preparation of powder samples sufficiently fine for x-ray powder diffraction analysis was carried out in two stages. Firstly, about 10 gm. of each section was reduced to a crude powder (mean particle size 1 - 2 mm) by making repeated cuts with a coarse-toothed, hardened steel, circular saw blade. The blade was mounted on a milling machine and set to rotate at medium speed (cutting edge velocity approximately 6m./sec.) The sample was gripped in a vice and, using the "compound

drive" mechanism of the milling machine, was caused to advance slowly toward the rotating saw blade (approximately 0.1 millimetre advance per 0.3 metre saw blade edge travel). A paper funnel was constructed to fit around each bone sample and convey bone powder into a container (Fig. 3). The powder collected was sufficiently fine to be suitable for further reduction in a McCrone Micronising Mill.\* The mill comprises a mechanism for vibrating an array of agate grinding elements contained in a sealed plastic jar. Bone powder was poured into the jar and washed down amongst the elements with about ten millilitres of isopropyl alcohol. A polythene cap was screwed securely on top of the jar which was then installed in the mill, and the jar and its contents were caused to vibrate for two minutes. This was adequate to produce a powder of particle size small enough for x-ray diffraction analysis (about 40 - 200 micron).

The advantages of using isopropyl alcohol as a grinding fluid are threefold. Firstly, it has

\* McCrone Research Associates Limited,  
Belsize Lane, London.

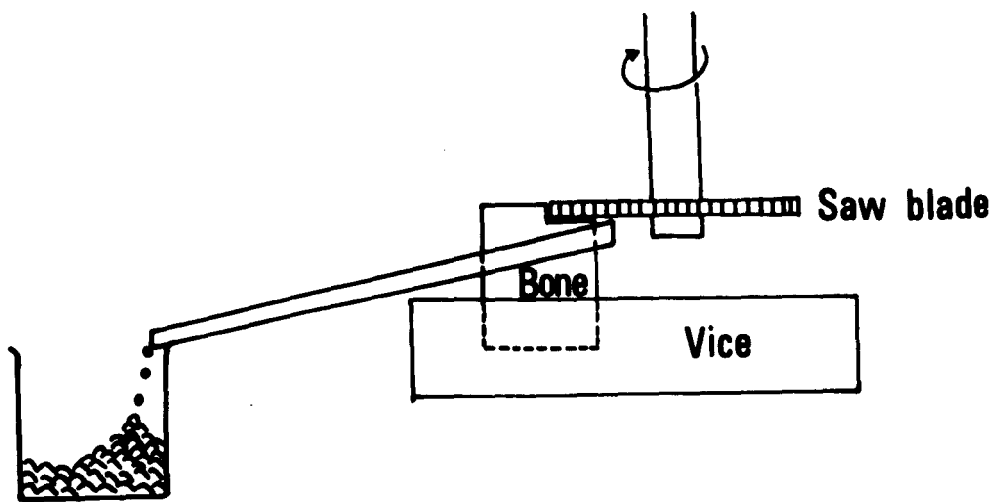


Fig. 3      Production of bone powder by the use of a circular saw blade mounted on a milling machine.

sufficiently high thermal conductivity to prevent localised heating during grinding of the sample. Secondly, it is volatile and rapidly evaporates after the grinding has been completed. Lastly, isopropyl alcohol presents no risk of explosion during the grinding process.

Immediately grinding had been accomplished, the jar was removed from the micronising mill and the cap was replaced with a "pouring cap" through which two holes were bored close to the circumference and diametrically opposite one another. The "slurry" of bone powder and alcohol was poured out of one of these holes and into a wide, shallow porcelain crucible. The pouring cap was removed, fifteen millilitres of isopropyl alcohol was poured into the jar, and the original cap was restored. The assembly was then vibrated in the mill for fifteen seconds before the fluid contents were added to the crucible. This procedure was repeated a further two times to flush out the grinding jar and leave it thoroughly clean to receive the next sample. The crucible was placed in a fume cupboard and left, with the extraction fan switched on, until the alcohol had completely evaporated (about twenty-four hours). The bone powder was left

deposited in the form of an aggregate layer, which was broken up by vigorous stirring with a soft brush before being passed through a no. 100 mesh sieve (150 micron mesh size), collected in a container, and stored ready for analysis.

#### METHOD OF RECORDING X-RAY DIFFRACTION PATTERNS

X-ray diffraction patterns were produced using nickel filtered radiation from the copper target of a Phillips X-ray generator type PW 1010/80\*. The machine was operated at an accelerating voltage of forty-four kilovolts and a tube current of twenty-two milliamps. A Phillips vertical goniometer type PW 1140\* with a sodium iodide scintillation detector, was employed to monitor the angular positions of diffraction maxima.

A 1.25 millimetre thick aluminium plate with a rectangular hole 20 millimetres wide and 11 millimetres high, served as specimen holder (Fig. 4). The holder was placed on a clean, flat sheet of glass and bone powder was poured into the rectangular aperture until it was amply filled. A paper tissue was laid over the specimen holder and pressed firmly down in such a way as to compress the bone powder into the

\* Pye-Unicam Limited, Phillips Analytical Department, York Street, Cambridge.

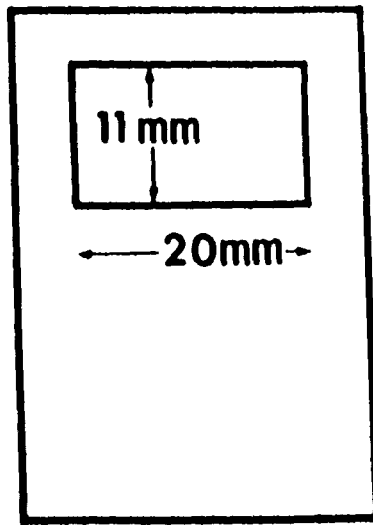
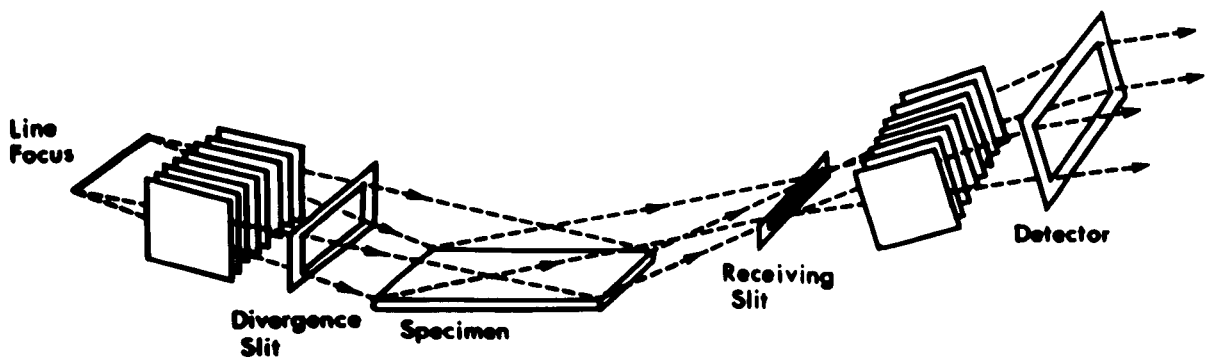


Fig. 4 Goniometer powder sample holder.

aperture. A heavy thumb pressure was sufficient to ensure that the powder remained in place during subsequent handling. The holder was then gently lifted and inserted in the goniometer.

The goniometer comprises a mechanism for exposing the flat surface of the sample to the x-ray beam, while rotating the sample, about an axis perpendicular to the incident beam, at exactly one half the angular velocity with which the scintillation detector is simultaneously rotated about the same axis. The zero angle positions of the sample and detector are coincident so that as the detector rotates, the angle it makes with the primary x-ray beam is always twice the angle of incidence the beam makes with the sample. Different speeds of rotation are set by employing various combinations of interchangeable spur gears. The x-ray optical design of the goniometer is illustrated in Fig. 5. A vertical divergence slit defines the angular divergence of the x-ray beam and restricts the beam to within the area of the specimen. A vertical receiving slit limits the width of the beam reflected from the sample and a vertical scatter slit in front of the detector completes the Bragg focussing system. In addition,



**Fig. 5** X-ray optical design of the Phillips PW1140 goniometer.

two parallel slit assemblies limit divergence in a horizontal direction.

A one degree angular aperture of the divergence slit was found appropriate to the size of specimen holder employed. The scatter slit, positioned the same distance from the specimen as the divergence slit, was also set at one degree. The size of the receiving slit affects both the angular resolution and the intensity of the reflected beam received by the detector. High resolution, achieved by using a very narrow slit, is normally required for accurate measurement of lattice parameters. However, with a poorly crystallized material such as bone tissue, reflections are very weak and the slit width cannot be reduced too much without producing intolerably low intensities. After investigating these considerations, a slit width of 0.1 millimetre was adopted.

The output of the scintillation detector was transmitted to a pulse height analyser which had been adjusted to pass only pulses in an energy range corresponding to the copper  $K\alpha$  radiations. A ratemeter converted these pulses into an analogue signal which was displayed graphically by a pen recorder.

With the detector rotating at an angular velocity of one degree per minute, continuous spectra were recorded over an angular range from twenty degrees to sixty degrees ( $2\theta$ ) for each bone powder sample. The maximum count rate observed was about 180 c.p.s. and the ratemeter was therefore set to provide a range of 200 c.p.s. for full scale deflection of the recorder. A ratemeter time constant of two seconds was used to smooth out statistical fluctuation in count rate during recording. The peak corresponding to the highest intensity bone powder reflection was recorded in detail, with the detector rotating at one eighth of a degree per minute, for several of the specimens. After subsequent positive identification of the crystal system of the sample material, peaks due to reflections from (002) planes and (222) planes were also recorded in detail at one eighth degree per minute detector angular velocity, for each sample. These reflections were of lower intensity than the principal reflection in the diffraction pattern and the ratemeter was adjusted to produce full scale recorder deflection at 100 c.p.s. During each of these detailed recordings, the ratemeter time constant was set at eight seconds. The measured d-spacings of the (002) and (222) reflections were used to

calculate accurately the unit cell parameters.

A powdered sample of sodium chloride was used as a standard and detailed recordings were made of the peaks corresponding to reflection from (111) and (220) sets of planes. These reflections occur at approximately the same angles of diffraction as the bone powder (002) and (222) reflections. Mean d-spacings calculated for the sodium chloride standard were compared with their known values to provide an estimate of any systematic error of determination. Sodium chloride gave more intense reflections than bone powder and counting ranges of 400 c.p.s. (111) and 2000 c.p.s. (220) were set. The time constant was kept at eight seconds.

During all recordings described above, the recorder chart speed was ten millimetre per minute.

## RESULTS AND CALCULATIONS

The x-ray spectrum emitted from a copper target contains discrete peaks of very high intensity at wavelengths corresponding to the characteristic copper  $K_{\beta}$  and  $K_{\alpha}$  radiations. Nickel has an absorption edge lying about midway between the  $CuK_{\beta}$  and  $CuK_{\alpha}$  wavelengths (Fig. 6). The nickel filter thus reduces the x-ray spectrum to a nearly monochromatic beam mainly comprised of the  $CuK_{\alpha}$  radiations at wavelengths of 1.54051 Angstroms ( $K_{\alpha 1}$ ) and 1.54433 Angstroms ( $K_{\alpha 2}$ ). These radiations, termed the copper  $K_{\alpha}$  doublet, have a weighted mean intensity occurring at a wavelength of 1.54178 Angstroms\*, and this value was used in all calculations involving the wavelength of the x-ray beam.

The mass absorption coefficient of whole bone for this wavelength of radiation is of the order of  $40 \text{ cm}^2/\text{gm}$ . and the density is about  $2.4 \text{ gm}/\text{cm}^3$ . Figure 7 shows the exponential relation between percent absorption and thickness of bone. Assuming compressed bone powder to be approximately equivalent to whole bone, the sample could be regarded as having infinite thickness with respect to transmission of

\* International Tables for X-ray Crystallography, The Kynoch Press, Birmingham.

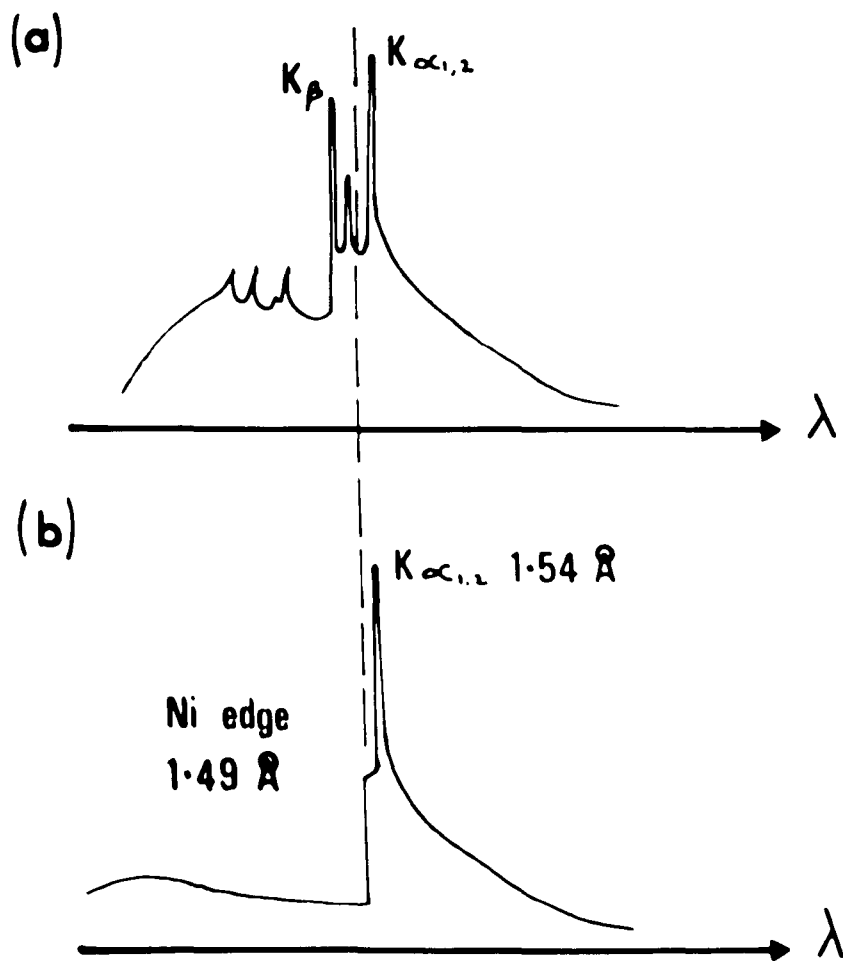


Fig. 6

- (a) Spectral distribution of x-rays emitted by a copper target.  
 (b) Spectral distribution of x-rays from copper target after nickel filtration.

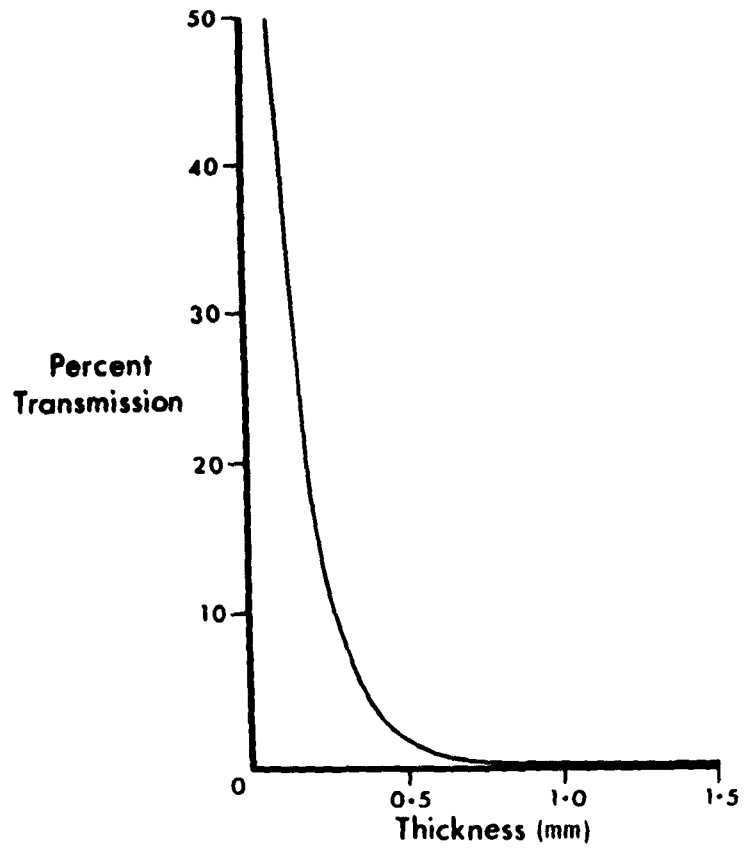
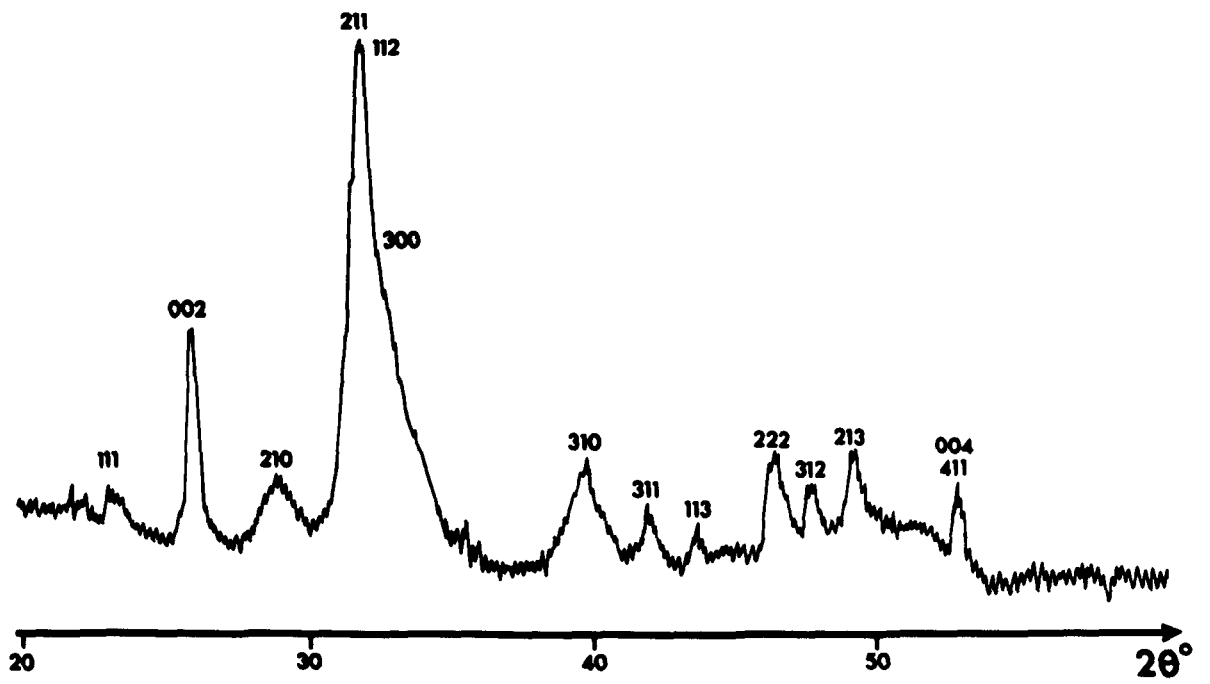


Fig. 7 Absorption versus specimen thickness for  $\text{CuK}\alpha$  x-rays incident on compact bone tissue.

the incident x-ray beam (transmission at 1.0 millimetre depth  $< 0.05\%$ ). Therefore, effects of varying sample thickness on intensity of reflection could be discounted.

A typical bone powder diffraction pattern, or diffractogram, is shown in figure 8. Eleven discrete peaks (diffraction lines) were identified and their angular positions, d-spacings, and relative intensities are recorded in Table 1. Peak height was taken to be an approximate measure of intensity and each measurement was expressed as a percentage of the height of the most intense reflection.

Intercomparison of diffractograms for the twenty-nine bone samples was facilitated with the aid of a horizontal illuminated viewing box. Two of the recorder tracings were laid on the box, one on top of the other, and the diffraction patterns were superimposed as closely as possible. In this way, the angular positions and relative intensities of the eleven main reflections were visually compared. The topmost tracing was then removed and replaced with another one. The procedure was repeated for each of the remaining recorder tracings. There was an almost exact superposition in every case and, taking into



**Fig. 8** Bone powder diffractogram (CuK $\alpha$  radiation).

account the number of reflections present, this was sufficient to confirm that each sample contained the same type of crystalline material.

The most intense reflection occurred at a diffraction angle of about 31.9 degrees (Table 1). Detailed profiles of this reflection for seven of the samples yielded the angular positions shown in Table 2. The mean value of 31.89 degrees was used to calculate accurately the d-spacing for the set of planes giving rise to this reflection. According to the Bragg law:

$$\lambda = 2 d \sin \theta$$

$$\therefore d = \frac{1.54178}{2 \cdot \sin \left[ \frac{31.89}{2} \right]^\circ} \quad \underline{\underline{2.81 \text{ Angstrom}}}$$

Thus 2.81 Angstrom was the principal d-spacing of the material. Comparison of the observed diffraction pattern with patterns of materials registered in the ASTM Powder Diffraction File, under principal d-spacing equal to 2.81 Angstrom, led to confirmation of the calcium hydroxyapatite-like structure of bone mineral. The substance with a diffraction pattern most resembling that of bone powder was the synthetic apatite  $\text{Ca}_{10}(\text{PO}_4)_6(\text{OH})_2$  listed under ASTM card number 9-432. This material possesses a hexagonal structure with unit cell parameters  $a = 9.418 \text{ \AA}$  and  $c = 6.884 \text{ \AA}$ .

Each of the d-spacings calculated for the eleven main reflections of bone powder agreed to within two decimal places with the data quoted for the equivalent reflections of synthetic apatite. However, it was discovered that some of the peaks resulted from partial superposition of more than one reflection. For this reason, only a very general agreement was found between measured relative intensities and the values referenced. Having identified the structure of crystalline bone mineral, the reflections were then indexed with the Miller indices of the sets of planes producing them (Fig. 8).

Examples of the detailed recordings of peaks due to (002) and (222) reflections are illustrated in Figs. 9a and 9b. These recordings were used to measure accurately the angular positions and d-spacings. Unit cell parameters were then calculated as follows:

$$\lambda = 2d \cdot \sin \theta \quad (1)$$

Thus for the (002) reflection:-

$$d_{002} = \frac{\lambda}{2 \cdot \sin (\theta_{002})} \quad (2)$$

For a hexagonal unit cell:-

$$d = \frac{1}{\left[ \frac{4(h^2 + hk + k^2)}{3a^2} + \frac{1}{c^2} \right]^{1/2}} \quad (3)$$

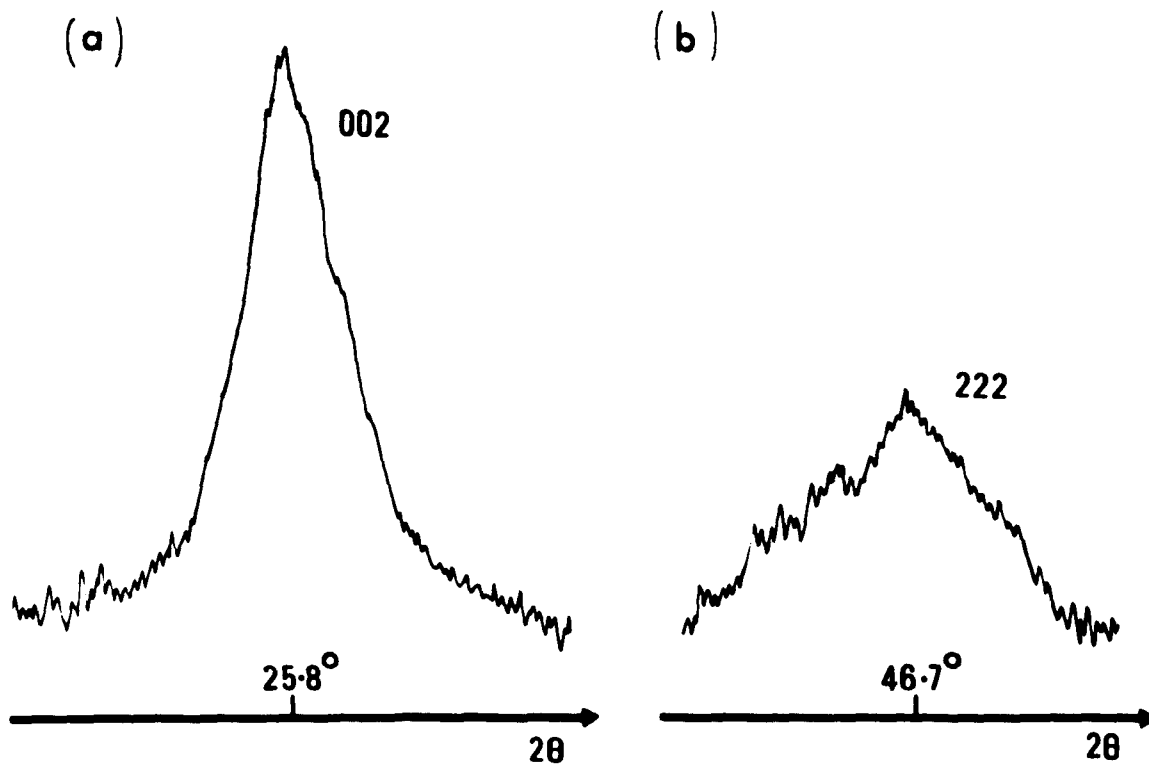


**Fig. 9** (a) Detailed recording of bone apatite (002) reflection.  
(b) Detailed recording of bone apatite (222) reflection.

For the (002) reflection, this reduces to:-

$$d = \frac{c}{2} \quad (4)$$

equating equations (2) and (4):-

$$c = \frac{\lambda}{\sin(\theta_{002})} \quad (5)$$

For the (222) reflection, equation (3) reduces to:-

$$d_{222} = \frac{1}{\left[ \frac{16}{a^2} + \frac{4}{c^2} \right]^{\frac{1}{2}}} \quad (6)$$

Equating equations (1) and (6), and rearranging:-

$$a = \frac{2}{\frac{\sin^2(\theta_{222})}{\lambda^2} - \frac{1}{c^2}} \quad (7)$$

Substituting equation (5) into equation (7):-

$$a = \frac{2\lambda^2}{\sin^2(\theta_{222}) - \sin^2(\theta_{002})} \quad (8)$$

Values of the unit cell parameters for each bone sample, calculated from equations (4) and (8), are listed in Table 3. The mean values were  $a = 9.409$  Angstrom and  $c = 6.893$  Angstrom, with coefficients of variation equal to 0.21% and 0.25% respectively.

Interplanar spacings calculated from the observed angular positions of the sodium chloride (111) and (220) reflections are listed in Table 4. The average values were within 0.05% of the values

quoted in the ASTM Powder Diffraction File (Card number 5-0628). The errors were thus considerably less than the coefficients of variation of the bone powder unit cell parameters and correction for systematic error of estimation was deemed unnecessary.

TABLE 1

X-RAY DIFFRACTION DATA OF THE ELEVEN MAIN REFLECTIONS  
OF BONE POWDER (CuK $\alpha$  radiation).

Angular Position	Relative Intensity ( $I/I_{\text{principal}}$ ) $\times$ 100%	Interplanar Spacing ( $d$ Angstrom)
22.95	17	3.88
25.9	47	3.44
28.95	18	3.08
31.9	100	2.81
39.95	20	2.26
42.1	9	2.15
43.8	8	2.07
46.7	23	1.94
48.05	15	1.89
49.45	28	1.84
53.15	16	1.72

TABLE 2

ANGULAR POSITION OF THE PRINCIPAL REFLECTION OF  
BONE POWDER (CuK $\alpha$  radiation).

Specimen	Diffraction angle of Principal Reflection (2 $\theta$ degrees)
N4	31.92
N5	31.85
RU 71	31.92
RU 73	31.83
RU 82	31.88
RU 85	31.95
RU 89	31.91

TABLE 3

BONE APATITE UNIT CELL PARAMETERS.

Sample	a (Angstrom)	c (Angstrom)
Y1	9.401	6.898
Y2	9.434	6.890
N1	9.410	6.898
N2	9.414	6.896
N3	9.425	6.882
N4	9.405	6.893
N5	9.407	6.893
RU 67	9.412	6.898
RU 69	9.395	6.882
RU 70	9.404	6.903
RU 71	9.415	6.890
RU 72	9.412	6.890
RU 73	9.416	6.888
RU 74	9.415	6.898
RU 75	9.418	6.890
RU 76	9.418	6.890
RU 77	9.397	6.901
RU 78	9.416	6.888
RU 79	9.409	6.899
RU 80	9.408	6.896
RU 81	9.404	6.911
RU 82	9.389	6.896
RU 83	9.409	6.890
RU 84	9.405	6.893
RU 85	9.402	6.861
RU 86	9.387	6.899
RU 87	9.406	6.888
RU 88	9.421	6.898
RU 89	9.405	6.896

TABLE 4

MEASURED d-SPACINGS OF SODIUM CHLORIDE (111) AND  
(220) REFLECTIONS (CuK $\alpha$  radiation).

Measurement	d <sub>111</sub> (Angstrom)	d <sub>220</sub> (Angstrom)
1	3.261	1.996
2	3.258	1.996
3	3.261	1.995
4	3.260	1.996
5	3.258	1.995
6	3.261	-
7	3.261	-
8	3.257	-

CHAPTER 3

DETERMINATION OF BONE APATITE CRYSTALLITE  
LENGTH BY X-RAY DIFFRACTION AND ELECTRON  
MICROSCOPY

## INTRODUCTION

Electron microscopy shows bone mineral to consist largely of approximately needle-shaped crystallites distributed throughout the collagen matrix (23, 25, 33, 54, 55). The crystallites are reported to range from about 200 to 500 Angstrom in length and 20 to 80 Angstrom in diameter, although measurement of electron micrographs has yielded rather higher figures than those obtained using x-ray diffraction techniques (36, 37, 47, 56).

Chatterji and Jeffery (57) have suggested that crystallite size increases with advancing age. In evidence, they published electron micrographs of human post mortem bone specimens aged seven, twenty-three and eighty-four years. Their results are difficult to interpret, but seem to indicate a GREATLY increased crystallite length in old age.

The present chapter describes the determination of mean crystallite length in femora excised from cadavera ranging in age from three and a half to eighty-seven years, by x-ray diffraction line-broadening. Electron microscopy provided a reference method with which the results were compared.

X-RAY DIFFRACTION MEASUREMENT OF CRYSTALLITE SIZE:  
THEORETICAL CONSIDERATIONS

Scherrer (58) first showed that diffraction line profiles of powder samples were subject to angular broadening when the crystallites present had average dimensions much less than  $10^{-4}$  millimetre. He explained this phenomenon in terms of the intensity contribution due to x-rays incident at angles slightly deviant from the Bragg angle. When such reflection occurs at closely adjacent parallel atomic planes, the resultant path difference between the reflected beams is short and does not produce sufficient phase discrepancy for their total mutual extinction. However, similar reflection of x-rays incident at widely separated atomic planes, causes a bigger phase discrepancy and a correspondingly greater degree of extinction. Thus, powder samples comprised of large crystallites produce well-defined diffraction lines within which most of the diffracted intensity results from summation of reflections from widely separated atomic planes. Conversely, when a sample contains only small crystallites, all reflections are from closely adjacent planes. The contribution of intensity reflected at angles deviant from the Bragg angle is then proportionately larger and creates increased angular broadening of the

diffraction lines. Scherrer derived an expression relating the extent of this increased broadening to the average crystallite dimension:

$$D_{hkl} = \frac{K \cdot \lambda}{\beta \cdot \cos(\theta_{hkl})} \quad (9)$$

where  $\theta_{hkl}$  is the Bragg angle of the reflecting planes (hkl) for radiation of wavelength  $\lambda$ ,  $D_{hkl}$  is the mean crystallite dimension in the direction normal to the reflecting planes,  $\beta$  is termed the "pure" or "intrinsic" line breadth and is a measure of the increase in the breadth due to small crystallite size, and  $K$  is a constant related to the crystallite shapes and the definition of  $\beta$ .

A major source of error in the estimation of crystallite sizes from line broadening, stems from uncertainty as to the value of  $K$ . Patterson (59, 60) has derived values of  $K$  for distributions of spherically shaped particles. More generally, Scherrer (58) and Bragg (61) have shown that in the absence of detailed information regarding the distribution of crystallite shapes, if  $\beta$  is defined as the pure line breadth at half maximum intensity ( $\beta_{\frac{1}{2}}$ ), then  $K$  takes a value of approximately 0.9 and is relatively insensitive to differences in crystallite shape. Thus

the Scherrer equation becomes:

$$D_{hkl} = \frac{0.9 \lambda}{\beta_{\frac{1}{2}} \cdot \cos(\theta_{hkl})} \quad (10)$$

Now, in order to deduce the pure diffraction breadth  $\beta$ , the experimentally observed line breadth must be corrected for all broadening other than the pure or intrinsic broadening due to small crystallite size. Additional broadening is caused by a variety of instrumental factors. Firstly, the primary x-ray beam cannot be made completely monochromatic, with the result that different wavelengths are present and these suffer Bragg reflection at differing Bragg angles. It can be shown (Appendix 1) that the angular separation  $S\theta$  between Bragg angles for wavelengths differing by  $S\lambda$  is:

$$S\theta = \frac{S\lambda}{\lambda} \cdot \tan \theta \quad (11)$$

This function increases sharply as  $\theta$  increases, tending toward infinity as  $\theta$  tends to ninety degrees. Figure 10 shows the separation  $S(2\theta)$  of diffraction angles for the copper  $K\alpha_1$  and  $K\alpha_2$  radiations, as a function of  $2\theta$ . A certain amount of line broadening results from the superposition of reflections of the two copper  $K\alpha$  radiations, which are only completely resolved at high Bragg angles.

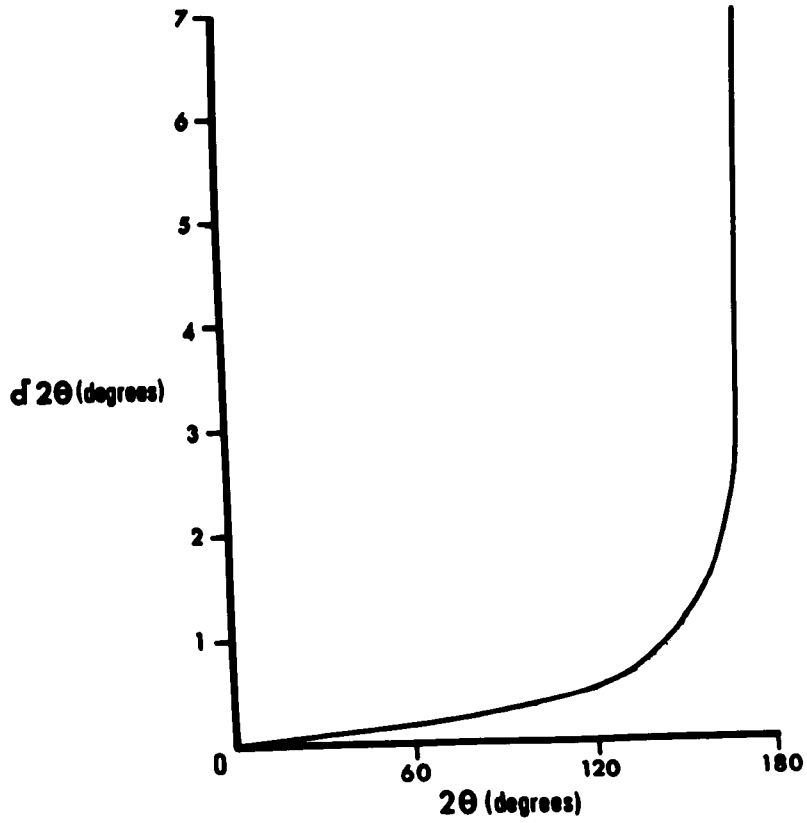


Fig. 10 Angular separation of diffraction angles of copper characteristic radiations, shown as a function of  $2\theta$ .

A second form of instrumental broadening results from geometrical sources. For example, the finite width of the x-ray focus means that a non-parallel primary beam is produced. Similarly, the finite height of the specimen and the fact that the incident x-rays penetrate to a finite depth (Fig. 7) contribute toward the lack of sharpness of diffraction lines. The combined effect of these geometrical factors has been expressed in mathematical form by Wilson (62).

The various intrinsic and instrumental determinants of line broadening interact in a complex way to produce the compound line breadths observed experimentally. Several different approaches toward tackling the problem of correcting observed breadth for total instrumental broadening, have been made. Spencer (63, 64, 65) has shown that the effect of instrumental factors in modifying a pure diffraction profile can be calculated using the "Superposition Theorem". This states that the profile of intensity distribution  $I = h(x)$  of the observed maximum will be the convolution (66) of the pure diffraction line profile  $f(x)$  and the weight function of the instrument or instrumental line profile  $g(x)$ :

$$h(x) = \int_{-\infty}^{+\infty} g(e) \cdot f(x-e) \cdot de \quad (12)$$

The variable  $x$  is the angular deviation from the theoretical diffraction angle (Fig. 11), and  $e$  is the "auxiliary variable".

NUMERICAL CORRECTION OF EXPERIMENTALLY OBSERVED  
LINE BREADTH

Stokes (67) has outlined a "Numerical Fourier analysis method for the correction of widths and shapes of lines on x-ray powder photographs". The functions  $h(x)$  and  $g(x)$  are each determined in numerical form by noting intensity at discrete intervals of  $x$ . In the former case, measurement is made of the profile of a diffraction maximum produced by the test sample. In the latter case, measurement is made of the profile of the corresponding maximum produced by a specimen comprised of the same material as the test sample but containing only large crystallites.

Equation (12) is then rewritten as:

$$h(x) = \sum_{-a}^{+a} g(e) \cdot f(x - e) \cdot Se \quad (13)$$

where the limits  $\pm a$  cover a sufficiently wide range of  $x$  to ensure that the summation includes the complete diffraction maximum. This summation constitutes a set of simultaneous equations which can be solved by the method of Fourier analysis.

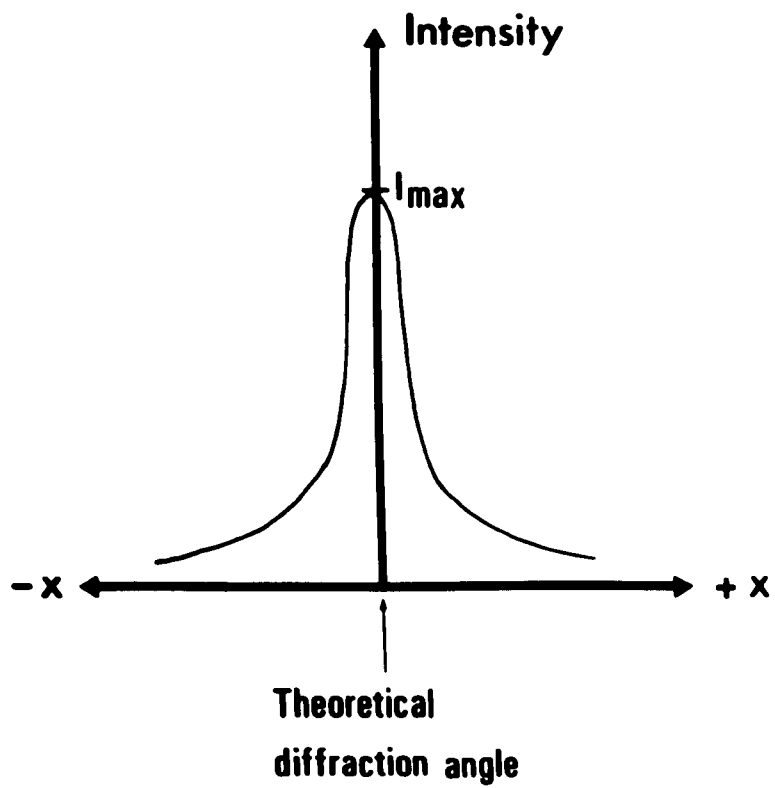


**Fig. 11** Diffraction line intensity distribution  $I=h(x)$  as assumed by Spencer (1949).

GRAPHICAL CORRECTION OF EXPERIMENTALLY OBSERVED  
LINE BREADTH

Jones (68) has described a convenient graphical method of correcting for the effects of instrumental line broadening. Initially, broadening due to wavelength spread which is superimposed over all other broadening, was evaluated. Using a sample comprised of crystallites sufficiently large to eliminate pure line broadening, Jones measured accurately the intensity profile of a diffraction line at a diffraction angle of one hundred and sixty degrees, where reflections of the copper  $K\alpha_1$  and  $K\alpha_2$  radiations were well resolved. He then investigated the profile for closeness of fit to equations of the form  $I = I_{\max.} (1 + k^2 x^2)^{-1}$  and  $I = I_{\max.} e^{-K^2 x^2}$ , where  $k$  and  $K$  were constants. Both of these equations had been shown previously by Von Laue to accurately describe x-ray diffraction line profile.

Jones first assumed profiles of the former type for reflections of the copper  $K\alpha$  radiations. Then, for differing angular separation  $S(2\theta)$ , he calculated the effect of compounding two such profiles both with the same breadth  $b$ , but one ( $K\alpha_1$ ) having twice the maximum intensity of the other ( $K\alpha_2$ ). From the results, the compound line breadth  $b_0$  was compared

to the angular separation  $S(2\theta)$ , and breadth ( $b$ ) of the original lines. Jones used the "Laue Integral Breadth" which is defined as the quotient of intensity integrated with respect to angle, divided by the maximum intensity. Integral breadth, like the breadth at half maximum intensity, is effectively independent of the intensity of primary radiation. Values of  $b/b_0$  were then plotted against  $S(2\theta)/b_0$ . This enabled subsequent interpolation of  $K\alpha$  corrected line breadths from experimentally observed breadths.

The whole procedure was repeated using the second of the Laue equations,  $I = I_0 e^{-k^2 x^2}$ . A correction curve, which differed only slightly from the first one, was obtained.

Further studies showed that both of the Laue equations described accurately the profiles of maxima produced when pure line broadening was present. This indicated that the line breadths of reflections from any sample, could be corrected for broadening due to wavelength spread by reference to the same correction curves.

Jones proceeded to show how a similar technique could be applied to the correction of geometrical broadening effects. Firstly, however, it was necessary to standardize the instrumental design. Then, detailed

diffraction line profiles were recorded for a sample known to contain only large crystallites. The observed breadth  $b_0$  of each line was corrected for  $K\alpha$  broadening. The corrected value  $b$ , constituted the geometrical broadening at the relevant angle of diffraction ( $2\theta$ ). Next, line profiles of reflections from a sample of test material were recorded under the same experimental conditions and  $K\alpha$  corrected breadth ( $B$ ) of lines of interest was determined. Jones showed how the pure breadth  $\beta$  of any of these lines could be evaluated from its  $K\alpha$  corrected breadth  $B$  and the geometrical breadth  $b$  for the same angle of diffraction. He plotted graphs of  $\beta/B$  versus  $b/B$  for each of the Laue forms of line profile.

Alexander and Klug (66, 69) published similar data for  $K\alpha$  and geometrical correction (Fig. 12) of breadth at half maximum intensity.

The graphs of Jones, and Alexander and Klug, provide standard data by which experimentally observed line breadths are corrected. Once the pure breadth at half maximum intensity has been determined and converted to radians, this value can be substituted directly into the modified Scherrer equation to yield an estimate of mean crystallite size in Angstrom units. Figure 13 shows the relation between pure line breadth and average

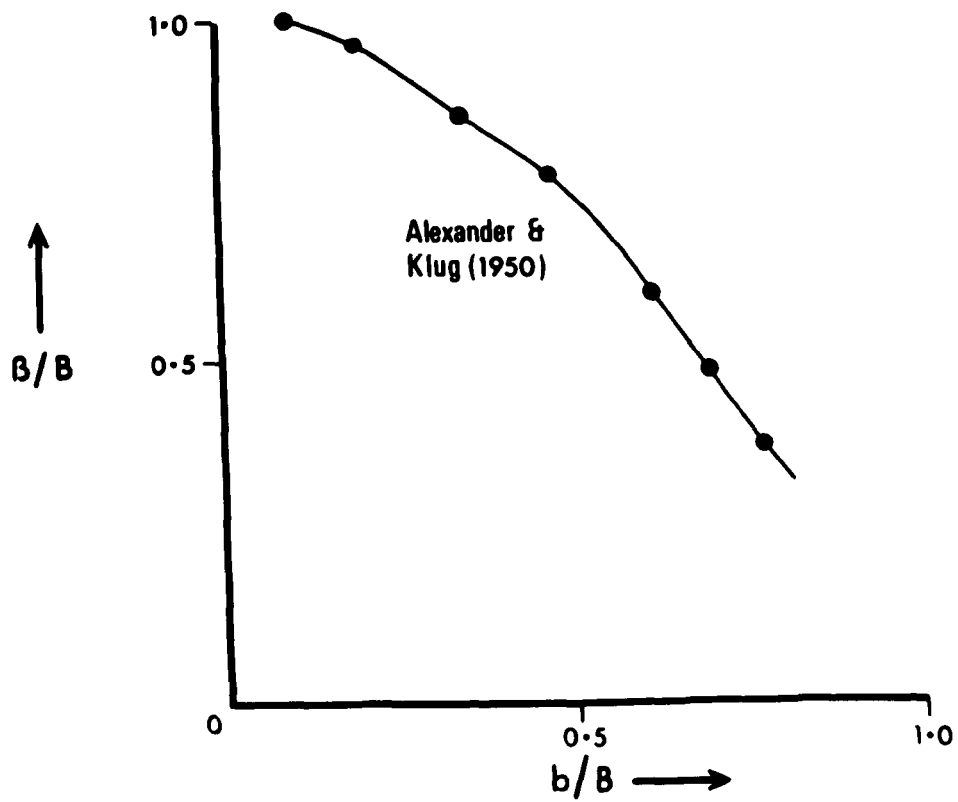


Fig. 12 Graph for correction of geometrical line broadening : constructed from data published by Alexander and Klug (1950).

crystallite dimension normal to the reflecting planes ( $D_{hkl}$ ) for different values of  $2\theta$  when  $\lambda$  is equal to the weighted mean of the copper  $K\alpha_1$  and  $K\alpha_2$  radiations.

Due to uncertainty regarding crystallite size distribution, and errors of evaluating instrumental broadening, absolute estimations of crystallite size are generally considered to be subject to errors of between twenty five and fifty percent (70). In most cases, however, we are concerned with the measurement of relative crystallite size, requiring only the determination of pure broadening. Repeatability can then be assessed on a statistical basis.

#### MATERIALS AND METHODS: X-RAY DIFFRACTION

Bone powder produced for studies described in the previous chapter provided sample material for crystallite size measurement. The powder was of sufficiently large particle size (50 - 150 micron) compared to the crystallite dimensions required to produce pure broadening, that no significant broadening could be attributable to crystallites damaged during grinding (Appendix 2). In addition to the bone powder samples, a number of powder specimens of sodium chloride having particle size in the range 50 - 150 micron, were prepared by crushing in a mortar and pestle followed by differential sieving.

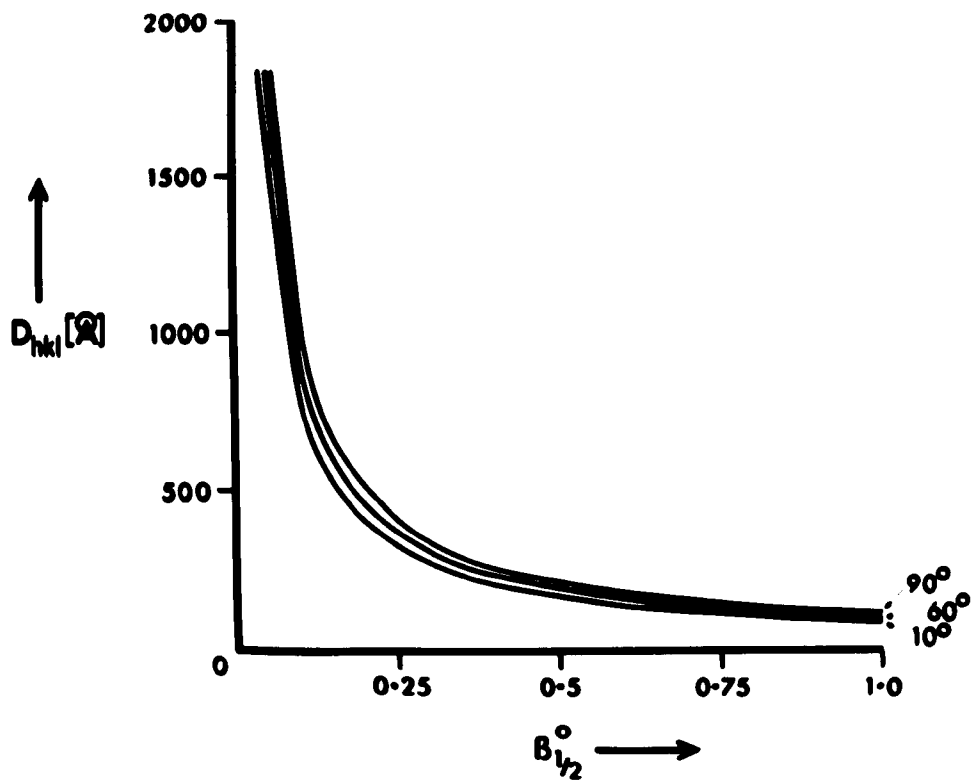


**Fig. 13** Relation between pure line breadth and average crystallite dimension normal to the reflecting planes, for different values of  $2\theta$  when  $\lambda$  is equal to the weighted mean of the copper  $K\alpha_1$  and  $K\alpha_2$  radiations.

Detailed recordings of the intensity profiles of bone powder (002) reflections were made using the goniometer and chart recorder described in Chapter 2. Copper K $\alpha$  radiation was employed. The scintillation detector was rotated at an angular velocity of one-eighth of a degree per minute, with the goniometer divergence, receiving and scatter slits set at one degree, one millimetre and one degree respectively. A ratemeter time constant of eight seconds, a chart speed of 600 mm/hour and a ratemeter range corresponding to 200 c.p.s. full scale recorder deflection, were chosen. Recording was carried out between diffraction angles two degrees either side of the theoretical angle of reflection, thus allowing accurate evaluation of the background intensity.

Similar recordings were made of the (111) reflections from each of the sodium chloride standards. Only the ratemeter range was altered, this being set to give 400 c.p.s. full scale deflection of the recorder. The (111) reflection was selected as this occurred at a Bragg angle close to that of the bone powder (002) reflection, and was thus used to estimate instrumental broadening at that angle.

On each recording a straight line was drawn joining the levels of background intensity on either

side of the diffraction profile (Fig. 14). This was used as a baseline above which the peak height  $I_{\max}$  was measured. Line breadth at half peak intensity was then noted.

Diffraction line profiles were investigated for degree of fit of each of the Laue equations  $I = I_{\max}/(1 + k^2 x^2)$  and  $I = I_{\max} \cdot e^{-K^2 x^2}$ . Each equation was reduced to a linear form and linear correlation coefficients for observed data were calculated.

After demonstrating that the former equation provided the better fit, this form was assumed in subsequent evaluation of  $K\alpha$  corrected breadth and pure breadth using the graphs published by Alexander and Klug (69)

#### RESULTS AND CALCULATIONS : X-RAY DIFFRACTION

Typical line profiles of bone (002) and sodium chloride (111) reflections are illustrated in Figure 14. Values of breadth at half maximum intensity are listed in Tables 5 and 6. The mean values for each reflection were expressed in millimetres of recorder chart travel and substituted into the Laue equations to yield values of the constants  $k$  and  $K$ :

$$I = I_{\max}/(1+k^2 x^2) \quad (14) \quad I = I_{\max} \cdot e^{-K^2 x^2} \quad (15)$$

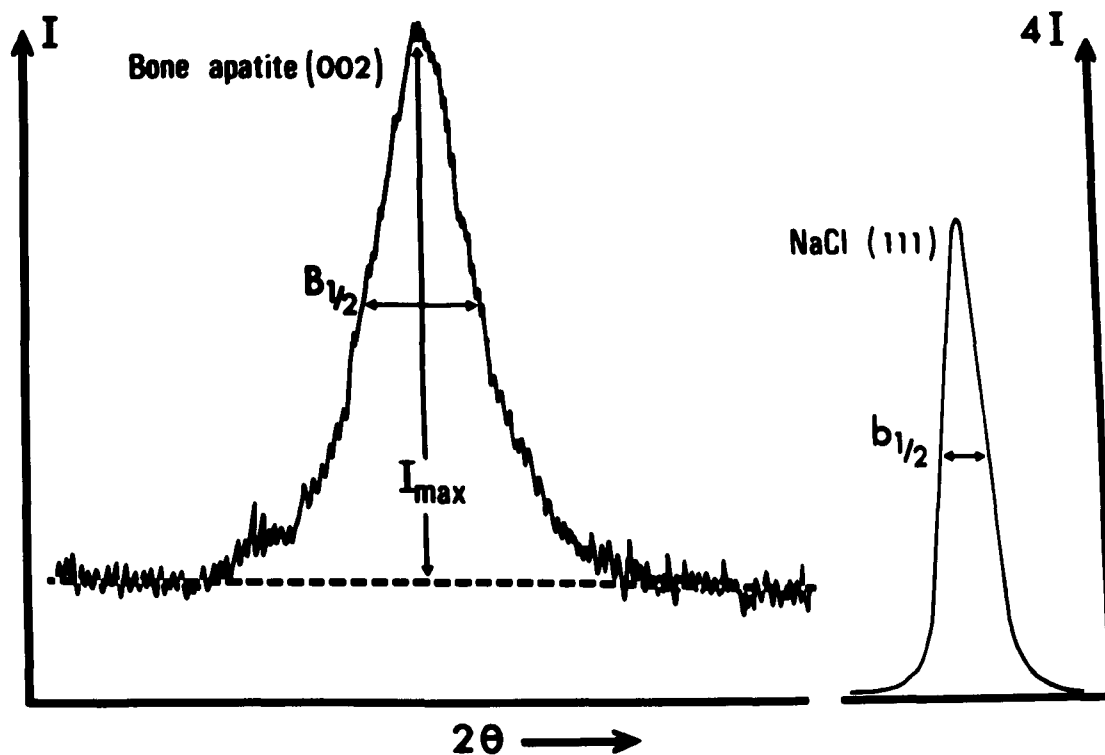


**Fig. 14** Line profiles of bone apatite (002) and sodium chloride (111) reflections, illustrating the definition of line breadth at half maximum intensity.

Now, for bone (002) reflections,  $B_{0\frac{1}{2}} = 0.355^\circ \cong 27.4 \text{ mm}$ .

Therefore, values of  $x$  at half maximum intensity are:

$$x = \pm \frac{(27.4)}{2}$$

Substituting into equation (14):

$$k_{\text{bone}}^2 = 0.0053 \text{ mm}^{-2}$$

And substituting  $x$  into equation (15):

$$K_{\text{bone}}^2 = 0.0037 \text{ mm}^{-2}$$

Similarly for NaCl (111) reflections,  $b_{0\frac{1}{2}} = 0.131^\circ \cong 10.5 \text{ mm}$ .

Hence from equation (14)

$$k_{\text{NaCl}}^2 = 0.0363 \text{ mm}^{-2}$$

And from equation (15)

$$K_{\text{NaCl}}^2 = 0.0251 \text{ mm}^{-2}$$

Thus for bone (002) reflections we have

$$I = I_{\text{max}} / (1 + 0.0053 x^2) \quad (16)$$

$$I = I_{\text{max}} \cdot e^{-0.0037 x^2} \quad (17)$$

And for NaCl (111) reflections

$$I = I_{\max} / (1 + 0.0363 x^2) \quad (18)$$

$$I = I_{\max} \cdot e^{-0.0251 x^2} \quad (19)$$

These equations can be reduced (Appendix 3) to the linear form:

$$Y = bX + C$$

Correlation coefficients for degree of fit of observed data to any of the linear equations are then given by:

$$r = \frac{N \cdot \Sigma(XY) - \Sigma X \cdot \Sigma Y}{\{ [N \cdot \Sigma(x^2) - (\Sigma X)^2] [N \cdot \Sigma(Y^2) - (\Sigma Y)^2] \}^{1/2}} \quad (20)$$

Now, for observed diffraction maxima, values of  $I$  were measured at discrete intervals of  $x$  spanning the complete profile. A Hewlett Packard 9100B Calculator\* was programmed to calculate correlation coefficients appropriate to each of the equations, and this was carried out for each set of data.

Using equations (16) and (18), the correlation coefficients for bone (002) profiles and sodium chloride (111) profiles were respectively greater than 0.99 and 0.95. With equations (17) and (19), coefficients for bone (002) reflections ranged from 0.95 to 0.99, while those for sodium chloride (111) reflections were about 0.94. Thus the results showed a close fit for both of the Laue equations, with a somewhat better fit for the equation  $I = I_{\max.} / (1 + k^2 x^2)$ . The equations (16) and (18) are therefore assumed valid in the following evaluation.

The  $K\alpha$  separation  $\delta(2\theta)$  was calculated at the observed diffraction angle of each bone (002) and sodium chloride (111) reflection. The values ranged from 0.0650 degrees to 0.0656 degrees in the former case, and from 0.0691 degrees to 0.0692 degrees in the latter case. Coefficients of variation were less than 0.2% and mean values are adopted in further calculations.

\*Hewlett Packard Limited, South Queensferry, West Lothian.

The ratio  $S(2\theta)/B_{0\frac{1}{2}}$  was calculated separately for each bone sample. A single value  $S(2\theta)/b_{0\frac{1}{2}}$  was calculated for sodium chloride using the mean breadth at half maximum intensity. Then, the ratios  $B_{\frac{1}{2}}/B_{0\frac{1}{2}}$  and  $b_{\frac{1}{2}}/b_{0\frac{1}{2}}$  were interpolated from the correction data of Alexander and Klug (66, 69). The product of each ratio and the observed breadth yielded the K $\alpha$  corrected breadth, which in the case of the sodium chloride standard represented the geometrical broadening  $b_{\frac{1}{2}}$ .

Then geometrical breadth was divided by the K $\alpha$  corrected breadth for bone  $B_{\frac{1}{2}}$ . This ratio enabled the interpolation of pure breadth divided by K $\alpha$  corrected breadth using the graph of Fig. 12 (after Alexander and Klug, 1950). Hence the pure breadth  $\beta_{\frac{1}{2}}$  of bone (002) reflection was calculated, converted to radians, and substituted into the modified Scherrer formula to yield the average crystallite length along the c-axis (Table 6).

The mean value was  $261 \pm 6.5$  Angstrom (2 S.E.). Values for different specimens are shown plotted against age of the parent bone in Fig. 15. No significant correlation with age was found ( $P = 0.31$ ).

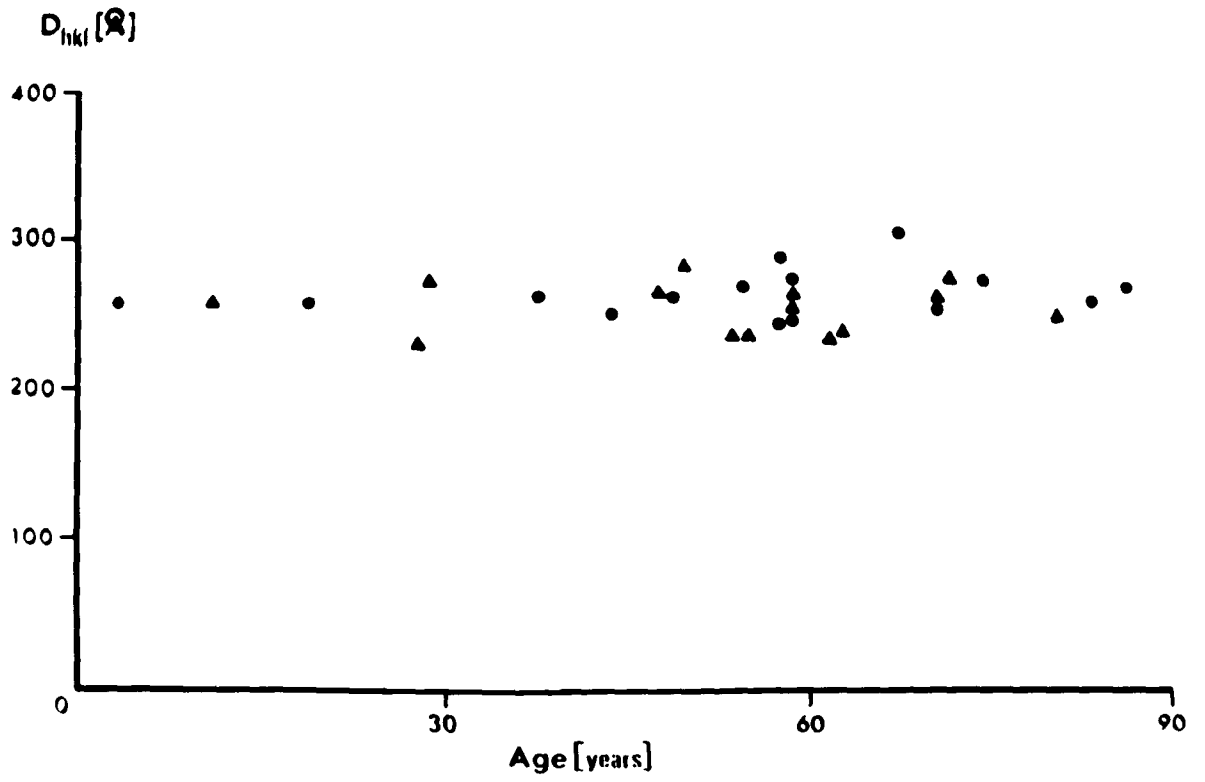


**Fig. 15** Average bone apatite crystallite length along c-axis, versus age.

## MATERIALS AND METHODS : ELECTRON MICROSCOPY

The Metals Research Macrotome II\* was used to cut 100 micron thick transverse sections from a proximal portion of the shaft of five femora. These bones were selected to cover a wide age range (three and a half to eighty-seven years). A one inch length of the shaft was first mounted on a vee block, which in turn was mounted on the macrotome swing arm attachment. Weights were added to the end of the swing arm, causing the specimen to be elevated toward the rotary blade cutting edge. The blade was rotated at about 1200 r.p.m. Ringer's solution was used as a coolant and lubricant, being continuously deposited near the centre of the blade by means of a drip feed system. Centrifugal forces dispersed the fluid over the blade surface and specimen. Bone sections were obtained by advancing the blade between sequential cuts. The thickness of each section was checked with the aid of a precision indicating gauge.

After dehydration in absolute ethanol for forty-eight hours, the sections were embedded in Araldite\*\* using an abbreviated version of the method described by Luft (71). Firstly, the sections were

\*Metals Research Limited, Royston, Herts.

\*\*Ciba Limited, Basle, Switzerland.

soaked in xylene at room temperature for about one hour. Then they were soaked for a further one hour at 60°C. in a mixture of one part xylene to two parts araldite. The araldite comprised a mixture of 27 ml CY212 resin, 23 ml. HY964 hardener and 0.75 ml DY064 accelerator. Next, the sections were removed, rinsed gently in freshly prepared araldite maintained at 60°C., and placed in a shallow polythene dish containing a previously prepared semi-hardened layer of araldite, also maintained at 60°C. The freshly prepared araldite was then added to the dish so that each specimen was completely covered. The dish was placed in an oven and kept at 60°C. until the contents formed a solid block (after about forty-eight hours). This block was removed and stored at room temperature for several weeks.

When the araldite was considered to be adequately cured, the block was cut into pieces, each piece containing a complete transverse section of bone. Each one was subdivided into four quadrants by cutting with the macrotome. One cut was made from the anterior aspect to the posterior aspect, and another cut was made at right angles to the first, from the medial aspect to the lateral aspect. These cuts exposed two edges of each bone quadrant (Fig. 16). Taking care to keep the exposed bone edges intact, the quadrants were

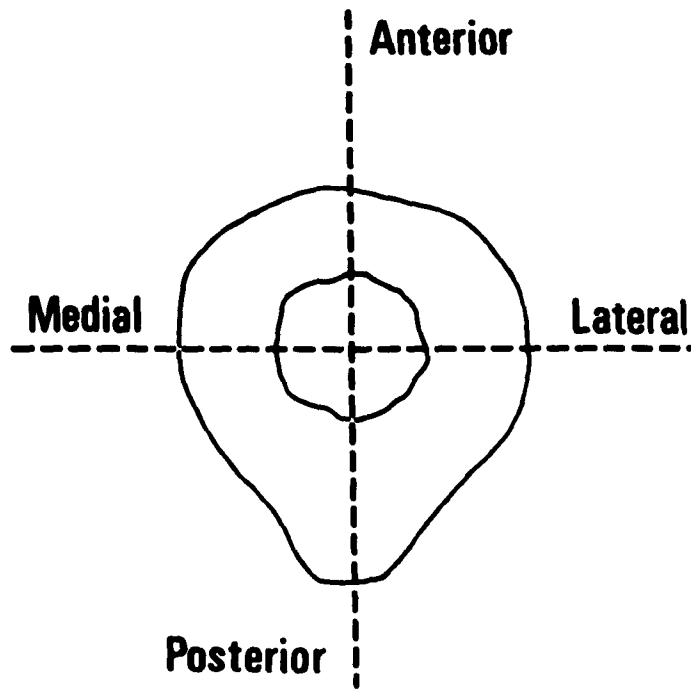


Fig. 16 Delineation of bone quadrants.

trimmed down to sizes suitable for mounting on the specimen arm of an L.K.B. Ultratome III\*. This instrument was used to cut ultrathin longitudinal bone sections from each of the exposed edges of the embedded specimens. A glass knife was employed.

Initially, a few sections about one micron thick were cut, stained with toluidene blue, and examined under an optical microscope to evaluate the effectiveness of the embedding schedule. This being deemed satisfactory, sections 500 - 700 Angstrom in thickness were cut and floated onto water. These sections were mounted on formvar coated copper grids and examined with a Phillips 201 electron microscope. Transmission electron micrographs were recorded with an electron accelerating voltage of 80 KV.

#### RESULTS : ELECTRON MICROSCOPY

Figures 17, 18 show typical transmission electron micrographs of bone sections. Visual examination showed a degree of preferred orientation of bone apatite crystals along a direction parallel to the long axis of each bone studied. The range of crystallite lengths observable varied from about 100 Angstrom to 1000 Angstrom.

\* L.K.B. Instruments Limited, 232 Addington Road, South Cr ydon, Surrey.

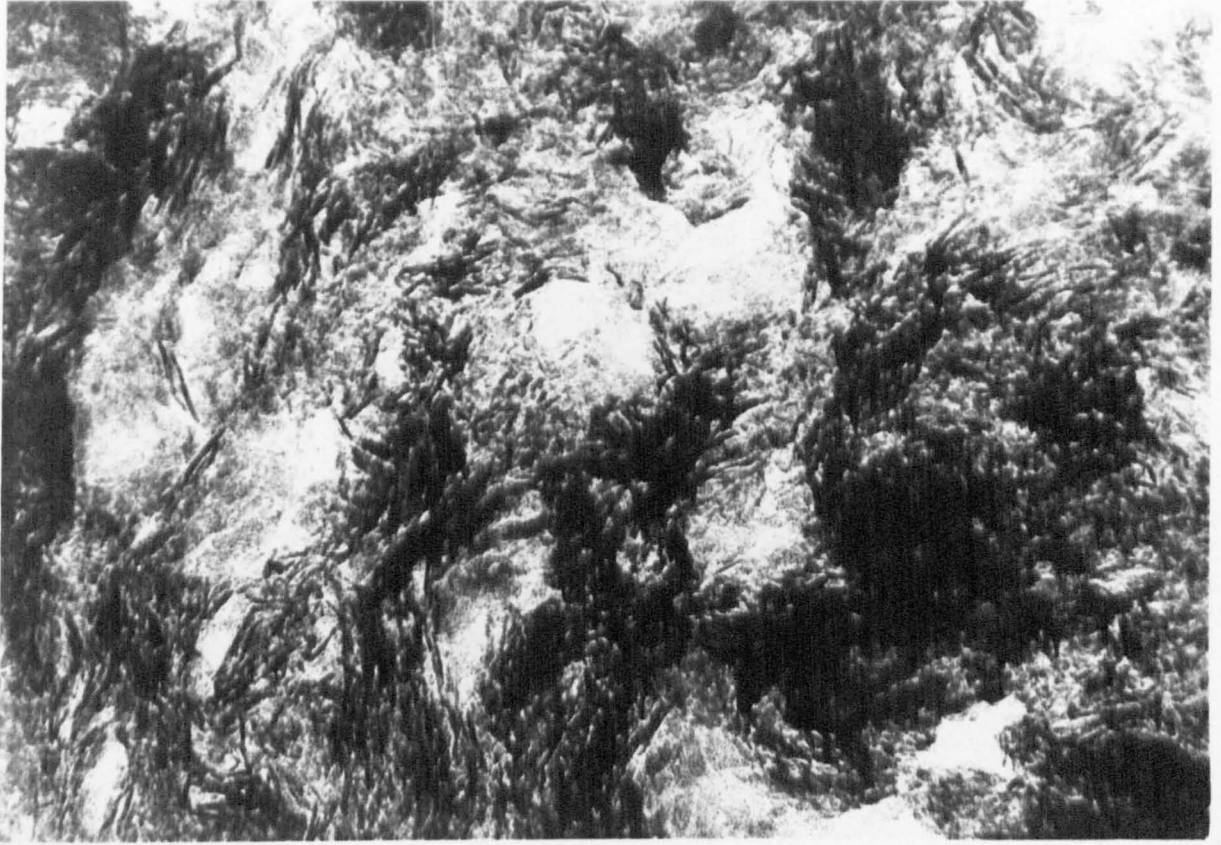


Fig. 17 Transmission electron micrograph of longitudinal bone section (approx. magnification X100,000).

TABLE I

LINE DENSITIES OF THE (111) REFLECTIONS OF BOSTON  
CERAMIC STRANDS.

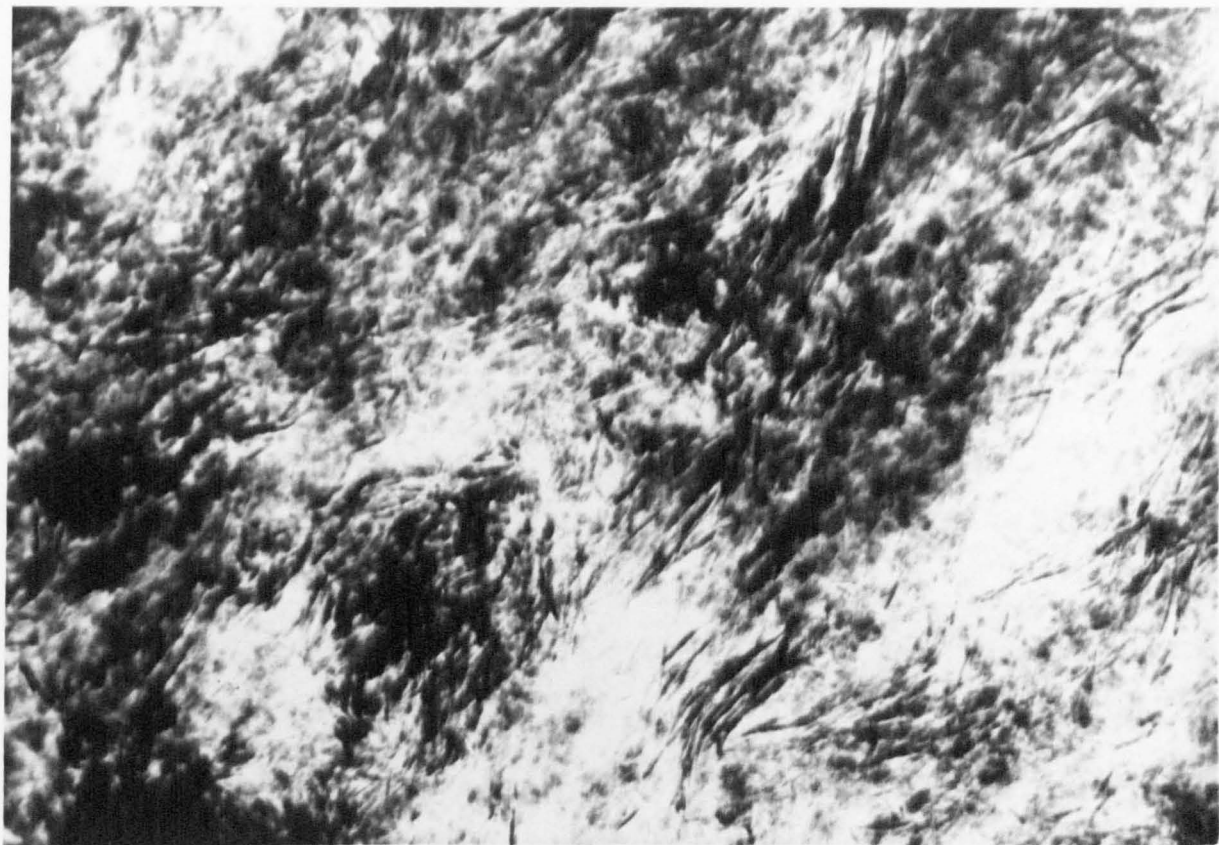


Fig. 18 Transmission electron micrograph of longitudinal  
bone section (approx. magnification X 200,000).

TABLE 5

LINE BREADTH OF THE (111) REFLECTION OF SODIUM  
CHLORIDE STANDARDS.

Sample	$\delta(2\theta)$ degrees	$b_{0\frac{1}{2}}$ degrees	$b_{\frac{1}{2}}$ degrees
1	0.0691	0.137	
2	0.0692	0.125	
3	0.0691	0.131	
4	0.0692	0.131	
5	0.0692	0.131	
6	0.0692	0.131	
7	0.0692	0.137	
8	0.0692	0.131	
Mean value	0.0692	0.132	<u>0.084</u>

TABLE 6

THE RELATION BETWEEN OBSERVED BREADTH  $B_{0\frac{1}{2}}$ ,  $K\alpha$  CORRECTED BREADTH  $B_{\frac{1}{2}}$ , AND PURE BREADTH  $\beta_{\frac{1}{2}}$  OF BONE APATITE (002) DIFFRACTION LINES.

Sample	Age (Years)	Sex	$K\alpha$ Separation degrees	$B_{0\frac{1}{2}}$ degrees	$B_{\frac{1}{2}}$ degrees	$\beta_{\frac{1}{2}}$ degrees	$D_{hkl}$ Angstrom
Y1	3½	F	0.0652	0.356	0.342	0.318	257
Y2	11	M	0.0652	0.356	0.342	0.318	257
N1	55	M	0.0652	0.381	0.368	0.346	236
N2	29	M	0.0652	0.344	0.327	0.301	271
N3	19	F	0.0653	0.356	0.342	0.318	257
N4	63	M	0.0652	0.375	0.362	0.340	240
N5	49	F	0.0652	0.350	0.333	0.310	263
RU 67	58	F	0.0652	0.325	0.307	0.281	290
RU 69	50	M	0.0653	0.331	0.313	0.286	285
RU 70	55	F	0.0651	0.344	0.327	0.301	271
RU 71	59	M	0.0652	0.356	0.342	0.318	257
RU 72	54	M	0.0652	0.381	0.368	0.346	236
RU 73	44	F	0.0653	0.363	0.348	0.325	251
RU 74	87	F	0.0652	0.344	0.327	0.301	271
RU 75	62	M	0.0652	0.381	0.368	0.346	236
RU 76	48	M	0.0652	0.350	0.333	0.310	263
RU 77	81	M	0.0651	0.363	0.348	0.325	251
RU 78	72	M	0.0653	0.338	0.321	0.295	277
RU 79	59	F	0.0652	0.338	0.321	0.295	276
RU 80	71	M	0.0652	0.350	0.333	0.310	263
RU 81	68	F	0.0650	0.313	0.294	0.265	308
RU 82	38	F	0.0652	0.350	0.333	0.310	263
RU 83	58	F	0.0652	0.369	0.354	0.331	246
RU 84	75	F	0.0652	0.338	0.321	0.295	277
RU 85	28	M	0.0654	0.391	0.377	0.357	230
RU 86	84	F	0.0652	0.353	0.335	0.312	261
RU 87	59	M	0.0653	0.350	0.333	0.310	263
RU 88	71	F	0.0652	0.356	0.342	0.318	257
RU 89	59	F	0.0652	0.369	0.354	0.331	246

CHAPTER 4

EVALUATION OF PREFERRED ORIENTATION OF APATITE  
CRYSTALLITES IN COMPACT BONE BY X-RAY DIFFRACTION

## INTRODUCTION

Several groups of researchers have provided information concerning the possible relation between degree of preferred orientation of bone apatite crystallites and age (33, 35, 39, 56, 72). Others have demonstrated preferred orientation parallel to adjacent bundles of collagen fibres (23, 54, 55). These studies indicate that a marked degree of preferred orientation is attained in human compact bone after, at most, a few years of age, although there is almost random orientation of apatite crystallites in foetal or very young calcified tissue. However, a literature search has failed to reveal any systematic study of crystallite orientation and its relation to age and mechanical properties of bone tissue.

## THEORETICAL CONSIDERATIONS

It has been explained in Chapter 2 that with a monochromatic x-ray beam, "the orientation of a crystal with respect to the direction of the incident beam decides which sets of atomic planes (hkl) produce diffraction maxima." Moreover, the disposition of the crystal in a plane normal to the incident beam determines the directions in which the maxima are diffracted. If we define the "inclination  $\theta$ ", and "disposition  $\psi$ " of a set of planes in the manner illustrated in fig. 19, then these two angles will completely describe the orientation of the planes with respect to the mutually perpendicular x, y, z axes. The angle  $\psi$  is termed the "azimuthal" angle.

Now, to obtain Bragg reflection, the inclination  $\theta$  of a set of planes (hkl) must be equal to their Bragg angle  $\theta_{hkl}$ . However, Bragg reflection can occur at ANY azimuthal angle. The possible orientations of (hkl) planes capable of producing Bragg reflection are illustrated schematically in fig. 20a. They form the planes lying tangentially to the curved surface of a cone with solid angle  $\pi \cdot \sin^2 \theta_{hkl}$  steradians. The corresponding directions of Bragg reflection lie along the inclined surface of a larger

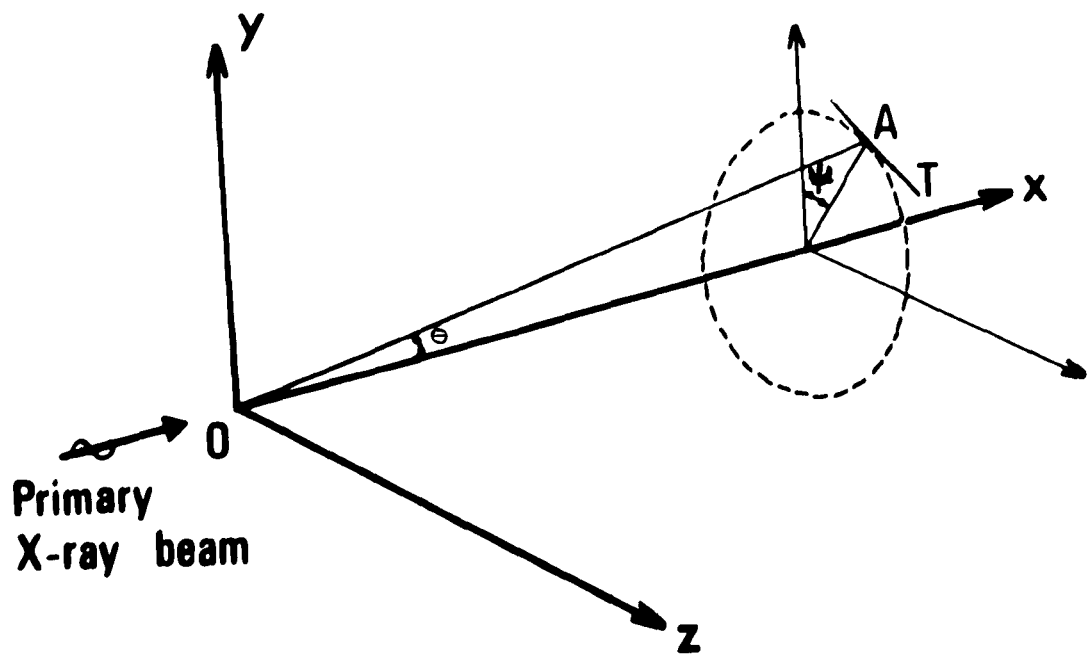
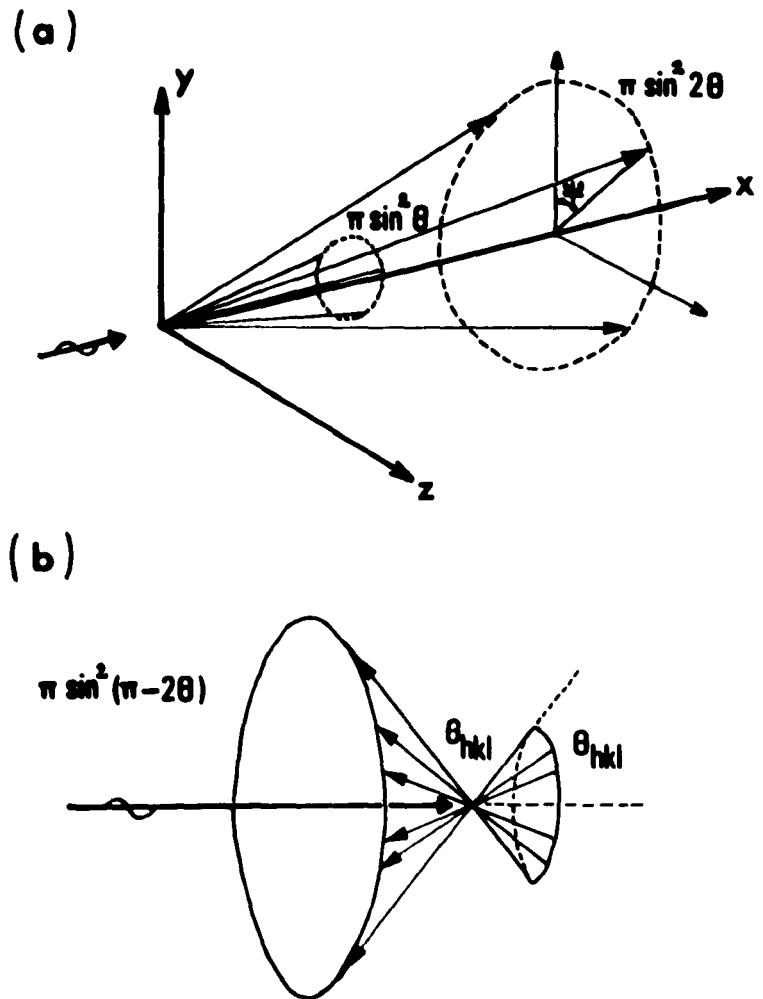


Fig. 19 Definition of orientation of a plane by its inclination  $\theta$  and disposition  $\psi$ .

cone of solid angle  $\pi \cdot \sin^2(2\theta_{hkl})$  steradians. Similar cones are described by Bragg reflections at differing azimuthal angles from each set of planes (hkl). At planes for which  $\theta_{hkl} > \pi/4$  radians, "back-reflection" occurs and a cone of solid angle  $\pi \cdot \sin^2(\pi - 2\theta_{hkl})$  steradians is delineated (Fig. 20b).

A flat plate camera (Fig. 21) can be employed to photographically record the patterns of both forward and back reflections. The camera incorporates a specimen holder fixed midway between two film cassettes, each placed normal to the direction of the primary x-ray beam. A pinhole collimator is located in the centre of the back reflection cassette, and a beam trap is situated in the centre of the forward reflection cassette. The beam trap, which is colinear with the collimator, absorbs any portion of the incident beam that is transmitted through the sample without angular deviation. Films placed in the forward and back reflection cassettes record intensity maxima diffracted in the approximate angular ranges five to sixty degrees and one hundred and twenty to one hundred and seventy-five degrees, respectively.

When forward patterns are to be recorded, the specimen must be sufficiently thick to contain



**Fig. 20** Orientations of (hkl) planes capable of producing Bragg reflection:  
 (a) Forward reflection  
 (b) Back reflection

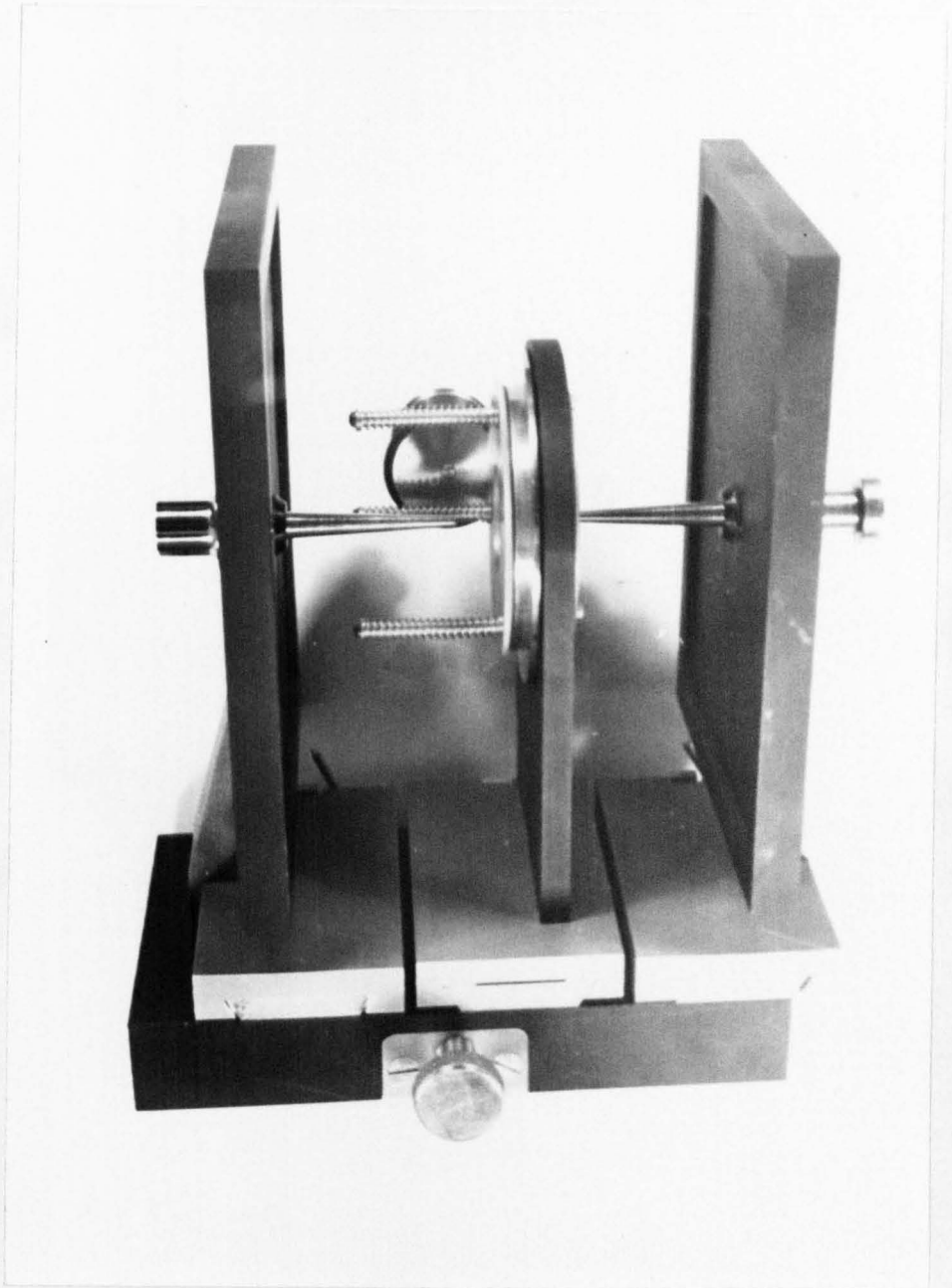


Fig. 21 Flat plate camera with spring-loaded specimen holder.

large numbers of reflecting planes, but not so thick that it prevents transmission of the diffracted x-rays. A thicker specimen is employed when recording back reflections in order to maximise the intensity of reflection.

Diffraction patterns produced by a specimen containing large numbers of randomly orientated crystallites (as in a powder sample) consist of concentric circles, each circle corresponding to reflection from a set of planes (hkl) and being of uniform intensity around its circumference. The intensity is related to the number of (hkl) planes inclined to the incident beam at their Bragg angle  $\theta_{hkl}$ . Thus, if a polycrystalline specimen possessing preferred crystallite orientation, or "texture", is inclined such that the angle between the primary x-ray beam and the texture direction is close to a Bragg angle  $\theta_{hkl}$ , then the (hkl) reflection in the diffraction pattern will be observed at an enhanced intensity. Furthermore, if the planes (hkl) are preferentially disposed AROUND the beam direction (i.e. with respect to the azimuthal angle), then the (hkl) diffraction ring will display varying intensity around its circumference. Therefore, investigation of the intensity of Bragg reflection

occurring when a monochromatic x-ray beam is incident on a sample at selected angles, allows the orientation of crystallites within the sample to be evaluated.

#### METHOD OF SAMPLE PREPARATION

A portion about one half inch in length was removed from close to the proximal end of the shaft of each of twenty-nine femora, as described in Chapter 1. From one of these pieces, a number of sections of compact bone varying in thickness from 50 micron to 1,000 micron were cut along each of three planes: (a) transverse to the long axis of the shaft, (b) parallel to the long axis and inclined radially, (c) parallel to the long axis and inclined tangentially, (Fig. 22). The sections were cut with the rotary blade macrotome, different thickness being obtained by varying the advance of the saw blade between consecutive cuts. Thickness was measured with a precision indicating gauge and noted. Sections were then transferred into separate containers and about 10 ml of absolute ethanol was added to each. After dehydration for at least forty-eight hours, each section was removed and positioned over a circular aperture punched in a small piece of thin card. It was then attached to

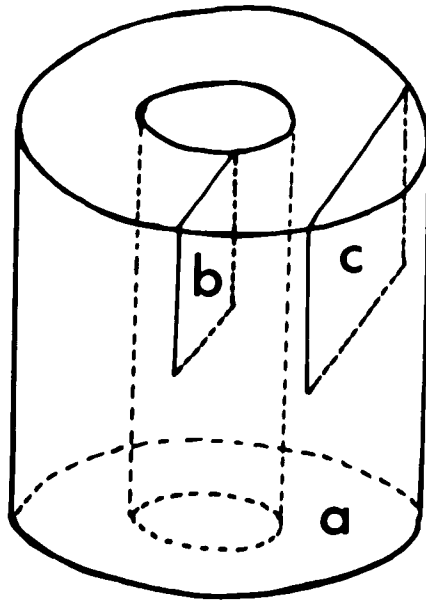


**Fig. 22** Delineation of sections for flat plate x-ray diffraction studies.

the card with adhesive tape (Fig. 23), care being taken to ensure that the tape only covered the section periphery. The section details were marked on the card.

After determination of the specimen thickness required for optimum intensity and contrast of the recorded diffraction pattern, longitudinal sections about 120 micron thick were cut from each of the remaining femoral specimens. These were mounted and labelled in the manner described above.

#### METHOD OF RECORDING X-RAY DIFFRACTION PATTERNS

Forward diffraction patterns were recorded with the aid of an A.E.I.\* flat plate camera and Raymax 60 X-ray generator. The cathode of the x-ray tube was adjusted to produce an electron focal spot approximately 1 mm by 10 mm in size on a polished copper target (anode). The camera mount was angled at six degrees to the plane of the anode, so that the x-ray image of the focal spot viewed along the camera axis was about 1 mm square (Fig. 24). A pinhole collimator 1 mm in diameter was employed.

The x-ray tube was evacuated to a pressure of  $10^{-6}$  torr and set at 40 KV electron accelerating

\*A.E.I. Scientific Apparatus Division, Urmston, Manchester.

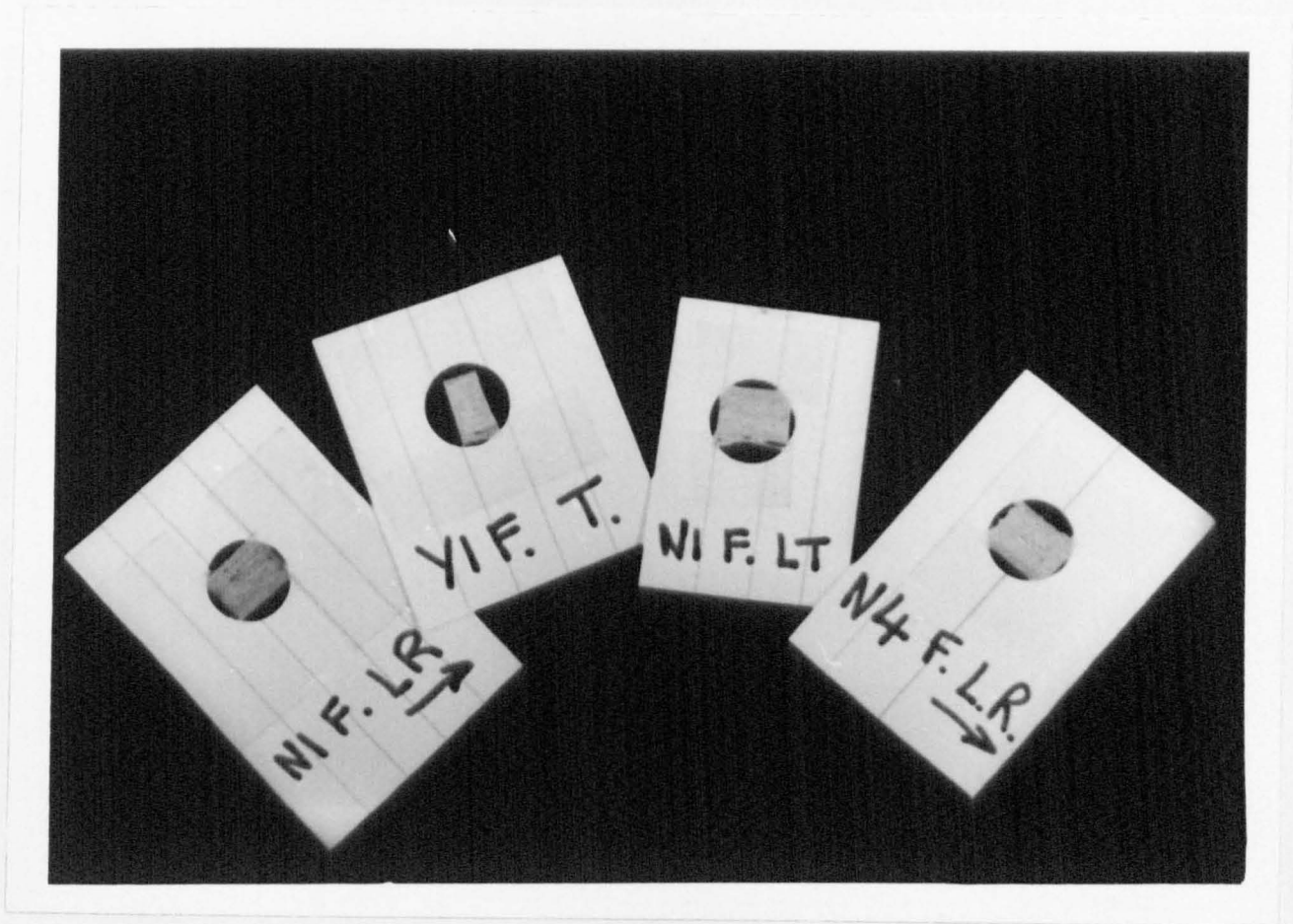


Fig. 23 Mounted flat plate specimens.

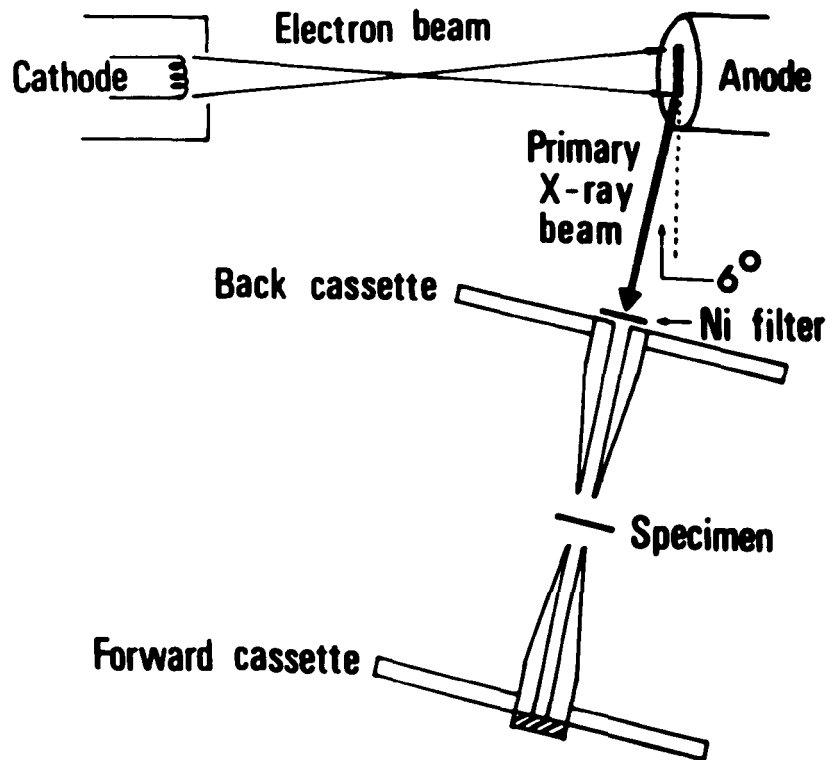


Fig. 24 Experimental arrangement for flat plate x-ray diffraction studies.

voltage and 20 mA tube current. X-rays produced by the copper target were filtered with a 13 micron thick nickel foil.

Firstly, the effect of specimen thickness on the diffraction pattern was investigated by recording patterns of samples ranging in thickness from 50 to 1,000 micron. Each specimen was located in turn on a spring-loaded holder fixed on the flat plate camera (Fig. 21). The holder gripped the specimen midway between, and parallel to, the flat plate film cassettes. These cassettes were designed to contain sheets of film four inches wide and five inches high, and they were positioned 8 cm apart. Before each exposure, the forward reflection cassette was loaded with Ilford Industrial G\* x-ray film, through the centre of which a hole had been punched to enable the film to be located around the beam trap fixture. The camera was then positioned with the collimator adjacent to the lead shutter of the x-ray tube window. Exposure commenced when the exposure timer was switched on and the lead shutter was opened by operation of the shutter switch. As a result of preliminary investigations, the timer was set at four hours for each exposure. After completion of the exposure the film

\*Ilford Limited, Ilford, Essex.

was removed and processed and the cassette was reloaded.

Developed films were visually examined. Diffraction patterns of specimens with thickness in the range 80 - 150 micron were observed to possess the optimum intensity and contrast. Thinner specimens produced insufficient reflection, while thicker specimens produced no forward diffraction pattern due to total absorption of forward reflected x-rays. On the basis of these results, a specimen thickness of about 120 micron was selected for further studies.

Next, the spring-loaded specimen holder was replaced by a goniometer specimen holder (Fig. 25). This was used to hold specimens at varying inclination to the incident x-ray beam. In this manner, forward diffraction patterns of transverse and longitudinal sections of one femoral sample were recorded at inclinations ranging from ninety degrees to forty-five degrees.

The distribution of intensity around the (002) ring in each diffraction pattern was studied in detail with the aid of a Barr and Stroud GN4\* spot densitometer. A circular stage with angular graduations around a central pivot, was constructed of cardboard. The

\* Barr and Stroud Limited, Anniesland, Glasgow.

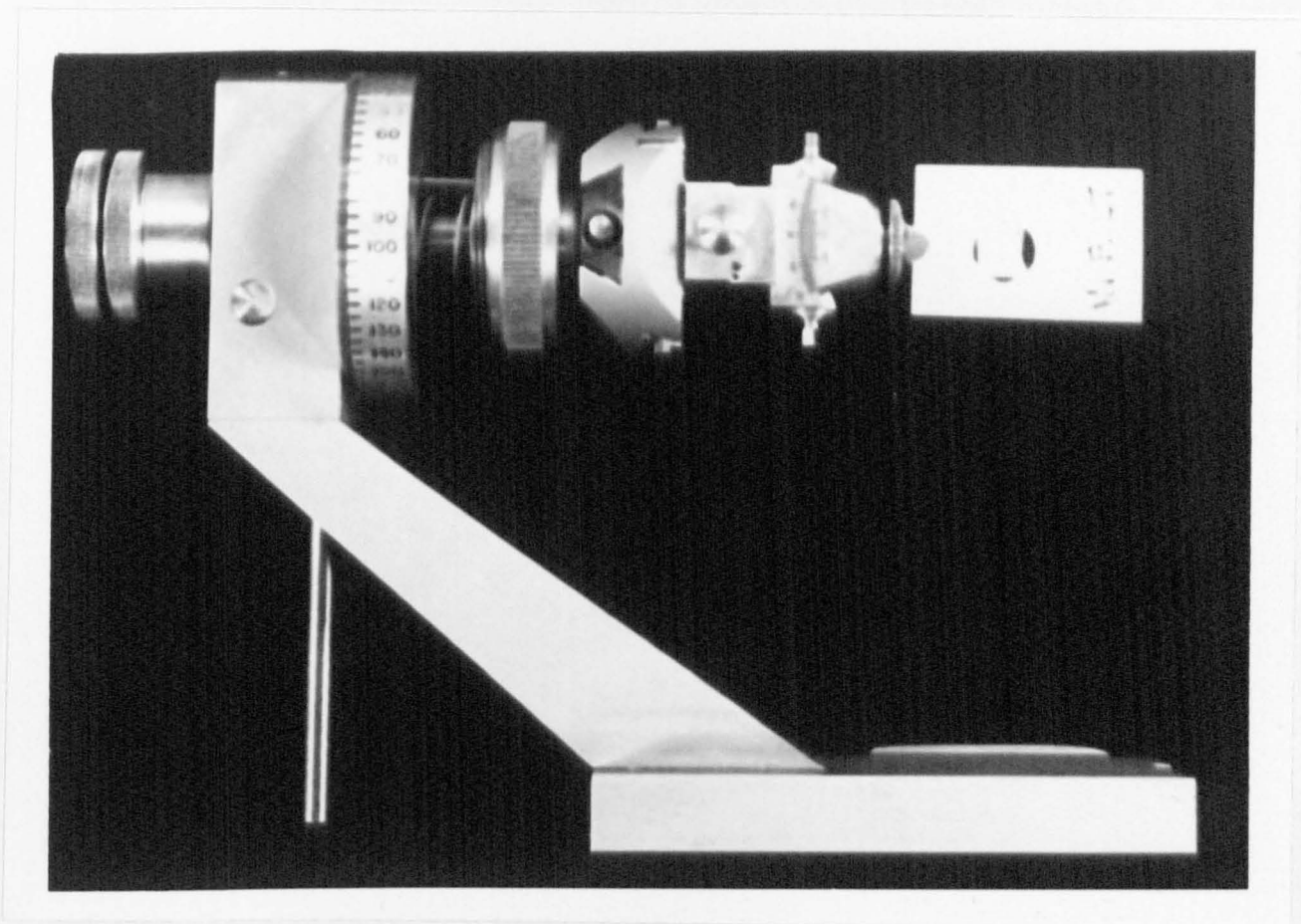


Fig. 25 Flat plate camera goniometer specimen holder.

pivot had the same diameter as the beam trap fixture of the flat plate camera. Thus, each processed film was in turn placed over the pivot and rotated around it so that optical transmission by different parts of the film was measured. The light spot diameter was set at 0.075 inches and percentage transmission around the circumference of the (002) diffraction ring and at points in the background region adjacent to the (002) ring, was determined at angular increments of 22.5 degrees. The angular positions of regions of the (002) ring giving maximum and minimum transmission were noted. Then, the ratio of the corresponding photographic density due to (002) reflection was deduced by correcting for background exposure as shown in Appendix 4.

Finally, the forward diffraction pattern of each radially cut longitudinal section was recorded with the x-ray beam incident at right angles to the specimen plane. These diffraction patterns were analysed in the manner described above, yielding the ratio of maximum to minimum photographic density due to (002) reflection.

## RESULTS

The (002) ring in the diffraction pattern of sections cut in a transverse plane was of uniform intensity around its circumference (Fig. 26). This was indicative of a random DISPOSITION of apatite (002) planes around the long axis of the bone shaft. However, longitudinally cut sections produced (002) reflection rings which displayed evidence of preferred INCLINATION of (002) planes (Fig. 27), normal to the long axis of the bone.

The ratio of maximum to minimum (002) reflected intensity of longitudinal sections cut from the same bone was considered in relation to the angle of inclination to the x-ray beam. Figure 28 shows the variation of observed degree of preferred orientation. This ranged from zero (ratio of photographic density  $D_{\max}/D_{\min} = 1$ ) when the beam was incident normally on a transverse section, to a maximum value when the beam was incident normally on a longitudinal section. These results confirm the findings indicated by figures 26, 27. Transverse and longitudinal sections inclined at forty-five degrees presented the long axis of the bone shaft at the same inclination to the x-ray beam and therefore produced similar diffraction patterns.

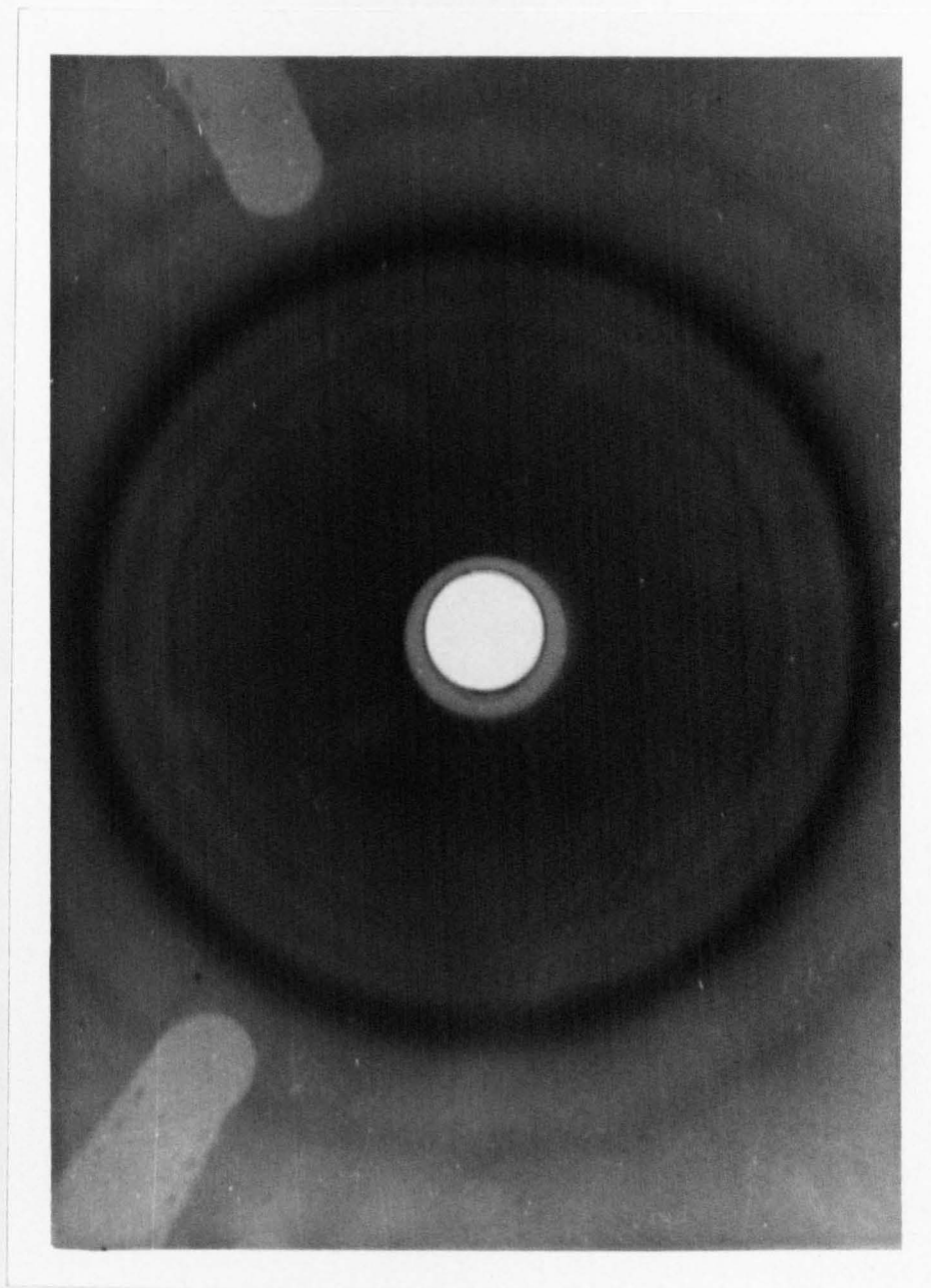


Fig. 26 Flat plate forward diffraction pattern of transverse bone section.

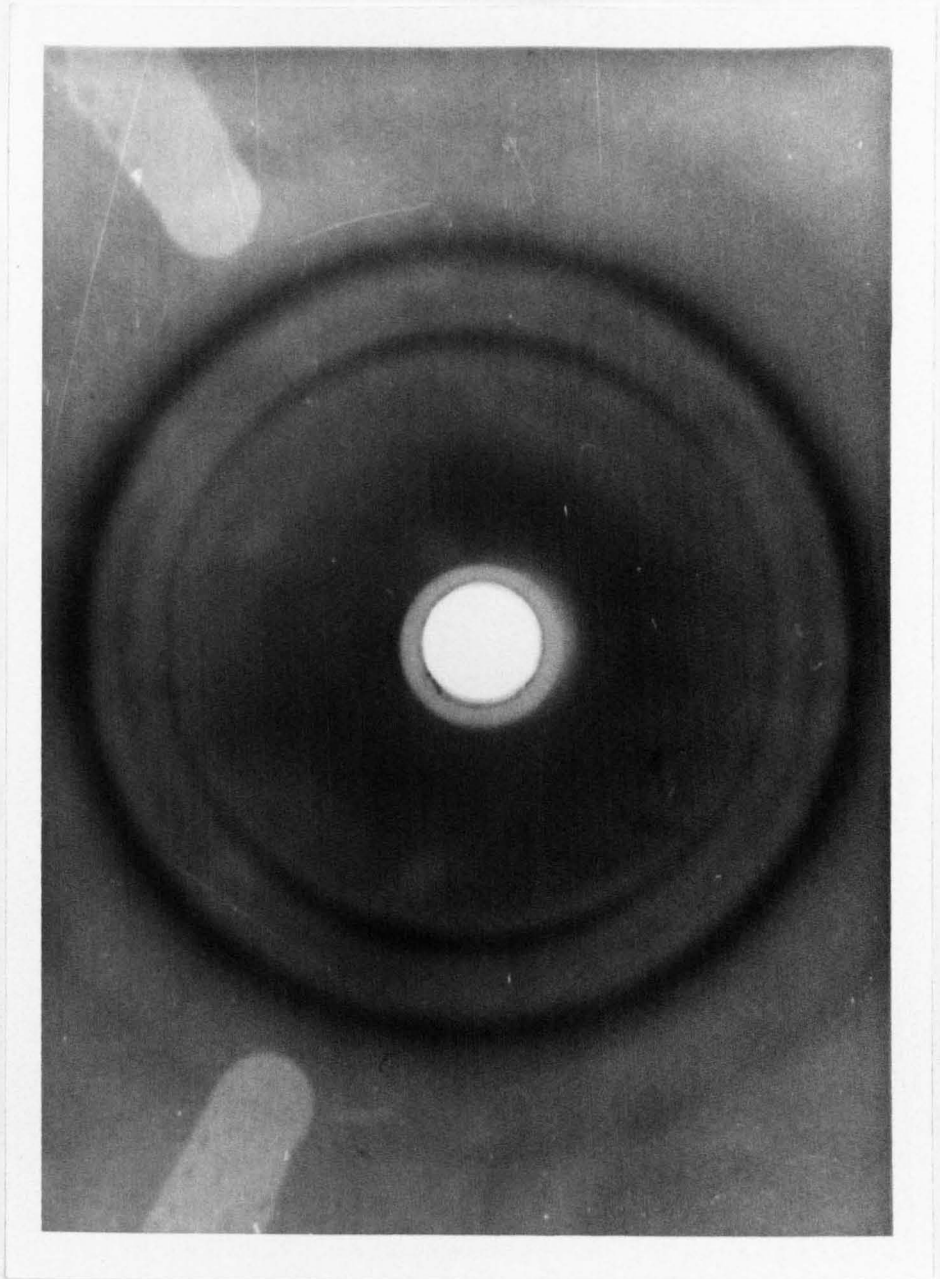


Fig. 27 Flat plate forward diffraction pattern of longitudinal bone section.

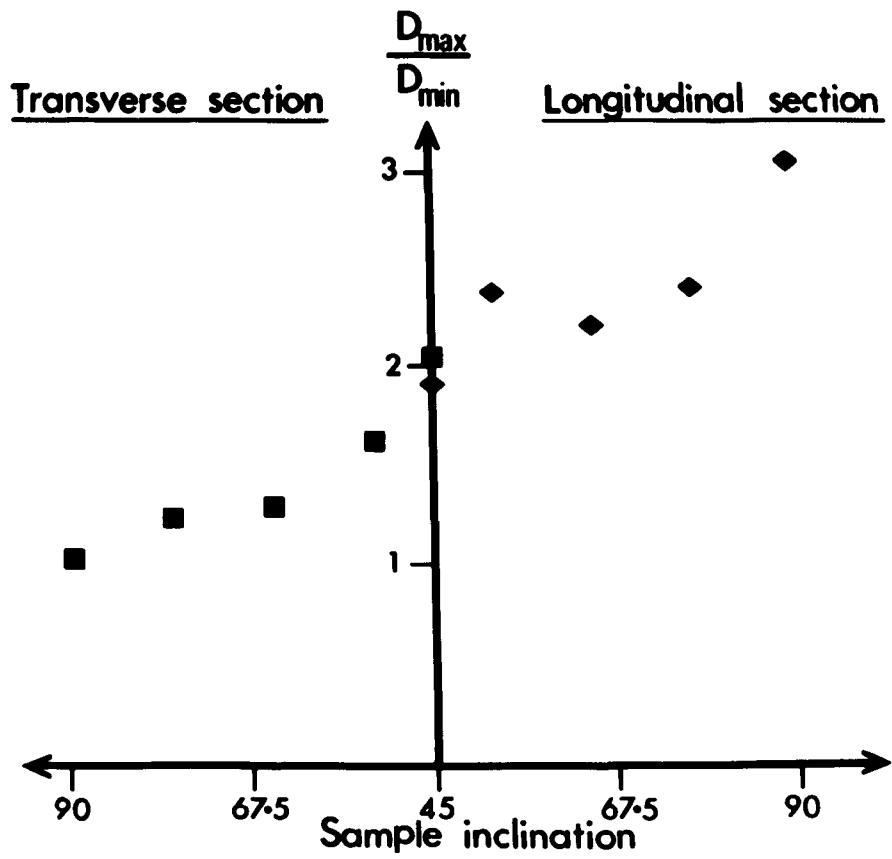


Fig. 28 Observed degree of preferred orientation versus specimen angle of inclination.

For several bones, preferred orientation observed for radially cut and tangentially cut longitudinal sections inclined at ninety degrees, was compared using Wilcoxon's statistical test and no significant difference was found.

The relation between the ratio  $D_{\max}/D_{\min}$  and age was investigated for radially cut longitudinal specimens. No significant correlation was observed. Values of  $D_{\max}/D_{\min}$  are listed in Table 7. The mean value was  $3.80 \pm 0.50$  (2 x S.E. of the mean).

TABLE 7

RATIO OF MAXIMUM TO MINIMUM PHOTOGRAPHIC DENSITY  
OF BONE APATITE (002) REFLECTION RECORDED BY A FLAT  
PLATE CAMERA.

SAMPLE	$D_{\max}/D_{\min}$
Y1	2.48
Y2	2.70
N1	3.88
N2	2.06
N3	7.74
N4	2.99
N5	5.57
RU 67	2.93
RU 69	2.97
RU 70	2.11
RU 71	2.10
RU 72	4.89
RU 73	4.69
RU 74	3.90
RU 75	4.89
RU 76	3.77
RU 77	4.91
RU 78	5.10
RU 79	3.47
RU 80	4.69
RU 81	3.59
RU 82	2.21
RU 83	2.61
RU 84	3.07
RU 85	4.88
RU 86	2.51
RU 87	3.70
RU 88	5.87
RU 89	3.83

CHAPTER 5

MECHANICAL TESTING OF BONE :  
THE STATE OF THE ART.

## INTRODUCTION

Structural materials are said to "fail" or "yield" when they lose their functional properties. This generally corresponds with the onset of inelastic deformation which may be due to plastic flow or fracture. A number of theories explaining the failure of various isotropic materials have been propounded. The most important are: (a) maximum principal stress theory, (b) maximum shearing stress theory, (c) maximum strain theory (d) total energy theory, (e) energy of distortion theory, (f) octahedral stress theory. Each theory attributes mechanical failure to the attainment of a "yield criterion" or critical value of one particular mechanical parameter. If this same critical value is always reached at failure regardless of the mode of application of the external forces producing failure, then the theory is considered to be valid for the material in question. Thus, the object of testing a sample of an isotropic structural material is to determine this parameter.

The situation is more complicated for materials which are anisotropic: their mechanical properties vary depending on the direction in which they are measured. Now, mechanical properties can be summarised

as, (i) elastic, (ii) rheologic, and (iii) strength. In anisotropic fibrous materials such as compact bone, the principal directional differences are between the "grain" direction or direction of preferred orientation of fibres, and directions transverse to this. It is invariably the case that such materials are best able to withstand stresses and strains suffered along the direction of the grain (29, 31). Any theory of yielding applicable to an anisotropic material must take these directional effects into account, and may be determined by testing a large number of specimens under uniaxial, biaxial and tri-axial stress states applied with differing orientation with respect to the grain direction. Due to the limited physical dimensions of human bones, it has proved impossible to prepare sufficient specimens to conduct such a systematic study of yielding in bone tissue. It is important, therefore, to carefully ponder the choice of an appropriate mechanical test which will yield mechanical factors relevant to the pathological fracture of whole bones.

From a consideration of the irregular geometrical configuration of most bones, it is clear that almost any externally applied force will result

in bending (or twisting which can be regarded as a three-dimensional case of bending) rather than simple compression or tension. When bending occurs, some regions of the bone suffer tensile stress and other regions suffer compressive stress. A "neutral surface" separating the two regions is under zero stress. Figure 29 shows a uniformly shaped specimen subjected to three-point bending. The shaded region is under tensile stress. Now, for a given arrangement of externally applied forces, the position of the neutral surface will depend on the relative values of Young's modulus of elasticity in tension ( $E_T$ ) and in compression ( $E_C$ ). If  $E_C$  is greater than  $E_T$  then it is likely that less bone will suffer compressive stress than suffers tensile stress. Since the region of bone under the highest strain is that farthest from the neutral surface, this strain will be tensile in nature. Moreover, as elastic modulus is defined as the quotient of stress divided by strain, then for the case where  $E_C > E_T$  the maximum tensile stress will be less than the maximum compressive stress. The opposite situation pertains when  $E_C < E_T$ .

For the reasons outlined above, experimental studies described in this thesis include both

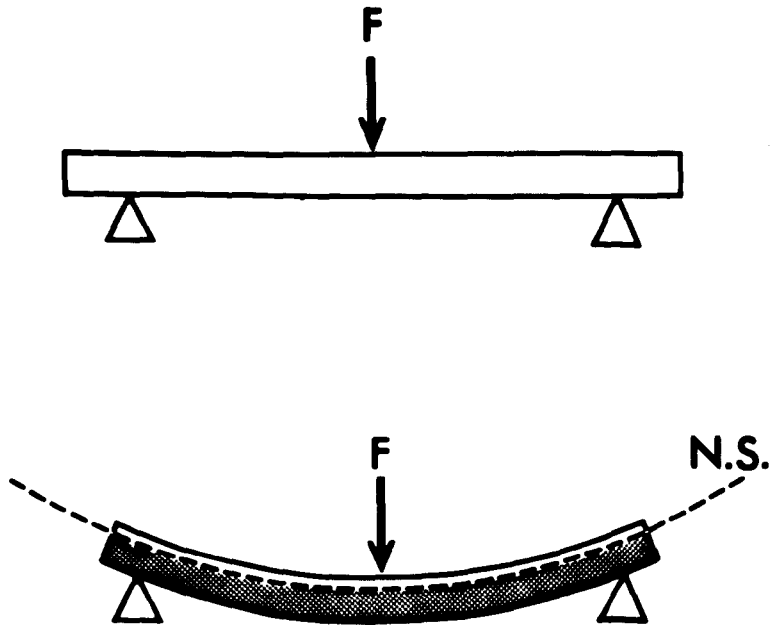


Fig. 29 Three point bending.

measurement of tensile and compressive properties of uniformly machined pieces of compact bone tissue. However, there were further complications to be considered prior to deciding the precise nature of tests to be conducted. The first problem arose from the "viscoelastic" nature of bone tissue: it responds differently to applied forces depending on their time rate of application. This phenomenon results from a variability of elastic resistance to deformation, caused by a relaxation mechanism. The stress produced by an externally induced strain is reduced by "creep" of the material at a rate characterised by a "relaxation time constant" (T). This rate may be sufficiently rapid to allow significant relaxation to occur during the time course of the mechanical test, so that a non-linear relation between stress and strain is observed. In such a situation, if the relaxation time constants of specimens are significantly different, then results obtained are not directly comparable. This difficulty can be obviated by conducting the test sufficiently rapidly to ensure that relaxation of stress during testing is small compared with the maximum stress attained.

A further complication may arise if the rate of application of force is now so rapid that the test can no longer be considered to be of a static nature. Many materials, bone included, are found to withstand highest ultimate stress when this is associated with a high strain rate. Under such circumstances, the test becomes a dynamic one and in the limiting case when the load is applied almost instantaneously constitutes an "impact test." The ultimate stress attained in dynamic or impact testing is highly dependent on strain rate and impact energy respectively. This creates difficulties in conducting tests in a repeatable fashion, and thus complicates the analysis of results. Moreover, since dynamic tests are by definition extremely short in duration, monitoring of the stress/strain relation requires high speed recording equipment. Due to these practical limitations on executing and interpreting dynamic tests, and because dynamic properties are related to static properties, it is usual to concentrate on static mechanical testing.

## BONE TISSUE : REVIEW OF PUBLISHED WORK

Mechanical properties of bone tissue have been measured and related to mineral content (28, 73, 74, 75, 76) and collagen fibre orientation (26, 27, 28, 77). However, methods of testing have differed greatly and comparison of results is difficult. Mechanical parameters most commonly measured include ultimate tensile stress (78, 79, 80, 81, 82, 83, 84, 85), ultimate tensile strain (78, 79, 80, 81), ultimate compressive stress (83, 84, 85) and Young's modulus of elasticity (78, 79, 80, 81). Some researchers have studied plastic behaviour of bone tissue (79, 82) while others have measured parameters such as the energy absorbed to failure (85, 88) and the limit of proportionality in tensile tests (78).

Usually, mechanical properties have been measured in the direction parallel to the haversian canals and therefore parallel to the grain. However, some researchers have produced evidence of anisotropic mechanical behaviour of bone tissue (77, 83, 86, 87, 88). Dempster and Liddicoat (83) measured compressive strength and compressive elastic modulus of cubes of human compact bone, along the grain and also at right angles to the grain. Values obtained in the

latter case were significantly lower than in the former case. Dempster and Coleman (86) and also Evans (87), published similar results for bone specimens tested in tension. Bonfield and Li (88) reported anisotropic behaviour of bovine bone tissue with respect to tensile and impact properties. A detailed study of directional effects in bending was undertaken by Hirsch and da Silva (77). They conducted tests of a series of uniformly machined lengths of human femoral compacta, successive specimens having been cut so that the angle between the long axis and the grain direction varied by increments of ten degrees, from zero to ninety degrees. They found that the strength of the specimen was inversely related to the magnitude of this angle.

Evans and Lebow (89) reported regional differences in mechanical properties of human compacta obtained from different parts of the femur. For example, the middle third of the shaft demonstrated the greatest ultimate tensile stress while the proximal third had the lowest value. Moreover, the lateral quadrant was stronger than the anterior quadrant.

WHOLE BONES : REVIEW OF PUBLISHED WORK

A number of researchers have reported results of tests conducted on excised whole bones. Pedersen, Evans and Lissner (90, 91) carried out "stresscoat" analysis of femora under bending, presenting evidence that in bending, fracture is initiated by tensile rather than compressive failure. Torsional and bending tests have been most commonly applied (76, 90, 91, 92, 93, 94, 95) and the mechanical parameters measured have sometimes been related to mineral content (76, 93). Burstein and Frankel (96) argue that the torsional shear stress at failure is the most useful parameter to measure. In general, however, due to difficulty in calculating the effect of varying bone geometry, testing of whole bones has yielded rather ambiguous results. Its main application lies in testing the bones of small experimental animals.

Bell, Cuthbertson and Orr (97) compared the bending and torsional strengths of bones from two groups of rats, one group having been maintained on a high calcium diet and the other on a low calcium diet. They found significantly higher values for bones from the first group. Conversely, Wolinsky, Suskin and Guggenheim (98) found that values of ultimate tensile stress, limit of elasticity and modulus of elasticity

of bones excised from rats which had been fed on a SUBSTANTIALLY fluoride-enriched diet were lower than values for bones from rats fed on a normal balanced diet.

Other groups of researchers who have utilised experimental animals in studying the effect on bone of dietary intake or metabolic state include Clarke, Bassin and Smith (99), Bell, Chambers and Dawson (100) and Weir, Bell and Chambers (101). The consequence of immobilisation was investigated by Semb (102) who immobilised, by denervation, one foreleg of each of a number of dogs. The dogs were slaughtered after varying periods of time had elapsed and the tensile strength and elastic modulus of bone tissue from the immobilised leg of each was compared with values of tissue from the opposite foreleg. No significant differences were observed. Similar studies carried out by Eichler (103) and Kazarian and von Gierke (104) yielded inconclusive results.

#### EFFECT OF STORAGE AND METHODS OF SAMPLE PREPARATION

An extensive investigation into methods of storage and preparation of mechanical test pieces was conducted by Sedlin (85). Firstly, he compared

the ultimate stress, Young's modulus, energy absorbed to failure and total deflection to failure in bending, of forty-three freshly prepared specimens of human femoral compacta, with corresponding values of thirty-one specimens which had been stored at  $-20^{\circ}\text{C}$  for about one month. Sedlin concluded that freezing at that temperature did not significantly alter their physical properties. Melick and Miller (105) reached a similar conclusion.

A contrasting situation was indicated when the effect of air-drying was investigated. Sedlin showed that as little as fifteen minutes drying in air at room temperature increased the ultimate stress attained during bending. Shorter periods of air-drying produced no significant effect. However, drying at higher temperature ( $100 - 105^{\circ}\text{C}$ ) produced even more marked changes in mechanical properties. These findings are consistent with earlier work reported by Dempster and Liddicoat (83), Dempster and Coleman (86), Evans (87), Evans and Lebow (89), Rauber (106) and Smith and Walmsley (107).

In addition, Sedlin considered the conditions under which testing was conducted. Specimens were tested by bending in Ringer's solution at temperatures of  $21^{\circ}\text{C}$  and  $37^{\circ}\text{C}$ . Ultimate stress, Young's

modulus, total deflection to failure, and energy absorbed to failure, were again measured. Total deflection and Young's modulus were both significantly different in the two cases, the former parameter being somewhat greater at the higher temperature and the latter parameter being rather lower. These results confirmed earlier findings of Smith and Walmsley (107).

**CHAPTER 6**

**TENSILE PROPERTIES OF COMPACT BONE :**  
**THEIR RELATION TO AGE AND MINERAL CONTENT**

## INTRODUCTION

Tensile testing entails inducing a uniaxial stress state in the specimen under investigation. This is achieved by locating the specimen in two suitably designed grips which are then pulled in opposite directions. Commercially available mechanical testing devices enable specimens to be stressed at either predetermined strain rate or predetermined rate of loading.

The geometrical design of tensile test pieces is governed primarily by the need to ensure that, in testing to destruction, failure does not occur at or near to the specimen grips where the specimen is weakened by their compressive effect. This possibility is eliminated by the use of a "waisted" specimen with a narrow portion in the centre, thus guaranteeing that failure occurs in this region well separated from the grips.

Since grips used for tensile tests are often liable to slip relative to the specimen during application of the load, strain is monitored most reliably by the use of strain gauges bonded directly to the specimen surface. This method was adopted in the studies described in the present chapter.

The most accurate non-destructive method of measuring the mineral content of bone tissue is the gamma ray absorption technique first described by Cameron and Sorenson (15). This procedure was used to estimate mineral content at the midpoint of each test piece prior to tensile testing.

### PREPARATION OF TENSILE TEST PIECES

Radiographs of twenty-four excised human femora were examined to enable selection of the section of the shaft from which to prepare tensile test pieces of compact bone. Portions extending approximately three inches toward the proximal extremity from about the midpoint of the shaft, were found to possess the greatest thickness of cortex.

The bones were removed from storage in the deep freezer and thawed to room temperature in a water bath. Then, a section defined as described above was removed from the shaft of each bone with a hacksaw. In a few cases, a longer piece was removed and divided into two portions of approximately equal length. The thickness of cortex was measured at different points around the circumference of the exposed ends of each of these detached portions of bone. Values were intercompared prior to deciding the optimum physical dimensions for tensile test pieces. It was desired to obtain a test piece from each of four bone quadrants (delineated as illustrated in Fig. 16) in each bone. In order to maintain consistency, it was decided that all test pieces should have the same dimensions. These were therefore governed by the size of the smaller

femora, and were chosen as described in the following paragraphs. Using a soft pencil, each femoral portion was then marked to indicate the parts from which it would be possible to remove sections of appropriate size.

The Metals Research Macrotome II was used to cut parallel sided beams about 6 cm. in length with the long axis parallel to the femoral shaft. Each femoral portion in turn was mounted on the macrotome sliding table as shown in figure 30. Elastic bands held the specimen in position while the sliding table advanced, under the action of a gravity feed, toward two rotating circular saw blades. Spacers separated the saw blades so that they produced parallel cuts 3.1 mm. apart. During cutting, the saw blades and specimen were cooled and lubricated with Ringer's solution dispensed as described in chapter 3. Cutting was terminated when the sliding table had advanced about 7 cm. The table was then returned to its starting position, the bone portion was rotated about its long axis so that another region of cortex was adjacent to the saw blades, and the cutting process was repeated. This procedure was continued until parallel longitudinal cuts had been made at all positions marked previously around the circumference

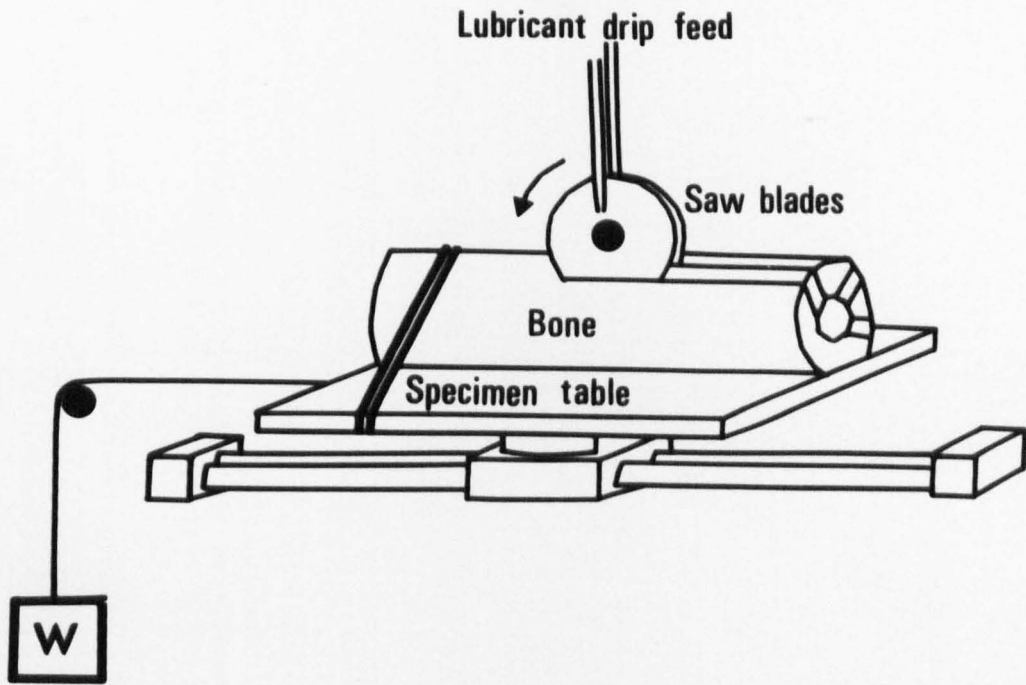
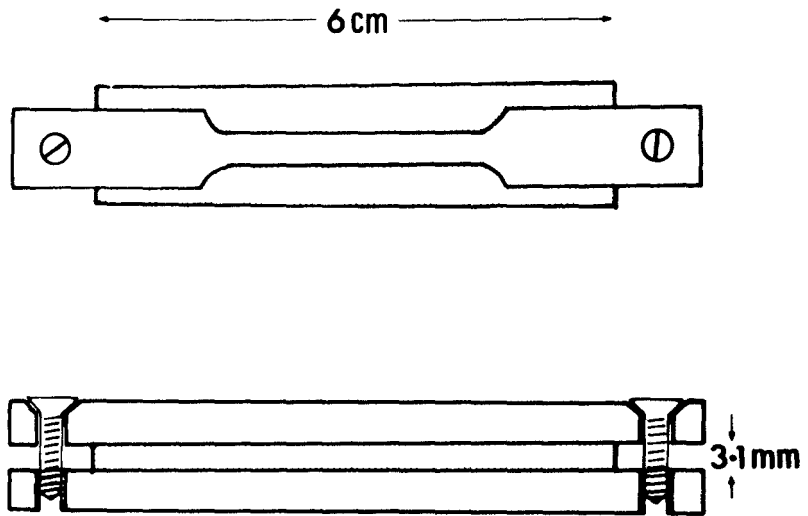


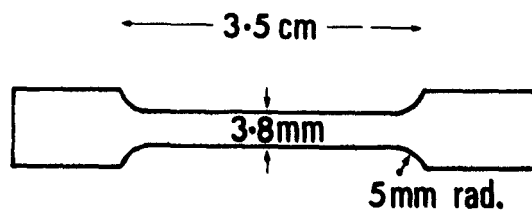
Fig. 30 Macrotome sliding table arrangement.

of the bone portion. The sample was then removed from the sliding table. The visible edge of each parallel sided piece was numbered and a note of its quadrant of origin was made. A hacksaw was used to separate these pieces from the uncut end of the bone portion, leaving them about 6 cm. in length, 3.1 mm in thickness and with width corresponding to the thickness of bone cortex.

These pieces were transformed, with the aid of hardened steel templates, into waisted tensile test pieces of approximately 3.8 mm minimum width (Fig. 31b). Firstly, each bone section in turn was placed between the two templates as shown in Fig. 31a. Screws linking the templates were tightened so that the specimen was firmly held, and the whole assembly was carefully clamped in a vice. Fine-toothed files were employed to reduce the protruding edges of bone until they were level with the edge surfaces of the templates, a small half-round file being used to shape the curved portions. The completed test piece was then released and loose grit and bone powder were removed by brushing and by rinsing in water. Next, the test piece was relabelled with a soft pencil and the precise dimensions at its midpoint were measured with a micrometer.



(a)



(b)

**Fig. 31**

- (a) Template production of tensile test piece.  
(b) Dimensions of completed test piece.

The time taken to complete the filing procedure was about three minutes. The test piece was placed, with other specimens prepared from the same bone, in a polythene bag. Care was taken to expel most of the air from the bag before it was sealed. The bag was then stored at  $-20^{\circ}\text{C}$  in a deep freezer. A total of one hundred and ten test pieces were prepared from twenty-four femora. In all cases except six, specimens were obtained from each of the four bone quadrants.

#### MEASUREMENT OF THE MINERAL CONTENT OF TENSILE TEST PIECES

Gamma ray absorption equipment described by Cameron and Sorenson (15, 17) and by other researchers (13, 14), which has been designed to measure mineral content at sites in intact human bones, is not suitable for the estimation of mineral content of small specimens. The problems are associated with the need to use a finely collimated gamma ray beam, while attaining a sufficiently high level of detection to restrict statistical errors of counting to within permissible limits.

A 'miniature' gamma densitometer (Fig. 32) was therefore constructed for the purpose of estimating the mineral content of mechanical test pieces. The

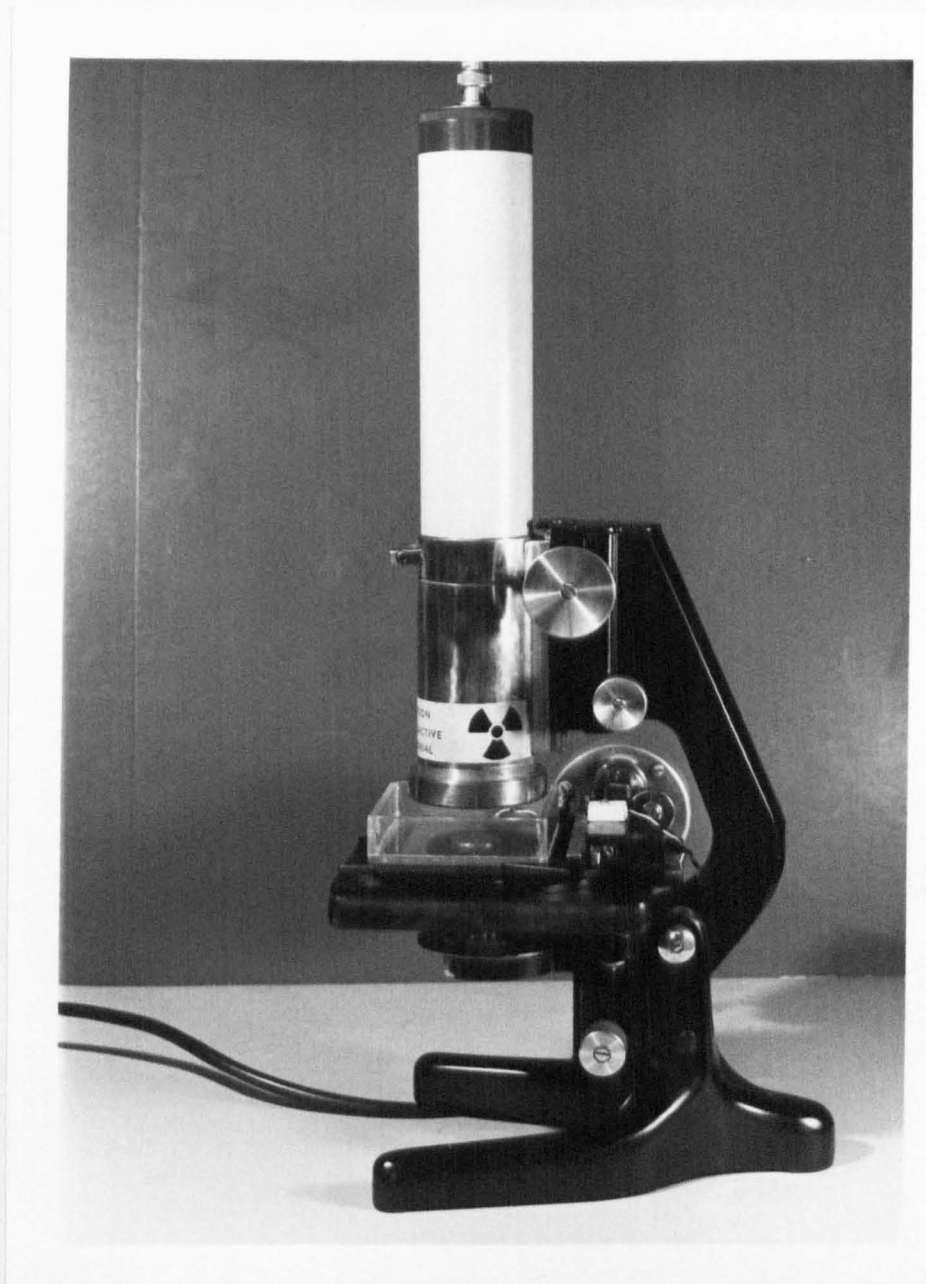


Fig. 32 Miniature gamma densitometer.

instrument was based on a discarded microscope stand equipped with an XY stage. The barrel of the microscope was replaced with a N.E.\* sodium iodide scintillation detector type DM1-1. A lead-lined holder, containing an  $I^{125}$  radioisotope source (about 25 millicurie), was mounted below the microscope stage in a position formerly occupied by the condenser lens. The top surface of the source holder was penetrated by a pinhole 1 mm. in diameter and was positioned so as to be colinear with a second pinhole collimator, 0.5 mm. in diameter, located below the sodium iodide detector. A fractional horse-power synchronous motor was linked, via a manually operated sliding pin clutch, to the X-movement of the stage. The motor was geared to drive the stage at 0.25 mm/sec. The scintillation detector was connected to an N.E. type 6900 multichannel analyser/multiscaler.

The midpoint of each tensile test piece in turn was scanned with the densitometer. Firstly, the specimen was immersed in about 1 cm. depth of water contained in a shallow trough constructed of perspex. The trough was located on the microscope stage and the specimen was positioned so that its

\*Nuclear Enterprises Limited, Sighthill, Edinburgh.

long axis lay along the Y direction. Manual adjustment of the stage ensured that the gamma ray beam was incident on the trough at a point adjacent to the midpoint of the specimen. Then, the clutch was engaged, the motor switched on, and the stage, the trough, and its contents were driven in the X direction. As the specimen traversed the gamma ray beam, sequential measurements of the intensity received by the detector during one second intervals were made with the multiscaler. After completion of the scan, the specimen was again placed in a polythene bag and stored at  $-20^{\circ}\text{C}$ .

Now, for the energy of gamma ray employed (27.3 KeV), water has attenuation properties similar to those of the organic constituents of bone tissue. Thus, any difference between transmission when the bone was interposed in the beam and transmission when only water was interposed, was related to the mineral content of the sample. The K-value parameter defined by Shimmins et al (13) was calculated from dead-time corrected transmission measurements for each sample. This value was proportional to the mineral content per unit length of specimen at its midpoint. A calibration equation (chapter 8) then yielded mineral

content in milligram per millimetre. Finally, the mineral content was divided by the specimen cross-sectional area to provide the mass of mineral per unit volume of bone ( $\text{mg}/\text{mm}^3$ ), or "degree of mineralisation."

#### ATTACHMENT OF STRAIN GAUGES TO TENSILE TEST PIECES

Specimens were thawed to room temperature in the plastic bags and then removed in order to facilitate the installation of strain gauges. Showa\* gauges type F-8 and Fb-2 proved suitable for monitoring longitudinal and lateral strain respectively. Both are polyester-backed foil gauges with resistance equal to 120 ohm. The foil dimensions were sufficiently small that the sensory portion of each gauge fitted within the geometrical limits of the specimen.

An F-8 and an Fb-2 gauge were mounted close to the midpoint and on opposite surfaces of each tensile test piece (Fig. 33). A quick-curing methacrylate cement, capable of withstanding high strain and a wide range of temperature, was employed to bond the gauges to the test pieces (Appendix 5). Installation was completed by applying, with a fine

\*Showa Measuring Instruments Limited, Tokyo, Japan.

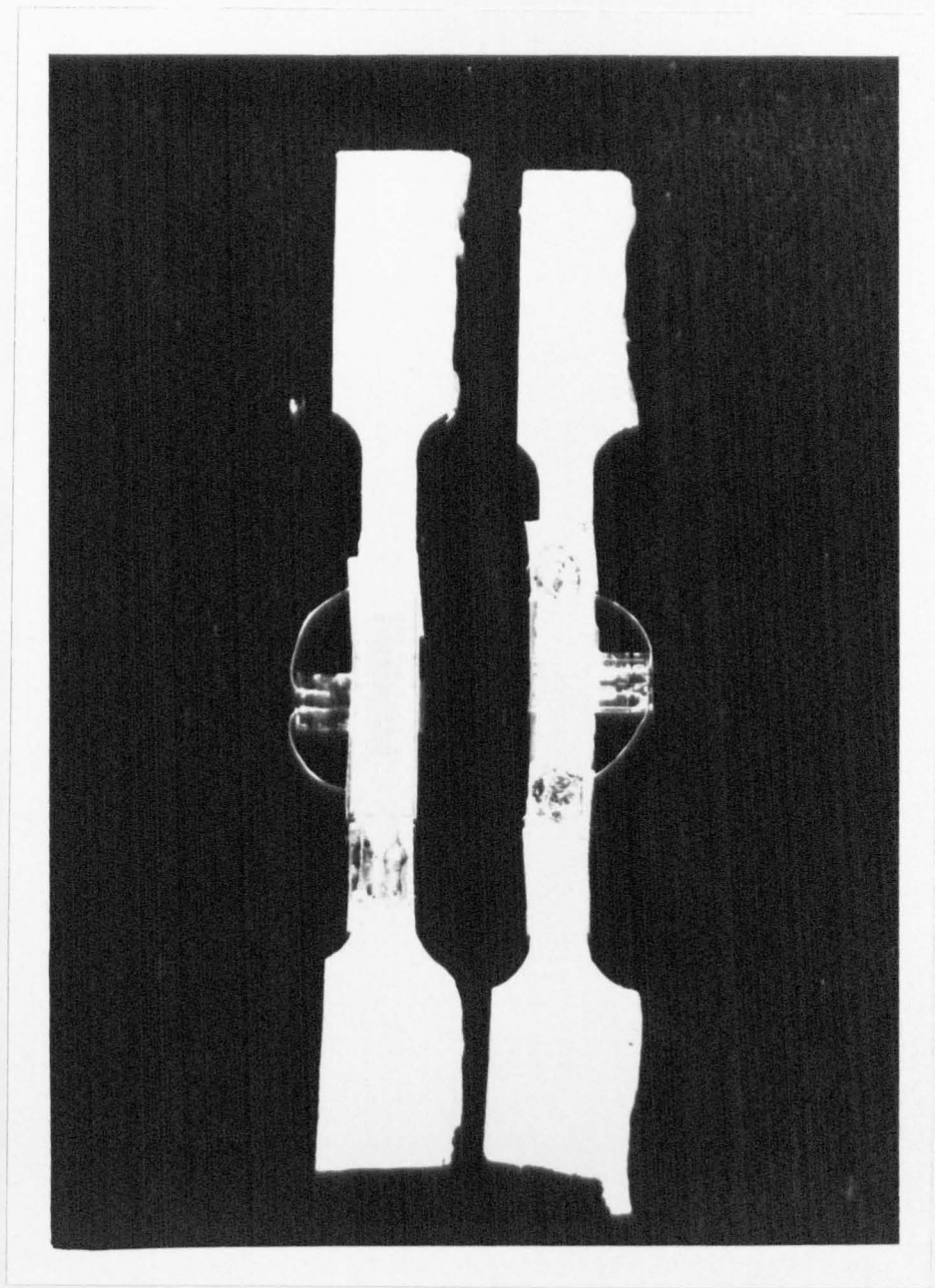


Fig. 33 Tensile test pieces with strain gauges attached.

brush, a thin coat of polyurethane. This served to protect the cement against penetration by moisture. The whole installation procedure took about five minutes. Each specimen was then maintained at 4 °C. in a refrigerator for about thirty minutes to allow the polyurethane coating to harden. It was intended that the high humidity within the refrigerator would prevent drying of the specimen WITHOUT causing damp penetration. Next, the connecting wires of each strain gauge were rapidly soldered onto adhesive terminal tags attached to the test piece at points adjacent to the gauges. Each specimen was then placed in a clean polythene bag and once again stored at -20°C until required for testing.

#### METHOD OF TENSILE TESTING

Tensile testing was carried out using an Instron\* Universal Testing Machine, model 1114. The machine comprises two vertical columns connected at top and bottom by rigid cross-heads, each of which is equipped with a mount to facilitate load cell installation. Worm gears situated adjacent to each column are used to vertically drive a mobile crosshead.

\*Instron Limited, High Wycombe, Bucks.

This may be propelled at speeds ranging from 0.5 to 500 mm/minute. In order to conduct tensile tests, a suitable load cell is mounted on the upper rigid crosshead and the test piece held by two appropriate specimen grips attached to the load cell and mobile crosshead. The mobile crosshead is then driven downward at the required speed, and the load cell output monitored by a potentiometric chart recorder which is incorporated into the Instron control console.

A pair of wedge grips was selected for the present investigation. A load cell having a dynamic range corresponding to loads up to 5,000 Kg. was employed. Using this load cell, it was possible to adjust the recorder to provide full scale deflection with loads of 100, 200, 500, 1,000, 2,000 or 5,000 Kg. A button on the Instron provided a calibration signal equivalent to that produced by the cell when a load of 1,000 Kg. was applied.

All specimens were removed from the deep freezer between one and three hours prior to testing. During this time they were sealed in the polythene bags and allowed to attain room temperature without losing moisture.

Then, each specimen in turn was extracted from its bag and flexible wire leads were rapidly soldered onto the strain gauge terminal tags. By means of these leads, each gauge was connected to the open arm of a separate Wheatstone bridge circuit (Fig. 34). These circuits had been constructed with the closed arms having resistance nominally equal to 120 ohm. Multiturn potentiometers were incorporated into the bridge arms to allow precise electrical balancing. A stabilised power supply provided a 2 volt d.c. excitation voltage to both of the bridges. The complete assembly was housed in a metal instrument box. Separate switches controlled the mains input to the stabilised supply and the excitation voltage to each bridge circuit. Terminals were provided for connection of strain gauge leads and additional terminals allowed the bridge imbalance voltages to be monitored by potentiometric chart recorders.

When both strain gauges were electrically connected, the mains input and excitation voltage were switched on. Any imbalance current was registered by recorder pen deflection. Bridge potentiometers were adjusted to give zero response when no load was applied to the specimen.

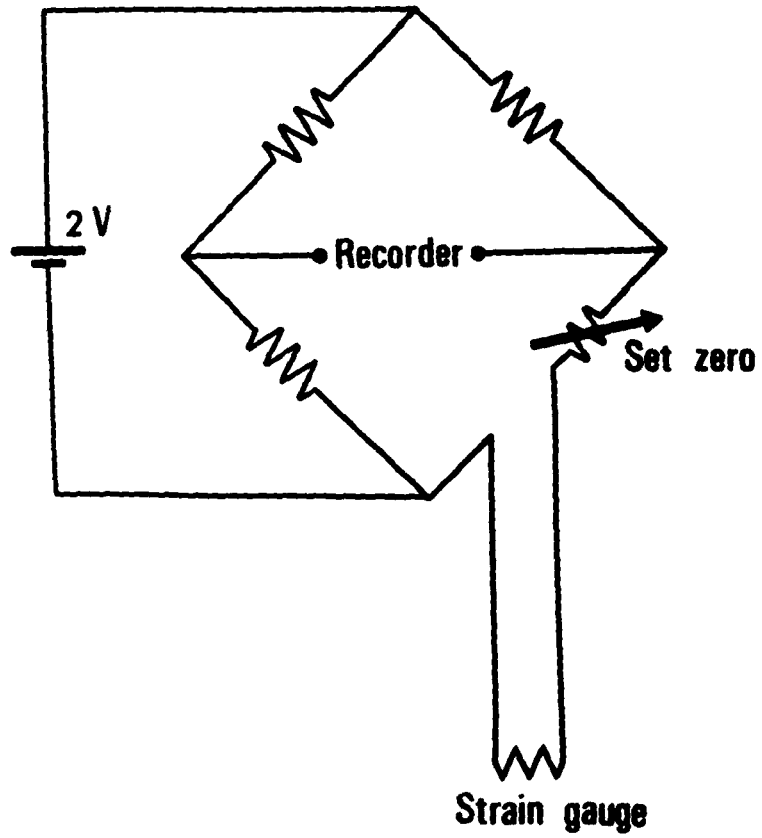


Fig. 34 Strain gauge bridge circuit.

The test piece was then mounted in the wedge grips (Fig. 35), and the Instron recorder was set to provide full scale deflection with a 100 Kg load and operated at a chart speed of 20 cm/min. Recorders monitoring longitudinal and lateral strain were respectively set for 2 mV and 0.5 mV per centimetre deflection. Both were operated at 0.2 cm/sec. chart speed.

Tests were carried out on several specimens to measure the relaxation time constant of bone tissue. The mobile crosshead was set to descend at a rate of 2 mm/minute and was stopped when the load reached about 40 Kg (corresponding to a tensile stress of about  $3.5 \text{ Kg/mm}^2$ ). Preliminary tests had indicated that this load would produce between fifty percent and seventy-five percent of the ultimate tensile stress. Applied load and specimen strain were monitored for several minutes after the crosshead had stopped. The relaxation curves obtained were investigated and relaxation time constants were determined. It became clear that relaxation of stress was not sufficiently rapid to create significant differences in the rate of increase of stress during application of the load. The distance between the points of

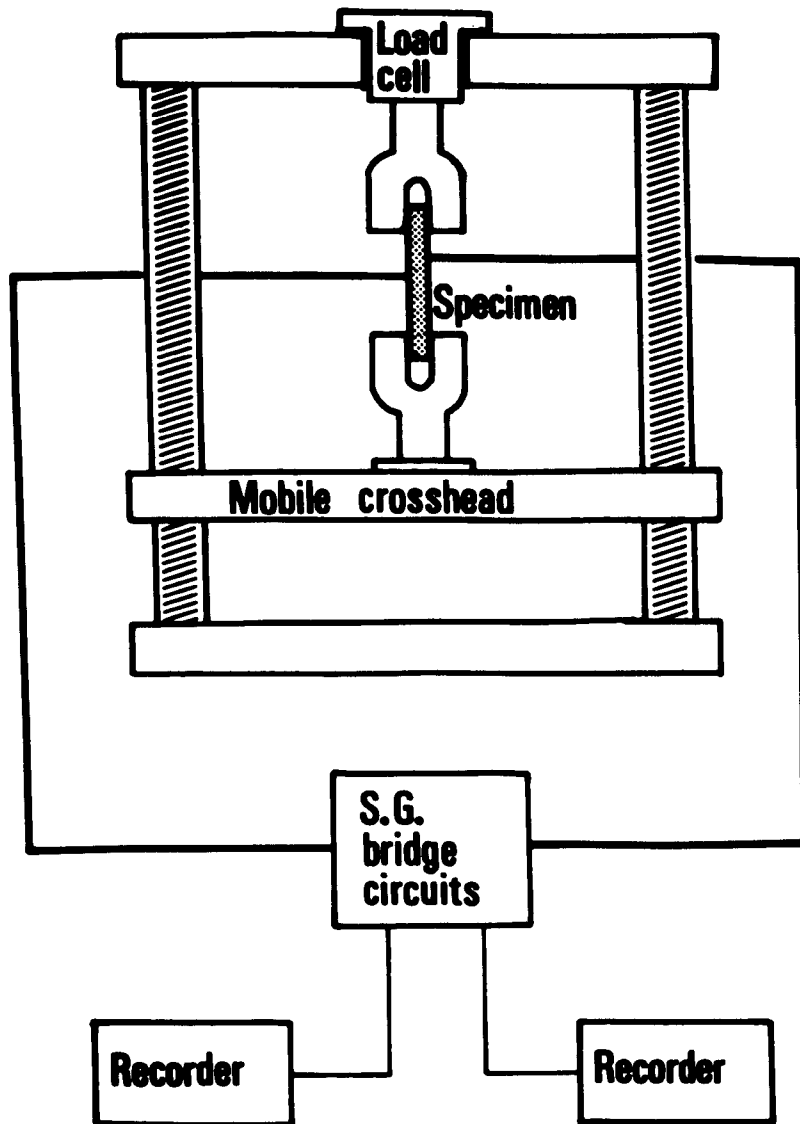


Fig. 35 Experimental arrangement of tensile testing equipment.

attachment of the grips was about 35 mm so that the crosshead speed of 2 mm/min. represented a strain rate of approximately  $10^{-3} \text{ sec}^{-1}$ .

Now, strain rate of  $10^{-3} \text{ sec}^{-1}$  is within the "static" range of testing indicated by other researchers (108). However, in order to determine the sensitivity to strain rate, a few specimens from one femur were tested to destruction using differing strain rate. Rates employed were  $10^{-4}$ ,  $10^{-3}$ ,  $2.5 \times 10^{-3}$  and  $10^{-2} \text{ sec}^{-1}$ . Values of ultimate tensile stress observed at the three slower rates were sufficiently similar to confirm the "static" nature of the test. All further studies were therefore conducted at a strain rate equal to  $10^{-3} \text{ sec}^{-1}$ . Each remaining specimen was tested to destruction in this manner.

## RESULTS AND CALCULATIONS

The rate of relaxation of stress in a visco-elastic material is generally proportional to the instantaneous stress. Thus, stress suffers an exponential decline with time, obeying an equation of the form  $\sigma_t = \sigma_0 \cdot e^{-t/T}$ . Figure 36 shows the stress relaxation curve of one of the tensile specimens. Best fitting exponential equations for such curves were calculated by the method of least squares. These equations, the corresponding correlation coefficients ( $r$ ), and the relaxation time constants ( $T$ ), are given in Table 8. The time constant is equal to the time taken for the initial stress to be reduced by the factor 0.368 ( $1/e$ ) due to relaxation. Table 9 lists observed values of ultimate tensile stress of specimens tested at differing strain rate.

Expressions relating strain suffered by a specimen, to resultant recorder deflection, were derived as detailed in appendix 6. Using these equations values of longitudinal and lateral strain were interpolated from recorder tracings at two second increments. Values of applied load at the corresponding times were similarly interpolated and divided by specimen cross-sectional area, to yield the stress. These interpolated

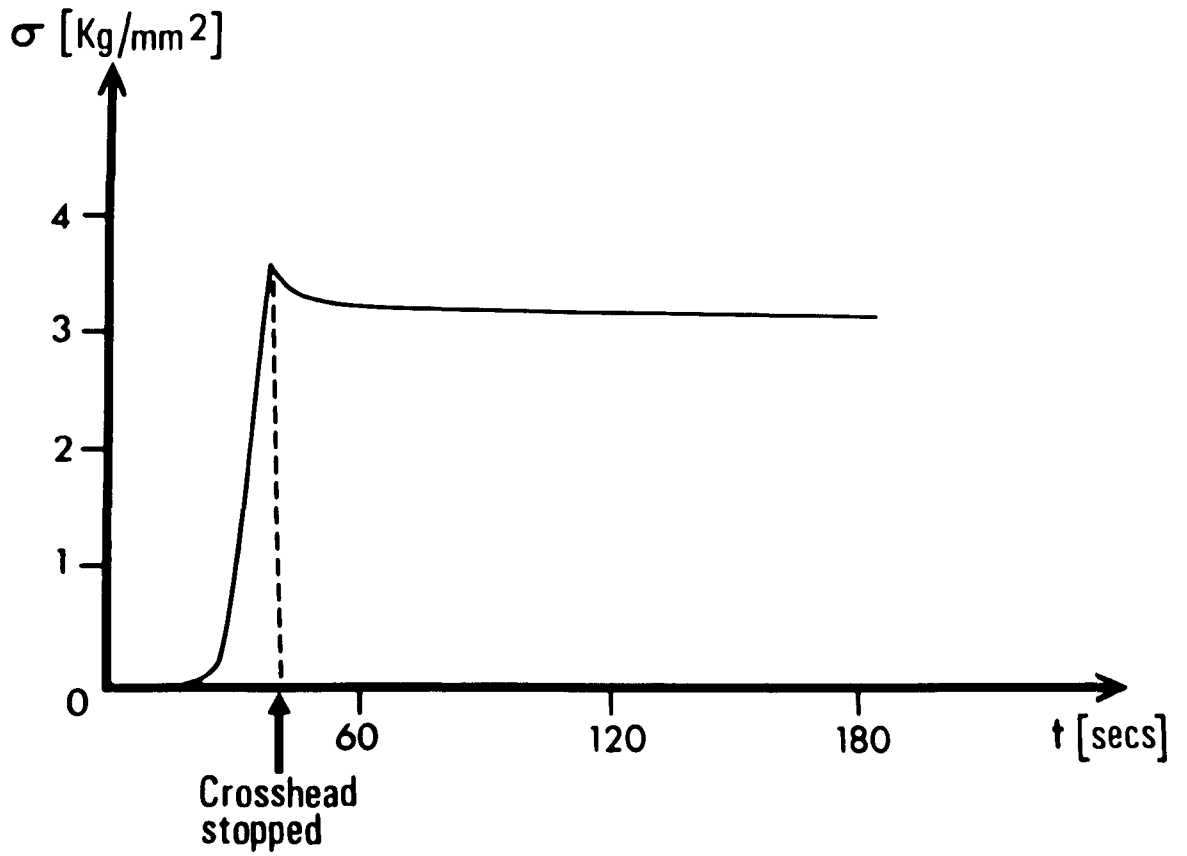


**Fig. 36** Tensile stress relaxation curve.

values were plotted to provide graphs of stress versus longitudinal strain, and also lateral strain versus longitudinal strain. Graphs obtained for specimens from one bone are illustrated in fig. 37. The linear portion of each stress/strain plot represented the region of proportionality within which strain was directly proportional to stress. The gradient of this line was equal to the quotient of tensile stress divided by tensile strain, or Young's modulus of elasticity (E). Similarly, the gradient of the linear portion of each graph of lateral versus longitudinal strain provided Poisson's ratio ( $\mu$ ).

Values of ultimate tensile stress, Young's modulus, tensile stress at the limit of proportionality, and Poisson's ratio, were calculated for each tensile test piece. The first two parameters are shown plotted against degree of mineralisation, in figures 38 and 39 respectively. Good exponential correlations between mechanical properties and mineralisation were found and these are summarized in Table 10.

The student's paired 't' test was used to compare mineral density and ultimate tensile stress of adjacent bone quadrants. Both were lowest for specimens derived from the lateral/proximal quadrant,

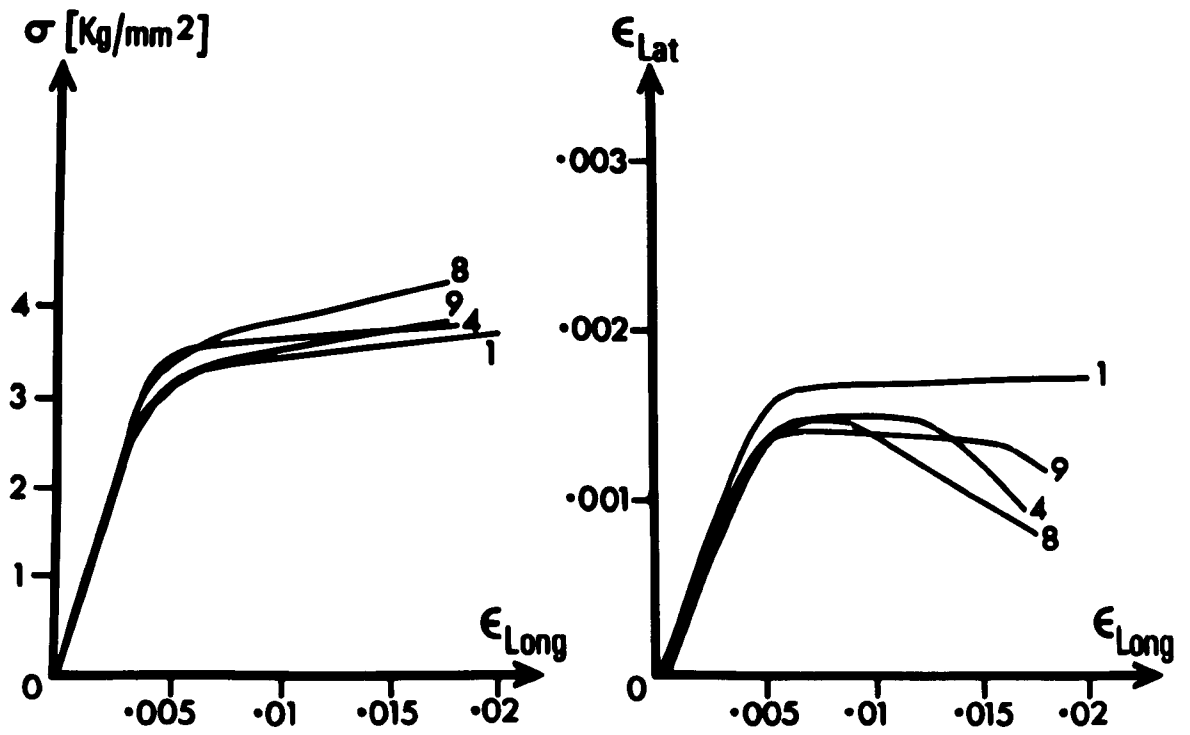


**Fig. 37** Graphs of tensile stress and lateral strain, versus longitudinal strain.

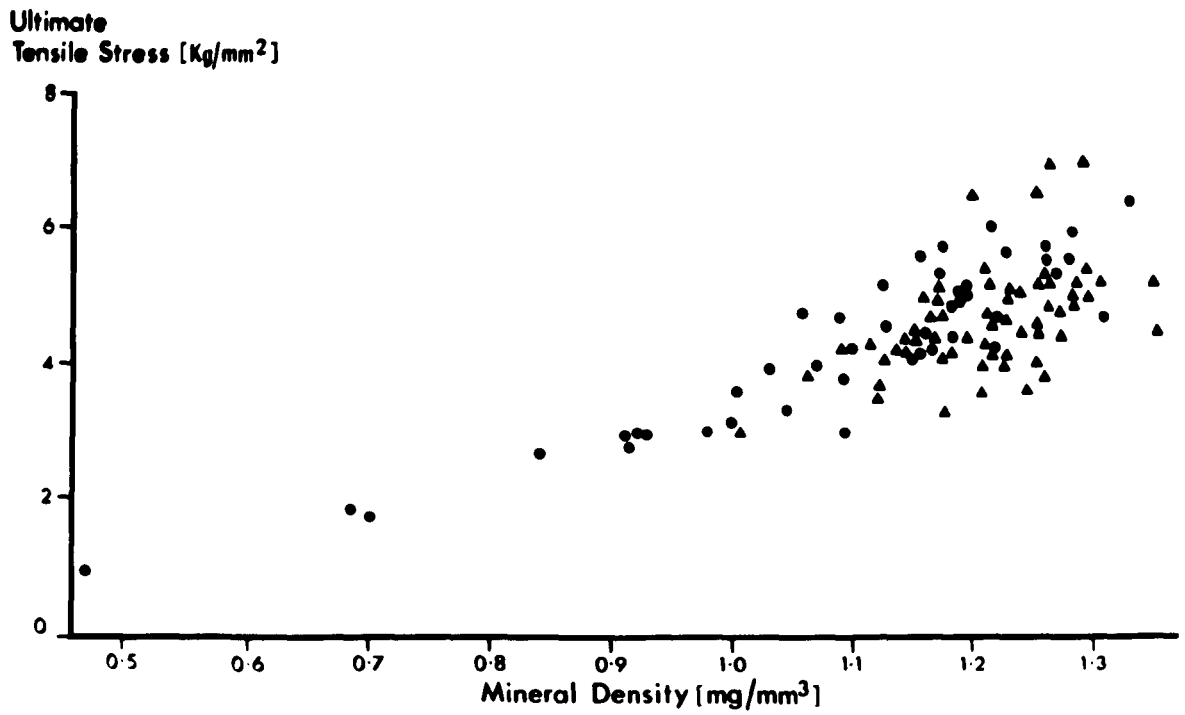


**Fig. 38** Ultimate tensile stress versus degree of mineralisation.

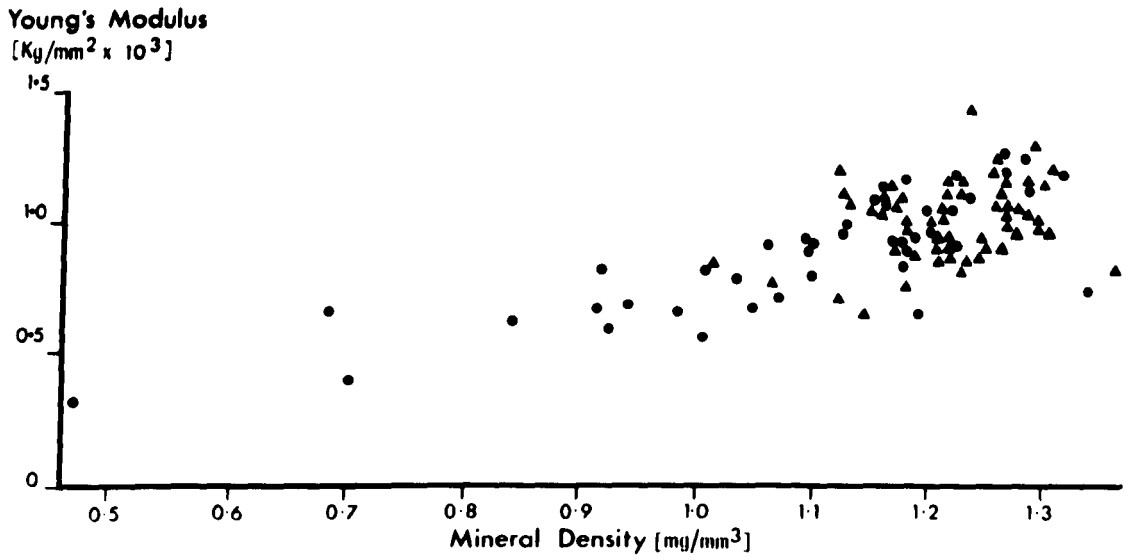


**Fig. 39** Young's modulus versus degree of mineralisation.

and greatest for specimens from the medial/anterior quadrant. These two quadrants were significantly different ( $P < 0.05$ ), the discrepancies averaging 7.6% and 17.3% of the means of mineralisation and ultimate tensile stress respectively.

Table 11 lists the age of each bone and the average value of degree of mineralisation, ultimate tensile stress, stress and strain at the limit of proportionality, Young's modulus, and Poisson's ratio, for test pieces from all four bone quadrants. A grand mean value is given at the foot of each column. Mineralisation, ultimate tensile stress, and stress at the limit of proportionality were related to age, obeying the relations detailed in Table 12.

In addition, ultimate tensile stress was considered in relation to mean apatite crystallite size and degree of preferred orientation determined as described in Chapters 3 and 4. No significant correlation ( $P = 0.70$ ) with degree of preferred orientation was observed. However, a significant negative correlation ( $P < 5 \cdot 10^{-3}$ ) with mean apatite crystallite length (fig. 40) yielded a linear correlation coefficient  $r = -0.60$ . Crystallite length also correlated with mineralisation ( $P < 10^{-3}$ ,  $r = -0.67$ ).

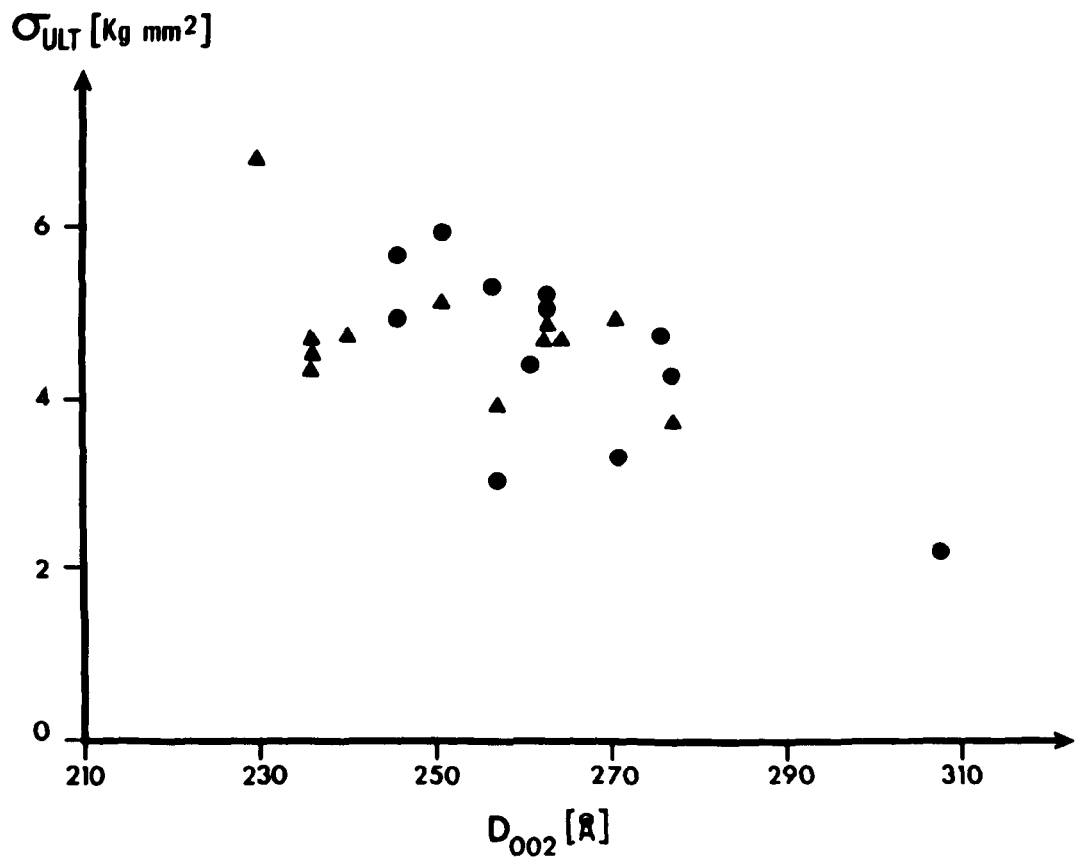


**Fig. 40** Ultimate tensile stress versus average bone apatite crystallite length.

Thus, the coefficients of PARTIAL correlation of crystallite length with ultimate tensile stress and mineralisation were  $r = -0.14$ , and  $r = -0.40$ , respectively.

TABLE 8

TENSILE STRESS RELAXATION DATA OF FEMORAL COMPACT BONE.

BONE	SPECIMEN	INITIAL STRESS (Kg/mm <sup>2</sup> )	CORRELATION COEFFICIENT (r) FOR EXPONENTIAL RELAXATION	RELAXATION TIME CONSTANT (Secs)
N2	A - T3	3.23	-0.86	692
N2	B - T2	4.52	-0.77	714
N2	B - T6	4.31	-0.81	610

TABLE 9

RESULTS OF TESTS TO EVALUATE SENSITIVITY OF ULTIMATE TENSILE STRESS TO VARIATION IN STRAIN RATE.

BONE	SPECIMEN	STRAIN RATE (Sec <sup>-1</sup> )	ULTIMATE TENSILE STRESS (Kg/mm <sup>2</sup> )
N2	B(1) - T7	10 <sup>-4</sup>	5.83
	B(11) - T4	10 <sup>-3</sup>	5.52
	B(1) - T4	2.5 x 10 <sup>-3</sup>	5.58
	B(1) - T5	10 <sup>-2</sup>	6.26

TABLE 10

EXPONENTIAL RELATIONS BETWEEN MECHANICAL PROPERTIES  
AND MINERALISATION.

X (mg/mm <sup>3</sup> )	Y (Kg/mm <sup>2</sup> )	N	Y = a.e <sup>bX</sup>		r	r <sup>2</sup>	S.E. OF ESTIMATE (Kg/mm <sup>2</sup> )
			a	b			
M	$\sigma_{ult}$	105	0.524	1.761	0.87	0.75	0.514
M	$E \times 10^3$	100	0.197	1.310	0.77	0.59	0.127
M	$\sigma_{lp}$	91	0.384	1.814	0.87	0.75	0.413

TABLE 11

MINERALISATION AND TENSILE PROPERTIES OF SAMPLES OF  
COMPACT BONE TISSUE OF DIFFERING AGE.

Bone	Sex	Age	$\bar{M}$ (mg/mm <sup>3</sup> )	$\sigma_{ult}$ (Kg/mm <sup>2</sup> )	$\bar{\sigma}_{LP}$ (Kg/mm <sup>2</sup> )	$\bar{\epsilon}_{LP}$ (x10 <sup>-3</sup> )	$\bar{E}$ (Kg/mm <sup>2</sup> x10 <sup>3</sup> )	$\bar{\mu}$
N1	M	55	1.27	4.60	3.49	3.41	1.02	0.330
N2	M	29	1.28	4.91	3.74	3.34	1.12	0.338
N3	F	19	1.26	5.30	3.73	3.97	0.94	0.292
N4	M	63	1.25	4.70	3.67	3.47	1.06	0.352
N5	F	49	1.17	5.01	3.97	3.95	1.01	0.310
RU71	M	59	1.26	3.90	3.12	3.34	0.94	0.442
RU72	M	54	1.23	4.31	3.36	3.92	0.86	0.230
RU73	F	44	1.26	5.96	4.37	4.33	1.01	0.293
RU74	F	87	1.07	3.33	2.67	3.36	0.80	0.275
RU75	M	62	1.28	4.54	4.07	3.70	1.10	0.316
RU76	M	48	1.25	4.65	3.60	3.28	1.10	0.323
RU77	M	81	1.27	5.08	3.95	3.82	1.04	0.310
RU78	M	72	1.15	3.69	3.20	3.27	0.98	0.337
RU79	F	59	1.18	4.75	3.17	3.82	0.83	0.361
RU80	M	71	1.29	4.90	3.37	2.88	1.17	0.364
RU81	F	68	0.80	2.23	1.74	2.87	0.61	0.311
RU82	F	38	1.31	5.16	4.50	3.79	1.19	0.316
RU83	F	58	1.26	4.89	4.50	3.77	1.19	0.354
RU84	F	75	1.16	4.33	3.36	3.66	0.92	0.320
RU85	M	28	1.30	6.82	5.70	5.91	0.97	0.351
RU86	F	84	1.21	4.39	3.62	3.59	1.01	0.341
RU87	M	59	1.27	4.75	3.73	3.34	1.12	0.306
RU88	F	71	0.98	3.01	2.40	3.83	0.63	0.320
RU89	F	58	1.27	5.72	3.80	3.39	1.12	0.336
GRAND MEAN VALUE			1.21	4.62	3.62	3.67	0.989	0.326
2xS.E. of MEAN			0.04	0.39	0.32	0.24	0.064	0.016

TABLE 12

LINEAR RELATIONS BETWEEN MINERALISATION, TENSILE PROPERTIES AND AGE

X (Years)	Y (Kg/mm <sup>2</sup> )	$\mu$	Y = a + bX		r	Level of Significance (P)	S.E. of estimate (Kg/mm <sup>2</sup> )
			a	b			
Age	$\sigma_{ult}$	24	6.468	-0.0318	-0.59	<0.005	0.754
Age	$E \times 10^3$	24	1.128	-0.0024	-0.27	N.S.	-
Age	$\sigma_{LP}$	24	4.984	-0.0236	-0.54	<0.005	0.638
	Y (mg/mm <sup>3</sup> )						S.E. <sup>3</sup> (mg/mm <sup>3</sup> )
Age	M	25	1.371	-0.0028	-0.41	<0.05	0.102

CHAPTER 7

COMPRESSIVE PROPERTIES OF COMPACT BONE : THEIR  
RELATION TO AGE AND MINERAL CONTENT

## INTRODUCTION

Compressive testing involves crushing the specimen under investigation between two parallel flat surfaces. Test pieces must satisfy certain basic criteria. Firstly, they should be of a size and shape that can be readily prepared from the sample material available. In the present study it was found that cylindrically shaped test pieces could be easily produced from compact bone tissue by a method described later in this chapter.

A second requirement was that test pieces should be designed to eliminate any possibility of "buckling". Now, buckling occurs when the specimen under stress is distorted in such a way that the effect of the force causing the initial distortion is amplified by that distortion. Bodies susceptible to buckling are described as "geometrically unstable". The critical force required to produce buckling in a cylindrical test piece under axial compression is given by Euler's formula,  $P_{crit.} = \pi^2 \cdot E \cdot I / L^2$ , where  $I$  is the second moment of area of the specimen cross-section about its centroid and  $L$  is the length of the cylinder. In order to prevent the occurrence of buckling during destructive compressive testing, it is necessary that  $P_{crit.}$  be

greater than the force required to produce failure. Appendix 7 shows that this condition is satisfied for compact bone when the ratio of specimen length divided by specimen diameter (L/D) is less than about 10.

#### PREPARATION OF COMPRESSIVE TEST PIECES

Parallel-ended transverse sections approximately 7.5 mm. long were cut from each of twenty-seven femora using the rotary blade macrotome. A one inch long proximal portion (Fig. 1) was first attached by elastic bands to the macrotome vee block specimen mount, and was positioned with about one half of its length protruding over the end of the vee block. The block was then adjusted so that the axis of the bone portion was normal to two parallel circular saw blades. These were mounted on the macrotome drive spindle separated by a 7.5 mm. thick spacer. A gravity loading system was used to bring the protruding portion of bone in contact with the edges of the rotating saw blades, both bone and blades being lubricated with Ringer's solution during cutting. Thus, a parallel-ended transverse section having the required length was obtained from each femur. Sections produced were clearly marked to indicate the anatomical alignment.

Next, cylindrically shaped compressive test pieces 5.1 mm. in diameter and 7.5 mm. in length, were produced with a diamond-tipped core drill. Each transverse section in turn was laid flat in a shallow trough filled with Ringer's solution to a depth of

about one inch. Then, using a bench-mounted drilling machine, test pieces were removed from each point of the bone cortex possessing sufficient thickness. A total of one hundred and sixteen specimens was obtained from the twenty-seven femora. The Ringer's solution acted as a coolant and lubricant during drilling. Completed test pieces were sealed in separate polythene bags, each labelled with details of the parent bone and quadrant of origin. They were then stored at  $-20^{\circ}\text{C}$  until required.

#### MEASUREMENT OF THE MINERAL CONTENT OF COMPRESSIVE TEST PIECES

Mineral per unit specimen length (mg/mm) at the midpoint of each compressive test piece was measured using the gamma densitometer described in chapter 6 (Fig. 32). Specimens were scanned in a shallow water bath to standardise for varying organic content. After completion of the scan, the precise diameter and length of each test piece was determined accurately with a micrometer and noted. The value of mineral content was then divided by the calculated cross-sectional area to yield the degree of mineralisation in milligram per cubic millimetre of compact bone.

### METHOD OF COMPRESSIVE TESTING

Compressive testing was performed with the Instron testing machine. A load cell equipped with a flat anvil was mounted on the lower rigid crosshead, and a flat compression unit was mounted on the underside of the mobile crosshead. The load cell employed had a dynamic range up to 5,000 Kg.

Each cylindrical test piece in turn was placed on end in the centre of the anvil (Fig. 41) and stressed by driving the mobile crosshead downward. Crosshead speed equal to 0.5 mm/minute was employed to obtain approximately the same strain rate as was used in tensile testing. During testing, the Instron recorder monitored force applied to the test piece. The recorder range was set so that full scale deflection corresponded to a load of 200 Kg. The chart speed was 5 cm/minute.

Initially, a few tests to evaluate the compressive relaxation time constant of bone tissue were conducted. In these tests, advance of the mobile crosshead was stopped when the applied load had produced about fifty percent of the estimated ultimate compressive stress: load was monitored for several minutes thereafter.

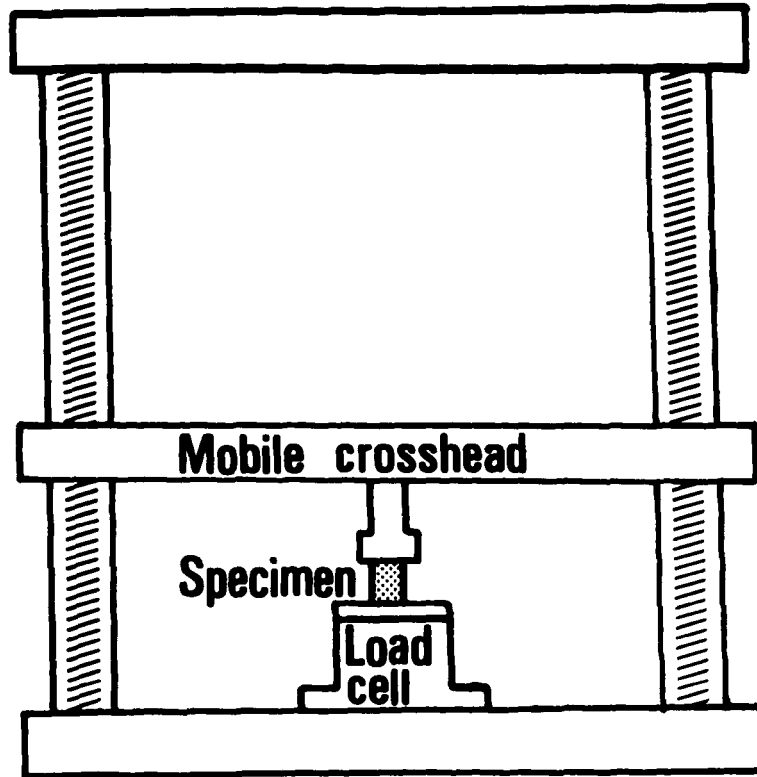


**Fig. 41** Experimental arrangement of compressive testing equipment.

All remaining compressive test pieces were tested to destruction under the experimental conditions described above.

### RESULTS AND CALCULATIONS

Figure 42 illustrates stress relaxation of a compressive test piece. Best fitting exponential relations of the form  $\sigma_t = \sigma_0 e^{-t/T}$  were calculated by the method of least squares for such curves, the relevant correlation coefficients and relaxation time constants being given in Table 13.

Good exponential correlation of both ultimate compressive stress and compressive stress at the limit of proportionality, with degree of mineralisation was demonstrated. Details of these relations are provided in Table 14. Ultimate compressive stress is shown plotted against mineralisation in figure 43.

No significant differences between the mineralisation or ultimate stress of different bone quadrants were observed. However, values for test pieces derived from the medial/anterior quadrant were, on average, higher than values for other test pieces.

Mean values of mineralisation, ultimate stress and stress at the limit of proportionality, of specimens

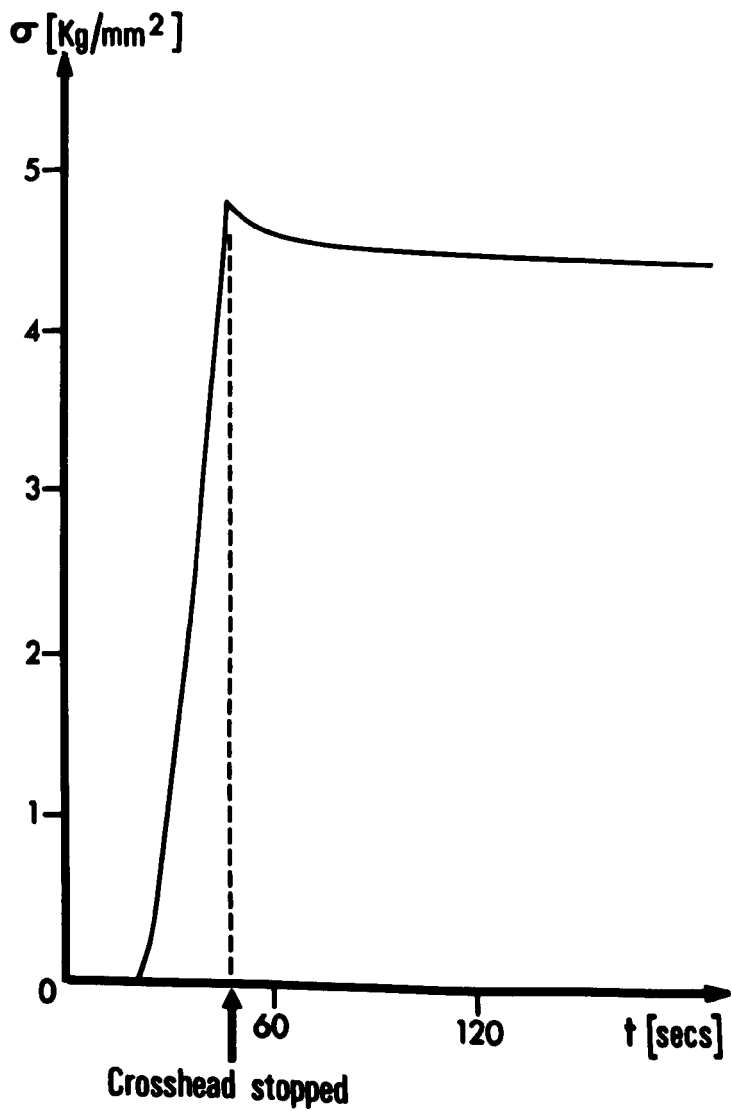
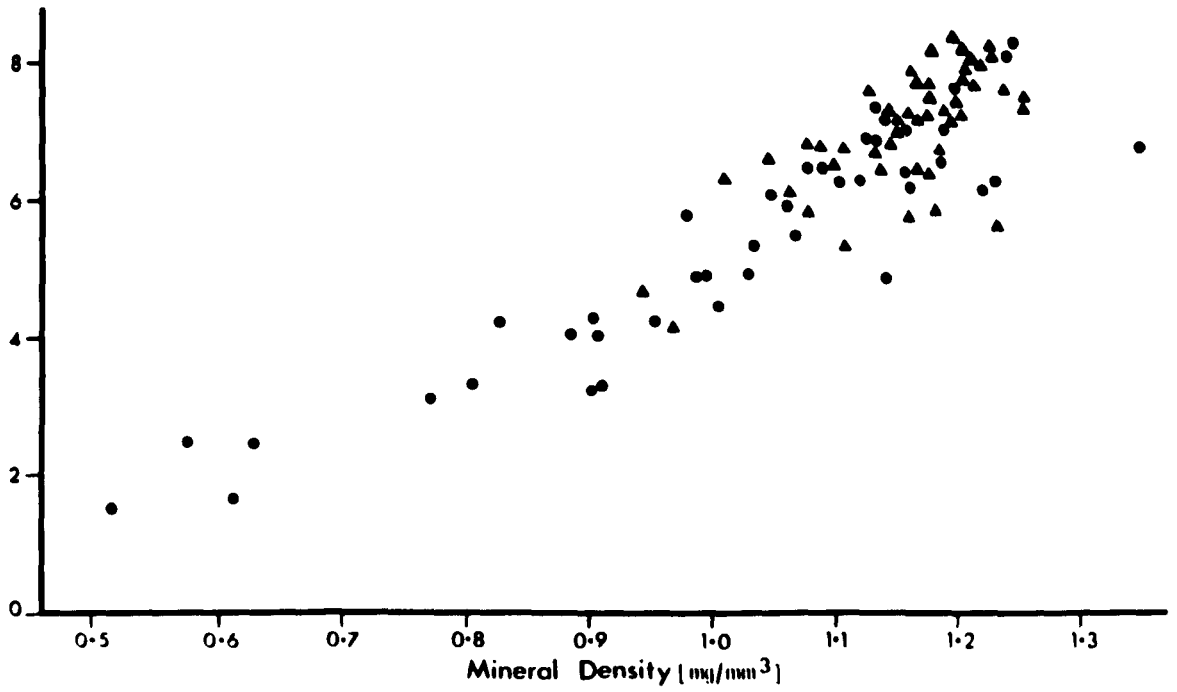


Fig. 42 Compressive stress relaxation curve.

Ultimate  
Compressive Stress (Kg/mm<sup>2</sup>)



**Fig. 43** Ultimate compressive stress versus degree of mineralisation.

derived from the same bone are given in Table 15. The grand mean value is listed at the foot of each column. No significant correlation between age and either ultimate stress or stress at the limit of proportionality, was observed.

Finally, relations between ultimate stress and bone apatite crystallite length and orientation were investigated. No significant correlation ( $P = 0.44$ ) with degree of preferred orientation was demonstrated. However, ultimate stress correlated ( $P < 0.005$ ) negatively with apatite crystallite length, yielding a correlation coefficient  $r = -0.53$  (Fig. 44). Correlation between crystallite length and mineralisation was also significant ( $r = -0.58$ ,  $P < 0.005$ ) and thus the coefficient of partial correlation between ultimate stress and mean crystallite length was only  $r = -0.03$ . Similarly, the partial correlation between crystallite length and mineralisation yielded  $r = -0.28$ .

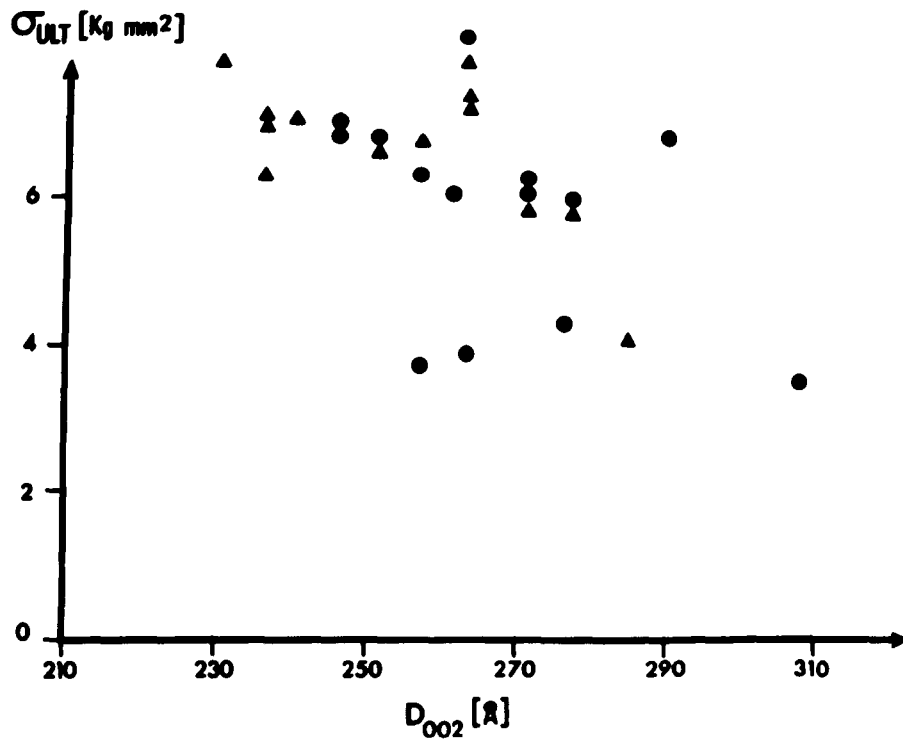


**Fig. 44** Ultimate compressive stress versus average bone apatite crystallite length.

TABLE 13

## COMPRESSIVE STRESS RELAXATION DATA OF FEMORAL COMPACT BONE

BONE	SPECIMEN	INITIAL STRESS (Kg/mm <sup>2</sup> )	CORRELATION COEFFICIENT (r) FOR EXPONENTIAL RELAXATION	RELAXATION TIME CONSTANT (Secs)
N4	C5	3.59	-0.89	1694
	C6	3.05	-0.89	1096
	C7	4.77	-0.87	1464

TABLE 14

EXPONENTIAL RELATIONS BETWEEN COMPRESSIVE MECHANICAL  
 PROPERTIES AND MINERALISATION

X (mg/mm <sup>3</sup> )	Y (Kg/mm <sup>2</sup> )	N	Y = a.e <sup>bX</sup>		r	r <sup>2</sup>	S.E. OF ESTIMATE (Kg/mm <sup>2</sup> )
			a	b			
M	$\sigma_{ult}$	91	0.547	2.017	0.92	0.85	0.605
M	$\sigma_{LP}$	91	0.409	2.143	0.91	0.84	0.598

TABLE 15

MINERALISATION AND COMPRESSIVE PROPERTIES OF SAMPLES  
OF COMPACT BONE TISSUE

BONE	SEX	AGE	$\bar{M}$ (mg/mm <sup>3</sup> )	$\bar{\sigma}_{ult}$ (Kg/mm <sup>2</sup> )	$\bar{\sigma}_{LP}$ (Kg/mm <sup>2</sup> )
N1	M	55	1.25	6.29	5.22
N2	M	29	1.24	5.85	5.29
N3	F	19	1.26	6.42	6.02
N4	M	63	1.32	7.10	6.32
N5	F	49	0.97	3.85	3.46
RU67	F	58	1.23	6.90	5.91
RU69	M	50	1.07	4.12	3.58
RU70	F	55	1.29	6.36	5.20
RU71	M	59	1.29	6.82	5.53
RU72	M	54	1.29	6.99	5.89
RU73	F	44	1.22	6.83	5.90
RU74	F	87	1.13	6.14	5.46
RU75	M	62	1.24	7.11	6.49
RU76	M	48	1.23	7.34	6.54
RU77	M	81	1.23	6.68	5.94
RU78	M	72	1.13	5.88	5.08
RU79	F	59	1.01	4.31	3.57
RU80	M	71	1.27	7.28	6.41
RU81	F	68	0.90	3.55	2.89
RU82	F	38	1.34	8.29	7.44
RU83	F	58	1.23	6.95	6.31
RU84	F	75	1.16	5.92	5.29
RU85	M	28	1.29	7.89	7.07
RU86	F	84	1.20	6.11	5.35
RU87	M	59	1.31	7.93	7.11
RU88	F	71	1.00	3.72	3.16
RU89	F	58	1.33	7.00	6.30
GRAND MEAN VALUE			1.201	6.283	5.509
2 x S.E. OF MEAN			0.045	0.503	0.471

CHAPTER 8

THE ESTIMATION OF BONE MINERAL CONTENT AT  
SELECTED SKELETAL SITES BY GAMMA RAY  
ABSORPTION

## INTRODUCTION

In previous chapters, mechanical properties of bone tissue have been related to degree of mineralisation and physical form of bone mineral. Indeed, in experimental measurements, seventy-five percent of variance of ultimate tensile stress and eighty-five percent of variance of ultimate compressive stress could be accounted for by variation in degree of mineralisation.

Now, the gamma ray absorption technique allows accurate in vivo estimation of mineral content per unit bone length at certain sites in some long bones (13, 15, 17, 18). This parameter represents a combined measure of the physical size and degree of mineralisation of a bone. Thus, gamma ray absorption measurement may provide an indication of susceptibility to fracture. However, many bone sites, including sites such as the femoral neck where fracture commonly occurs, are not amenable to precise in vivo measurement. Difficulties arise in accurately locating the site to be measured and correcting for varying covering thickness of soft tissue. Therefore, it is important to establish whether mineral content at an accessible site can be regarded as representative of other sites and hence be used to diagnose skeletal status.

In the present chapter, calibration for gamma ray absorption determination of bone mineral is described, and the inter-relation of mineral content at selected skeletal sites is investigated.

### MATERIAL PREPARATION

One hundred and seven sets of bones comprising the right third metacarpal, radius and femur, were obtained from human cadavera of wide age range (14 - 90 years). Each bone was stripped of soft tissue and stored at  $-20^{\circ}\text{C}$ . until required.

### MEASUREMENT OF K-VALUE BY GAMMA RAY ABSORPTION

Using equipment described by Shimmins et al (13, 109), gamma ray absorption properties were measured at selected sites chosen to be representative of each bone and independent of the bone dimensions. Thus, gamma ray absorption scans at the midpoint of each bone, at sites one eighth way from the distal end of radius and femur, and at the midpoint of the femoral neck (in forty-one bones), were conducted.

Figure 45 shows a schematic illustration of the gamma ray absorption equipment. A radioisotope source provided a beam of monoenergetic gamma rays. Americium-241 (59.6KeV) was used to make measurement at each site, and iodine-125 (27.3KeV) was used to make additional measurement of metacarpal and radius. Beam collimation was achieved with lead lined collimators, a slit 6 mm. long and 1.5 mm. wide being employed for measurement at

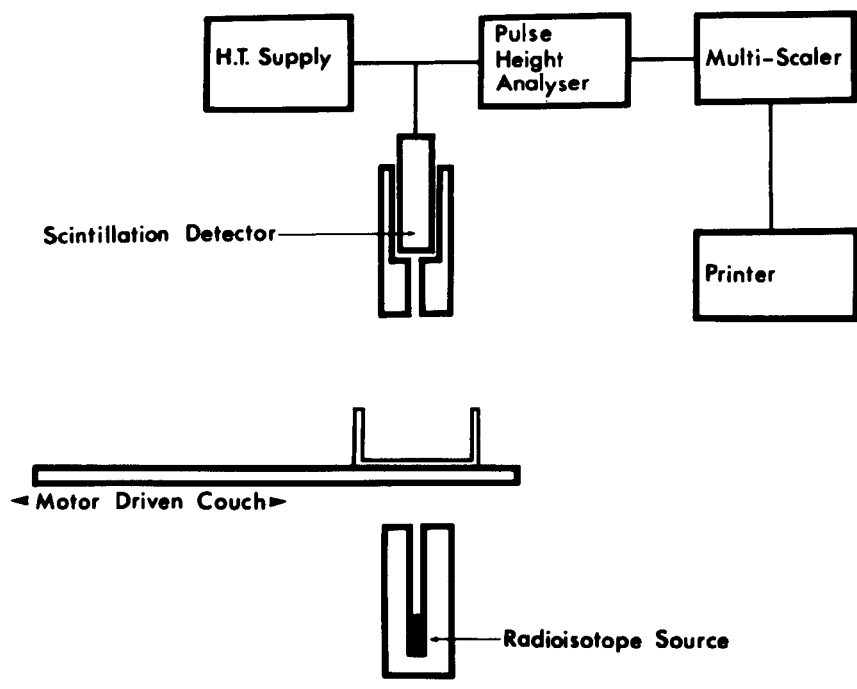


**Fig. 45** Schematic illustration of gamma ray absorption equipment.

all sites except the femoral neck. Due to its restricted length and irregular geometrical configuration, measurement of the neck of femur was most repeatable when a circular collimator 3 mm. in diameter was used.

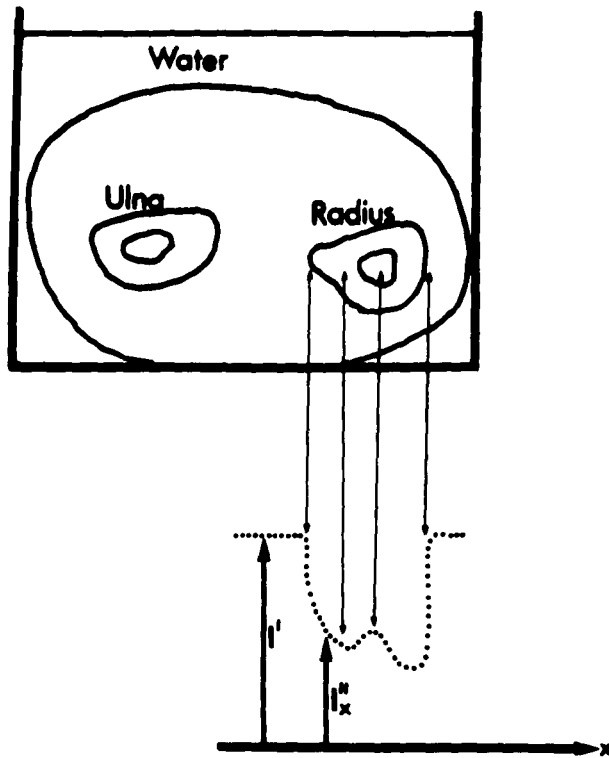
Scanning was conducted with the bone immersed in a water bath to standardize for varying organic content. The water bath was placed on a perspex window located in a motor driven couch, and was positioned so that the proposed site of measurement was adjacent to the gamma ray beam. A sodium iodide scintillation detector was connected to an 144-channel multiscaler, which sequentially recorded intensity transmitted through the bone as it traversed the gamma ray beam. The duration of each individual measurement (the channel "dwell time") was made sufficiently long to allow the bone to completely traverse the beam during available recording time. Channel dwell time was thus varied from one to four seconds depending on the width of bone under examination.

Measurements of intensity transmitted through the bone and water cover, and also through the water adjacent to the bone, were used to compute the "K-value" parameter defined by Shimmins et al (13). Figure 46

illustrates a typical scan profile obtained on the multiscaler display after scanning a site in the radius, shown here in situ. The K-value for each site was calculated from the logarithms of the inverse ratios of counts accumulated in equal time intervals while the bone was traversing the beam to counts accumulated during similar periods when only the water was interposed. The summation of these logarithms was multiplied by the distance traversed during each of the time intervals. Since the couch speed was known to be 0.192 mm/sec., the distance traversed was equal to  $0.192 \times \text{DWELL TIME}$ .

#### MEASUREMENT OF MINERAL CONTENT BY ASHING

After completion of gamma ray absorption studies, sections about 10 mm. in length were removed from each scan site except the femoral neck, in forty-five sets of bones. Section lengths were determined accurately with a micrometer. Each section was then placed in a muffle furnace and maintained at  $600^{\circ}\text{C}$ . for twenty-four hours. The weight of ash residue was divided by the section length to yield bone mineral content at the site in question, in milligram per millimetre length.



$$K\text{-Value} = \Delta x \times \sum \log_{10} \left( \frac{I_0}{I_x} \right)$$

$$\text{Mineral/unit bone length } M = \text{Constant} \times K$$

Fig. 46 Gamma ray absorption scan profile.

## RESULTS AND CALCULATIONS

Measurements of K-value were considered in relation to the corresponding ash values at sites in forty-five bone sets. Good linear correlation between ash and K-value (Fig. 47) measured both with americium-241 and iodine-125 was found, yielding  $r = 0.98$  in each case. These relations constituted calibration equations (Table 16) by which mineral content could be determined accurately from gamma ray absorption data. Using iodine-125 the standard error of estimate was 6.39 mg/mm within the range 21 - 151 mg/mm, and using americium-241 the standard error of estimate was 33.41 mg/mm. within the range 21 - 770 mg/mm.

Now, confidence limits ( $P \geq 0.95$ ) for percent error in determination of K-value arising from statistical fluctuation in count rate, depended on the magnitude of count rate involved. Such limits were typically 0.35% for iodine-125 and 2.25% for americium-241, never exceeding 0.75% and 4% respectively.

The assumption that water has the same absorption properties as the organic constituents of bone leads to systematic error in determination of K-value. In practice, however, fat is the only organic constituent with absorption properties very different

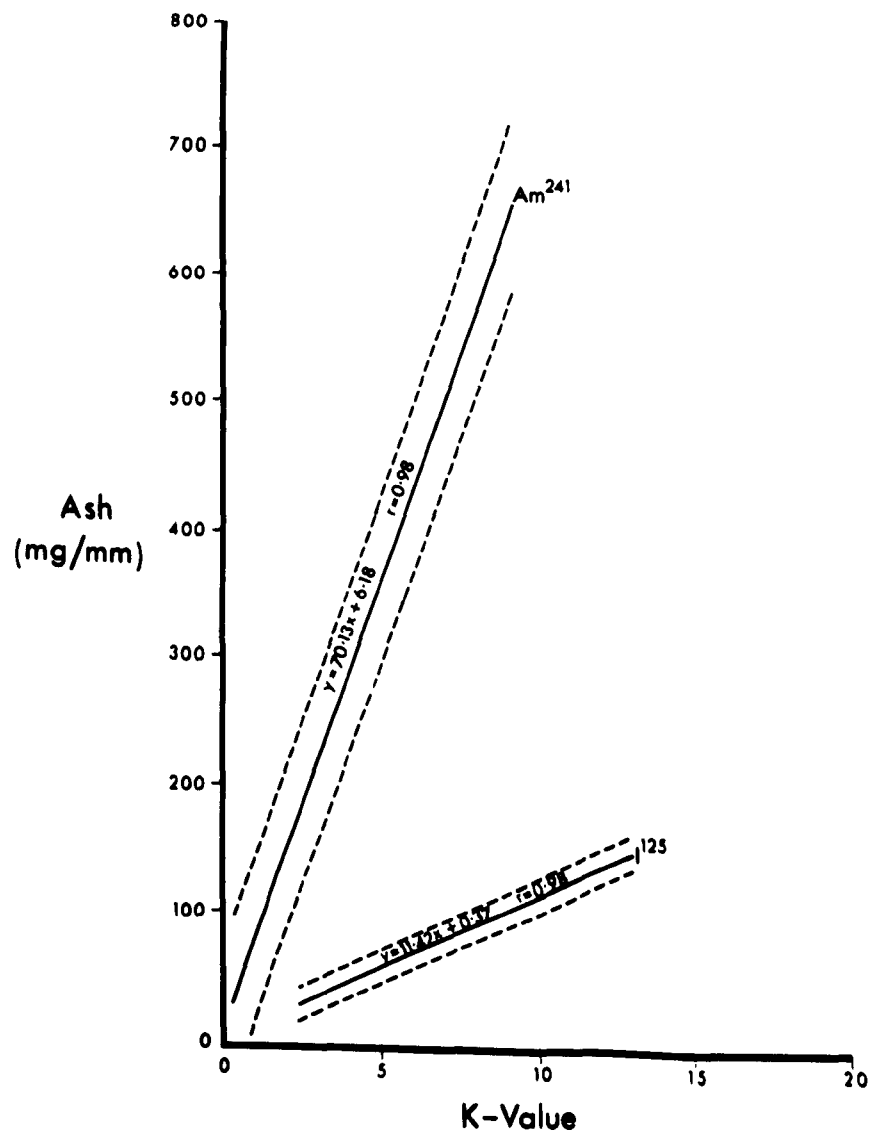


**Fig. 47** Ash value versus iodine-125 and americium-241 K-value.

from those of water. Significant errors thus only arise when appreciable quantities of fat are present. For example, if the medullary cavity of a typical metacarpal were completely full of fat, then the K-value would be underestimated by about 3% for iodine-125 and by about 5% for americium-241. Smaller underestimates occur at other sites. The presence of fat is largely taken into account by the empirical calibration of K-value against ash weight. Nevertheless, biological variation in fat content will introduce random error, although the magnitude will be much less than quoted above.

Mineral content at each site scanned in all one hundred and seven sets of bones was calculated using the equations of table 16. Iodine-125 K-values were substituted into the appropriate equation for sites in metacarpal and radius, and americium-241 K-values were used for sites in femur. Then, interrelation of mineral content at different sites was investigated separately for males and females and also for the combined population. Significant correlation ( $P < 0.005$ ) between all pairs of sites was found for each group. Table 17 provides details of linear correlation between mineral content at the mid metacarpal

site and at other sites. Correlation coefficients ranged from 0.54 to 0.80 in males, from 0.49 to 0.91 in females, and from 0.72 to 0.89 for the combined population. The corresponding values of  $r^2$  indicate the proportion of total data variance accounted for by variation within the respective relations. Figure 48 shows mineral content at the distal radius site plotted against mineral at the mid metacarpal site.

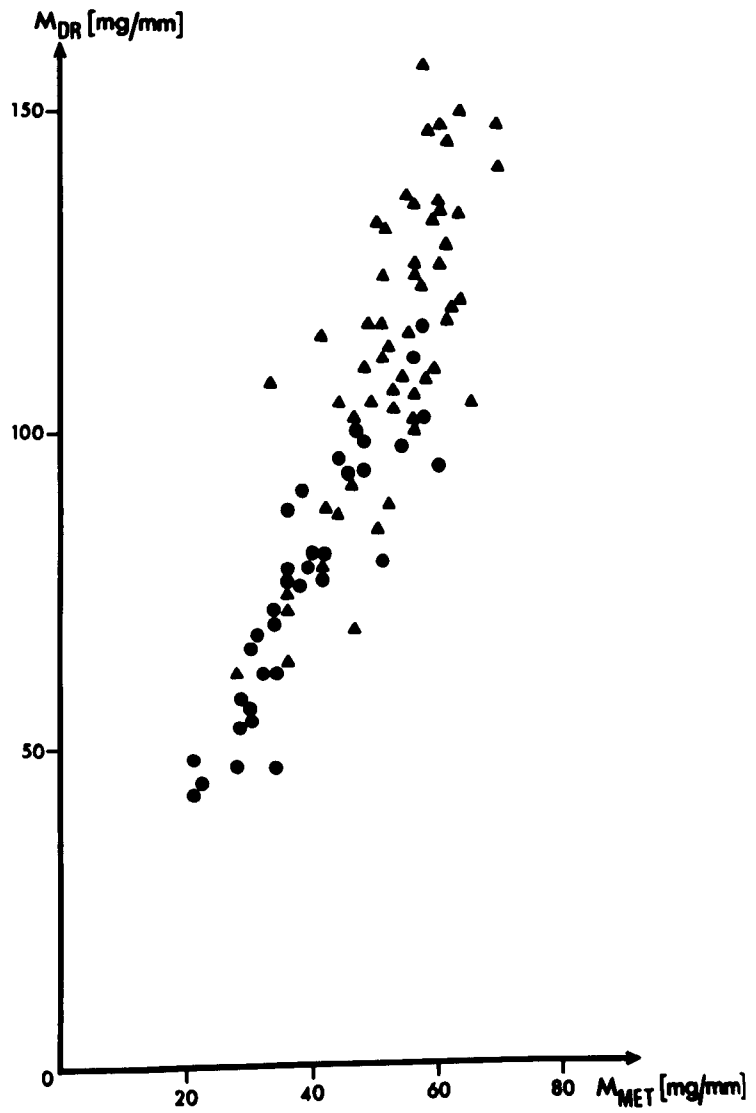


Fig. 48 Distal radius mineral content versus mid metacarpal mineral content.

TABLE 16

CALIBRATION EQUATIONS FOR DETERMINATION OF MINERAL  
CONTENT FROM K-VALUE

X	Bone sites included in correlation	N	Mineral content (mg/mm) = a + b.X		r	S.E. of estimate (mg/mm)
			a	b		
K <sub>I</sub> -125	mid.met., mid. rad., dist. rad.	132	0.37	11.42	0.98	6.39
Kam-241	mid. met., mid. rad., dist. rad., mid. fem. dist. fem.	216	6.18	70.13	0.98	33.41

TABLE 17

RELATIONS BETWEEN MINERAL CONTENT AT MID METACARPAL SITE  
AND AT OTHER SELECTED SKELETAL SITES

Group	Site X	Site Y	N	Y = a + bX (mg/mm)		r	r <sup>2</sup>	S.E. of estimate (mg/mm)
				a	b			
Males	mid. met	fem. neck	22	-36.2	5.93	0.54	0.29	51.3
	"	mid. fem	56	203	5.67	0.58	0.34	70.7
	"	dist. fem	54	129	4.94	0.55	0.30	68.9
	"	mid. rad	56	18.6	1.94	0.80	0.64	13.2
	"	Dist. rad	55	14.2	1.89	0.73	0.53	15.8
Females	mid. met	fem. neck	19	115.5	2.67	0.49	0.24	39.8
	"	mid. fem	36	124.6	5.95	0.67	0.45	64.6
	"	dist. fem	36	73.9	5.16	0.64	0.41	63.0
	"	mid. rad	36	17.6	1.68	0.86	0.74	10.0
	"	dist. rad	35	8.95	1.74	0.91	0.83	8.46
Combined	mid. met	fem. neck	41	51.5	4.35	0.72	0.52	47.8
	"	mid. fem	92	100	7.46	0.77	0.59	73.0
	"	dist. fem	90	56.2	6.10	0.72	0.52	69.3
	"	mid. rad	92	5.31	2.13	0.89	0.79	13.1
	"	dist. rad	90	-1.02	2.12	0.87	0.76	14.4

CHAPTER 9

THE RELATION BETWEEN FRACTURE OF THE DISTAL END  
OF RADIUS AND DEGREE OF MINERALISATION OF THE  
THIRD METACARPAL.

## INTRODUCTION

Incidence of Colles' fracture of the distal end of radius in the general population increases with age. Knowelden, Buhr and Dunbar (1), recorded a particularly sharp increase for women over about forty years of age. Because of this relation with ageing, and on the basis of clinical observation, Colles' fracture is commonly considered to be associated with skeletal degeneration (4). This raises the possibility of diagnosing an individual's susceptibility to Colles' fracture, and indeed any other fracture resulting from generalised skeletal degeneration, by evaluating status of the skeleton with respect to its ability to fulfil its structural role.

Now, as has been stated in chapter 1, values of bone mineral content (Mg/mm), measured by gamma ray absorptiometry, must be normalised for varying individual physical size before meaningful assessment of skeletal status can be made. This problem may be obviated by use of an absolute parameter, such as degree of mineralisation ( $\text{mg}/\text{mm}^3$ ). Unfortunately, in order to determine degree of mineralisation from gamma ray absorption measurement in vivo, cross-sectional area of bone at the site scanned must be known. Now,

precise determination of bone cross-sectional area at the distal radius site, which contains a substantial proportion of trabecular bone, is not possible. However, at sites where bone tissue is primarily compact, cross-sectional area can be estimated accurately from radiographs (7). Moreover, relations between mineral content at different skeletal sites established in the previous chapter (Table 17), indicate the validity of comparing groups of individuals on the basis of mineral density at an arbitrarily chosen site.

In the present study, gamma ray absorption measurement of mineral content and radiographic estimation of bone cross-sectional area at the midpoint of third metacarpal, were used to evaluate degree of mineralisation. Values for male and female groups of patients who had recently sustained Colles' fracture, were respectively compared with values for groups of normal male and female subjects.

#### METHOD OF GAMMA RAY ABSORPTION MEASUREMENT

Gamma ray absorption equipment described in the previous chapter (Fig. 45), was used to measure mineral content (mg/mm) at the midpoint of left or right third metacarpal in fifteen male and one hundred and twenty-one female patients, who had suffered Colles' fracture of the corresponding radius six weeks earlier. Measurement was made in the manner described by Shimmings (109). Each patient was asked to lie on the motor driven couch, with the hand under investigation held palm downward on a water-filled polythene bag situated in an open ended perspex box. The ends of the third metacarpal were identified by palpation, and hence its midpoint was located and the skin surface was marked at the appropriate point. Then, a second water-filled bag was placed over the hand and a thin perspex plate firmly clamped on top, thus producing uniform covering thickness of soft tissue and tissue equivalent material above and below the metacarpals. The complete assembly rested on the couch perspex window. Next, the iodine-125 radioisotope source was moved into line with the beam collimators, and the couch was manually positioned so that the midpoint of the third metacarpal was adjacent to the collimated gamma ray beam. Each scan was conducted using a

detector collimator aperture 12.5 mm. long and 1.5 mm wide. The multiscaler dwell time was set at one second. Finally, K-value of the measured bone site was calculated from the dead-time corrected transmission data and substituted into the appropriate calibration equation (table 16) to yield mineral content.

Similar evaluation of mineral content was carried out on the right third metacarpal of thirty-two normal male and thirty-six normal female volunteers.

#### METHOD OF RADIOGRAPHIC ESTIMATION OF BONE CROSS-SECTIONAL AREA

After completion of gamma ray absorption measurement, the hand was positioned palm downward on an x-ray film and radiographed at a focus to skin distance of fifty inches. Non-screen film was employed in order to obtain maximum resolution. The film was subsequently developed and the radiographic image of the third metacarpal was examined. Because of the close proximity of the metacarpal to the x-ray film during x-ray exposure, and the relatively long focus to skin distance, film magnification was approximately equal to unity. Thus, a pair of Vernier precision calipers was used to measure accurately total bone width ( $D_0$ ) and width of the medullary cavity ( $D_I$ )

at the midpoint of the third metacarpal. Then, the cortical bone cross-sectional area was calculated using the approximation  $A = \pi (D_o^2 - D_i^2)/4$ , which gives the area of a circular annulus possessing outer diameter  $D_o$  and inner diameter  $D_i$ .

## RESULTS AND CALCULATIONS

In order to check the accuracy of estimation of cortical bone area, values were plotted against measured mineral content (Fig. 49) in normal subjects. Good linear correlation was obtained ( $r = 0.87$ ), accounting for seventy-six percent of total data variance. The remaining data variance was due to experimental error and true difference in degree of mineralisation, which is of interest in the present study.

Next, each value of mineral content (mg/mm) was divided by the corresponding estimated cortical area ( $\text{mm}^2$ ), to yield degree of mineralisation, or mass of mineral per unit volume of cortical bone ( $\text{mg}/\text{mm}^3$ ).

Colles' fracture patients were divided into groups defined according to sex and side of fracture. Mean mineral density and standard error of the mean were computed for each group (Table 18). Mean estimate of left third metacarpal (measurements on patients who had sustained fracture of the left radius) was compared with mean estimate of right third metacarpal (measurements on patients with fracture of the right radius) using the student's t-test. In addition, in view of the small number of male patients, males with left fracture were compared with those



having right fracture using the non-parametric Wilcoxon statistical test. In no case was any significant difference between groups established ( $P \gg 0.10$ ). The right and left fracture groups were therefore combined for each sex, and overall mean values were calculated (Table 18).

Normal male and female subjects were similarly compared on the basis of right third metacarpal mineral density. The students t-test indicated a strong possibility ( $P = 0.11$ ) that the two groups were different. Thus, comparison between Colles' and normal groups was carried out separately for males and females. Once again, the t-test was used for both comparisons, and in addition the Wilcoxon test was employed in the case of the males. For both males and females, third metacarpal mineral density was significantly lower ( $P \ll 10^{-2}$ ) in the Colles' group than in the normal group. Figures 50 and 51 show histograms of the distribution of mineral density values in Colles' and normal subjects of both sexes.

Table 18 lists the mean degree of mineralisation and standard error of the mean for each group investigated, and also summarizes results of the statistical comparisons described above. In addition, corresponding

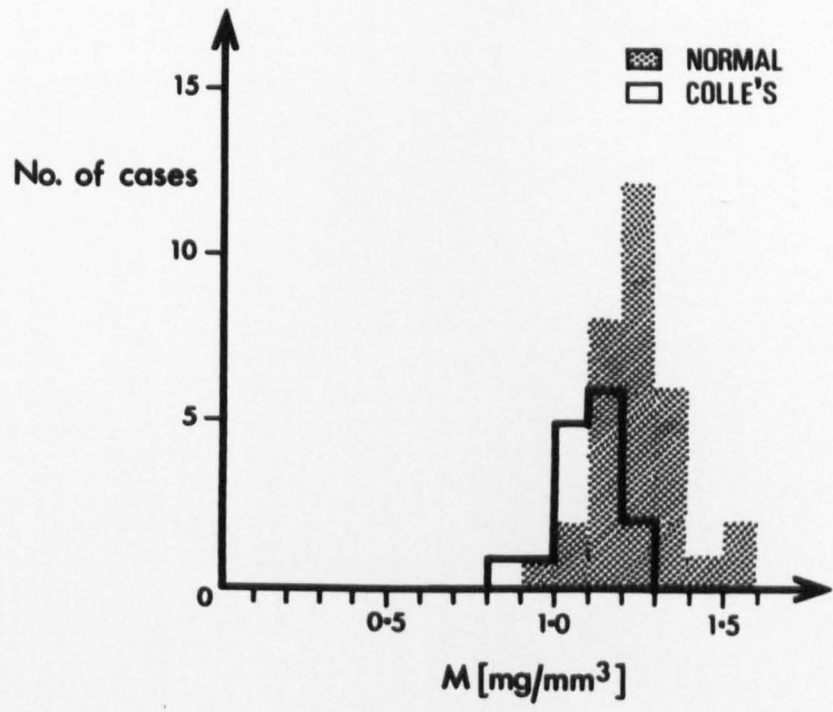


Fig. 50 Histograms showing distribution of values of mineral density of third metacarpal in male patients with Colles' fracture, and in normal male subjects.

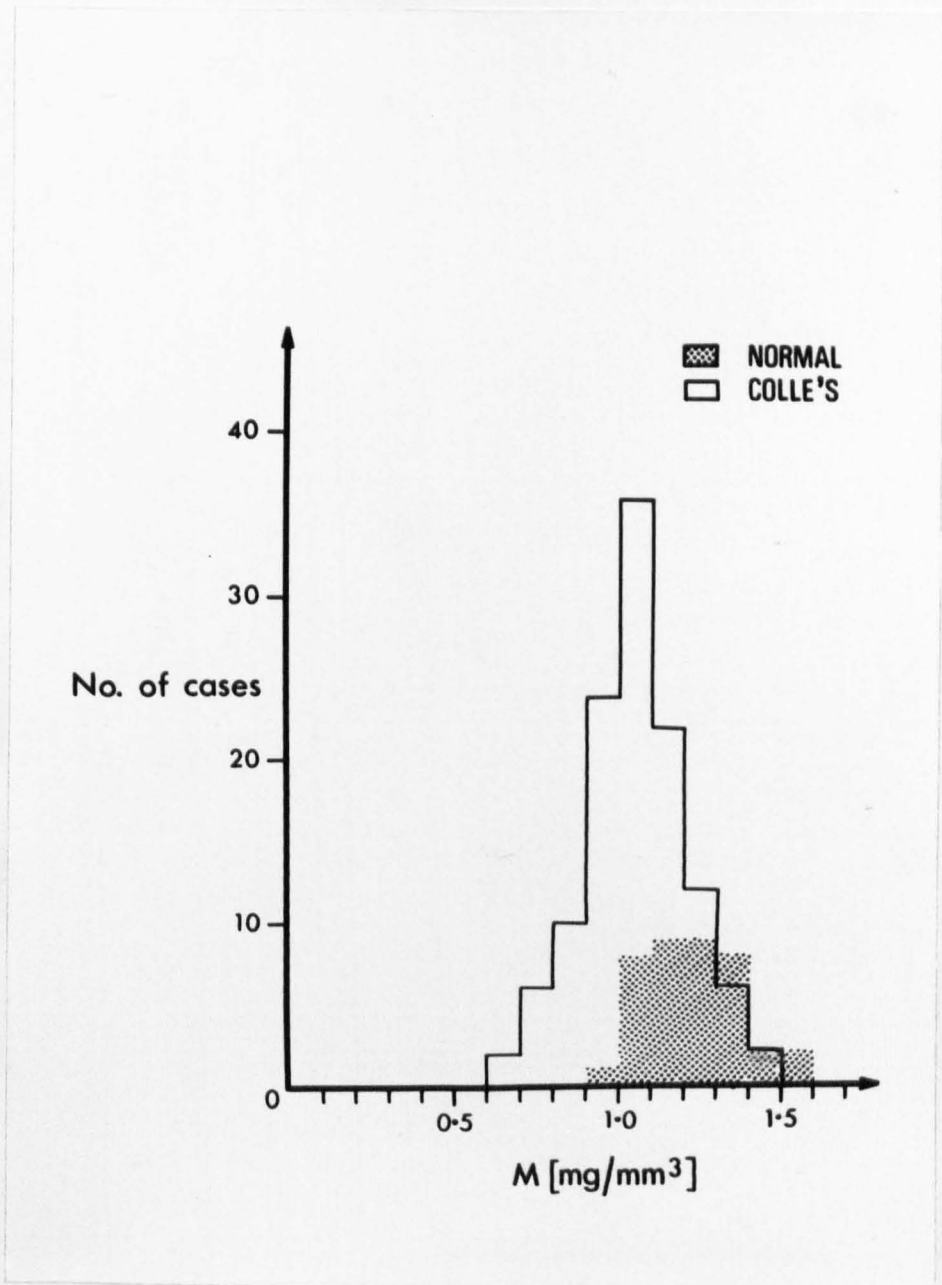


Fig. 51 Histograms showing distribution of values of mineral density of third metacarpal in female patients with Colles' fracture, and in normal female subjects.

data for the accurately measured femoral sections used as sample material for tests described in chapters 6 and 7, is provided.

TABLE 18

METACARPAL AND FEMORAL MINERAL DENSITY: SIGNIFICANCE OF DIFFERENCE BETWEEN GROUPS

Group	N	Mean mineral density (mg/mm <sup>3</sup> )	S.E. of mean (mg/mm <sup>3</sup> )	Statistical test/significance of difference between groups (P)
Colles' males right	4	1.112	0.028	t-test/P = 0.56 Wilcoxon/P >> 0.10
Colles' males left	11	1.077	0.034	
Colles' males combined	15	1.087	0.026	
Normal males right	32	1.241	0.024	t-test/p < 5.10 <sup>-4</sup> Wilcoxon/P << 10 <sup>-2</sup>
Normal females right	36	1.190	0.020	
Colles' females right	50	1.033	0.019	t-test/P = 0.44 t-test/P < 5.10 <sup>-6</sup>
Colles' females left	71	1.057	0.022	
Colles' females combined	121	1.047	0.015	
Femoral tensile section male	12	1.258	0.011	t-test/P < 0.05
Femoral tensile section female	12	1.161	0.042	Wilcoxon/P < 0.05
Femoral compressive section male	14	1.243	0.020	t-test/P < 0.10
Femoral compressive section female	13	1.162	0.037	Wilcoxon/P < 0.10

**CHAPTER 10**

**DISCUSSION AND CONCLUSIONS**

X-ray powder diffraction analysis has confirmed the apatitic nature of crystalline bone mineral. Precise evaluation of unit cell parameters revealed a hexagonal crystal structure very similar to that of calcium hydroxyapatite. No evidence of any other crystalline bone mineral was found.

Although the possible existence of amorphous calcium phosphate in bone was not specifically investigated, it was noted that bone powder diffractograms were not consistent with the presence of large quantities of amorphous mineral. Diffraction lines were generally well-defined (Fig. 8) and the relative intensity of diffusely scattered radiation was much less than that recorded for femoral bone powder by Harper and Posner (110).

Average bone apatite crystallite length was determined from powder diffraction line broadening (Table 6). The mean value for samples studied was  $261 \pm 6.5$  Angstrom ( $2 \times \text{S.E.}$ ), with coefficient of variation equalling 6.7%. No significant correlation with age ( $P = 0.31$ ) was indicated (Fig. 15). This contradicts the theory of bone ageing proposed by Chatterji and Jeffery (57). Transmission electron microscopy enabled "order of magnitude" assessment of

crystallite size, the results of which were consistent with findings described above.

Preferred orientation of bone apatite crystallites, in the direction of propagation of haversian canals in femoral compacta, was demonstrated by a flat plate camera x-ray diffraction technique. However, angular disposition of crystallites (Fig. 19) was completely uniform around the haversian canals. No significant correlation between degree of preferred orientation and age was shown.

Tensile and compressive mechanical properties of compact bone tissue were investigated in relation to age and bone mineral. Although mineral density, ultimate tensile stress, and tensile stress at the limit of proportionality correlated significantly with age ( $P < 0.05$ ), regression coefficients were small and age could not be shown to account for more than thirty-five percent of observed data variance. Good correlation between mechanical properties and mineral density was demonstrated (Table 10). Indeed, seventy-five percent of variance of ultimate tensile stress, and eighty-five percent of variance of ultimate compressive stress could be attributed to variation in mineral density. Thus, mineral density, or degree of mineralisation, has been established as an important determinant of bone strength.

Statistical analysis of results of x-ray diffraction measurement and mechanical testing, revealed the effect on mechanical properties produced by differing physical form of bone apatite. Significant ( $P < 0.005$ ) negative correlation of both ultimate tensile and ultimate compressive stress with average bone apatite crystallite length was exhibited (Figs. 40, 44). These relations indicate the deleterious effect on bone strength associated with any substantial increase in average crystallite length. However, this may be due to the significant ( $P < 0.005$ ) negative correlation between average crystallite length and mineral density.

No significant correlation of degree of preferred orientation of bone apatite crystallites with age, mineralisation, or mechanical properties, was observed.

Calibration equations (Table 16, fig. 47) enabling direct estimation of mineral content by gamma ray absorptiometry, using either an iodine-125 or americium-241 radioisotope source have been determined. Measurements made by this technique were used to establish significant relations ( $P < 0.005$ ) between mineral content at selected skeletal sites. These relations provide evidence of a general pattern of

distribution of skeletal mineral. Thus, the possibility of assessing skeletal status by measurement at an arbitrarily chosen bone site, is indicated. Alternatively, localised bone disease may be diagnosed and quantified by comparison of mineral content at several skeletal sites.

In view of the good correlation between mechanical properties and mineralisation of bone tissue, the effect of variation in this latter parameter was studied. A method by which third metacarpal mineral density can be evaluated by in vivo measurement of mineral content and cortical bone cross-sectional area, has been presented. Male and female groups of Colles' fracture patients had significantly lower ( $P \ll 10^{-2}$ ) metacarpal mineral density than had groups of normal subjects.

Compact bone mineral density is proposed as a parameter of skeletal status, relevant to the skeleton's ability to fulfil its structural role, and therefore appropriate to the assessment of susceptibility to fracture. Clinical interpretation of mineral density values does not depend on their normalisation for differing physical size of subjects, neither does it require the accumulation of data concerning the general

population. Moreover, since mechanical properties of bone tissue are closely related to mineral density, (whole) bone strength will be more readily evaluated if mineral density is known.

LIST OF REFERENCES

1. KNOWELDEN, J., Buhr, A.J., Dunbar, O., 1964. Incidence of fractures in persons over 35 years of age. A report to the M.R.C. working party on fractures in the elderly. BRIT. J. SOC. & PREV. MED., 18, 130 - 141.
2. CHALMERS, J., Conacher, W.D.M., Gardner, D.L., Scott, P.J., 1967. Osteomalacia: a common disease in elderly women. J. BONE & JT. SURG., 49B, 403 - 423.
3. BARNES, R., 1967. Fracture of the neck of femur. J. BONE & JT. SURG., 49B, 607 - 617.
4. SMITH, D.A., 1970. Osteoporosis. M.D. THESIS, UNIVERSITY OF GLASGOW.
5. BARNETT, E., Nordin, B.E.C., 1960. The radiological diagnosis of osteoporosis: A new approach. CLIN. RADIOL., 11, 166 - 174.
6. SPENCER, R.P., Coulombe, M.J., 1966. Quantitation of the radiographically determined age dependence of bone thickness. INVEST. RADIOL., 1, 144 - 147.
7. EXTON-SMITH, A.N., Millard, P.H., Payne, P.R., Wheeler, E.F., 1969. Pattern of development and loss of bone with age. LANCET, (ii), 1154 - 1156.
8. DOYLE, F.H., 1961. Ulnar bone mineral concentration in metabolic bone diseases. BRIT. J. RADIOL., 34, 698 - 712.

9. KEANE, B.E., Spiegler, G., Davis, R., 1959. Quantitative evaluation of bone mineral by a radiographic method. BRIT. J. RADIOL., 32, 162 - 167.
10. SMITH, D.A., Anderson, J.B., Shimmins, J., Speirs, C.F., Barnett, E., 1969. Changes in metacarpal mineral content and density in normal male and female subjects with age. CLIN. RADIOL., 20, 23 - 31.
11. ANDERSON, J.B., Shimmins, J., Smith, D.A., 1966. A new technique for the measurement of metacarpal density. BRIT. J. RADIOL., 39, 443 - 450.
12. MULLIGAN, P.J., Smith, D.A., Smith, C.B., Anderson, J.B., Barnes, R., 1975. The relation between sub-capital fracture of the femur and mineral content of the right third metacarpal. BRIT. J. RADIOL., 48, 370 - 373.
13. SHIMMINS, J., Smith, D.A., Aitken, M., Anderson, J.B., Gillespie, F.C., 1972. The accuracy and reproducibility of bone mineral measurements in vivo: (b) Methods using sealed isotope sources. CLIN. RADIOL., 23, 47 - 51.
14. WEST, R.R., Reed, G.W., 1970. The measurement of bone mineral in vivo by photon beam scanning. BRIT. J. RADIOL., 43, 886 - 893.
15. CAMERON, J.R., Sorenson, J.A., 1963. Measurement of bone mineral in vivo: An improved method. SCIENCE, 142, 230 - 232.
16. MAZESS, R.B., Cameron, J.R., O'Connor, R. Knutzen, D., 1964. Accuracy of bone mineral measurement. SCIENCE, 145, 388 - 389

17. SORENSON, J.A., Cameron, J.R., 1967. A reliable in vivo measurement of bone mineral content. J. BONE & JT. SURG., 49A, 481 - 497.
18. MAZESS, R.B., 1971. Estimation of bone and skeletal weight by direct photon absorptiometry. INVEST. RADIOL., 6, 52 - 60.
19. MAZESS, R.B., Cameron, J.R., 1973. Bone mineral content in normal U.S. whites. In "Proceedings International Conference on Bone Mineral Measurement", Chicago, Illinois, pp. 228 - 238.
20. McLEAN, F.C., Urist, M.R., 1961. In "Bone: An Introduction to the Physiology of Skeletal Tissue", University of Chicago Press, Illinois, page 35.
21. RAMACHANDRAN, G.N., Kartha, G., 1955. Structure of collagen. NATURE, 176, 593 - 595.
22. RICH, A., Crick, F.H.C., 1961. The molecular structure of collagen. J. MOL. BIOL., 3, 483 - 506.
23. ROBINSON, R.A., Watson, M.L., 1952. Collagen - crystal relationships in bone as observed in the electron microscope. ANAT. REC., 114, 383 - 410.
24. JACKSON, S.F., Randall, J.T., 1956. The fine structure of bone. NATURE, 178, p. 798.
25. FERNANDEZ-MORAN, H., Engstrom, A., 1957. Electron microscopy and x-ray diffraction on bone. BIOCHIM. et BIOPHYS. ACTA., 23, 260 - 264.

26. ASCENZI, A., Bonucci, E., 1967. The compressive properties of single osteons. ANAT. REC., 161, 377 - 392.
27. EVANS, F.G., Vincentelli, R., 1969. Relation of collagen fibre orientation to some mechanical properties of human cortical bone. J. BIOMECHS., 2, 63 - 72.
28. VINCENTELLI, R., Evans, F.G., 1971. Relations among mechanical properties, collagen fibres and calcification in adult human cortical bone. J. BIOMECHS., 4, 193 - 201.
29. ROSEN, B.W., Dow, N.F., 1972. Mechanics of failure of fibrous composites. In "Fracture: an Advanced Treatise - Vol. VII Fracture of Non-metals and Composites", ACADEMIC PRESS, LONDON, pp. 611 - 674.
30. CHATTERJI, S., Jeffery, J.W., 1967. Strength development in calcareous cements. NATURE, 214, 559 - 561.
31. BIGGS, W.D., 1966. Theoretical background. In "Composite Materials", ELSEVIER PUB. CO., NEW YORK, pp. 28 - 57.
32. DE JONG, W.F., 1926. Recueil des travaux chimiques des pays-bas, 45, 445.
33. ENGSTROM, A., Zettersohm, R., 1951. Studies on the ultrastructure of bone. EXP. CELL RES., 2, 268 - 274.
34. DALLEMAGNE, M.J., 1948. The theory of primary calcification in bone. NATURE, 161, p. 115.

35. ENGSTROM, A., Finean, J.B., 1953. Micro x-ray diffraction in histochemistry. EXP. CELL RES., 4, 484 - 486.
36. FINEAN, J.B., Engstrom, A., 1953. Low angle x-ray diffraction of bone. NATURE, 171, p. 564.
37. FINEAN, J.B., Engstrom, A., 1953. The low angle scatter of x-rays from bone tissue. BIOCHIM. et BIOPHYS. ACTA., 11, 178 - 189.
38. AMPRINO, R., Engstrom, A., 1952. Studies on x-ray absorption and diffraction of bone tissue. ACTA. ANAT. 15, 1 - 22.
39. CHATTERJI, S., Wall, J.C., Jeffery, J.W., 1972. Changes in the degree of orientation of bone minerals with age in the human femur. EXPERIENTIA, 28, 156 - 157.
40. CHEN, H.L., Gundjian, A.A., 1974. Determination of the bone crystallites distribution function by x-ray diffraction. MED. & BIOL. ENG., 12, 531 - 536.
41. BALE, W.F., 1940. A comparative roentgen-ray diffraction study of several natural apatites and the apatite-like constituent of bone and tooth substance. AM. J. ROENTGENOL., 43, 735 - 747.
42. REED, C.I., Reed, C.P., 1942/3. An attempted correlation of mechanical properties of bone with antirachitic healing and with molecular structure as determined by x-ray diffraction techniques. AM. J. PHYSIOL., 138, 34 - 40.

43. TRAUTZ, O.R., 1954/5. X-ray diffraction of apatites. ANN. N.Y. ACAD. SCI., 60, 696 - 713.
44. POSNER, A.S., Eanes, E.D., Harper, R.A., Zipkin, I., 1963. X-ray diffraction analysis of the effect of fluoride on human bone apatite. ARCH. ORAL BIOL., 8, 549 - 570.
45. KAY, M.I., Young, R.A., Posner, A.S., 1964. Crystal structure of hydroxyapatite. NATURE, 204, 1050 - 1052.
46. POSNER, A.S., Eanes, E.D., Zipkin, I., 1964. X-ray diffraction analysis of the effect of fluoride on bone. In "Proceedings Second European Symposium of Calcified Tissues", LIEGE, pp. 79 - 88.
47. MOSEBACH, R., 1965. A propos des dimensions et des proprietes crystallographiques des particules primaires de l'apatite. BULL. GROUP INT. RECH. SC. STOMAT, 8, 325 - 340.
48. LENART, G., Bidlo, G., Pinter, J., 1968. Use of x-ray diffraction method in investigations on mineral substances of bone and callus. ACTA. BIOCHIM. et BIOPHYS. ACAD. SCI. HUNG., 3, 305 - 316.
49. LENART, G., Bidlo, G., Pinter, J., 1971. X-ray diffraction investigations in the growing zone of long bones. ACTA. BIOCHIM. et BIOPHYS. ACAD. SCI. HUNG., 6, 306 - 309.
50. EANES, E.D., Termine, J.D., Posner, A.S., 1967, Amorphous calcium phosphate in skeletal tissue. CLIN. ORTHOP., 53, 223 - 235.
51. POSNER, A.S., Eanes, E.D., Low angle x-ray scattering of bone.

52. TERMINE, J.D., Posner, A.S., 1966. Infra-red determination of the percentage of crystallinity in apatitic calcium phosphates. NATURE, 211, 268 - 270.
53. TERMINE, J.D., Posner, A.S., 1966. Infra-red analysis of rat bone : age dependency of amorphous and crystalline mineral fractions. SCIENCE, 153, 1523 - 1525.
54. ROBINSON, R.A., 1952. An electron microscope study of the crystalline inorganic component of bone and its relationship to the organic matrix. J. BONE & JT. SURG., 34A, 389 - 434.
55. ROBINSON, R.A., Watson, M.L., 1955. Collagen-crystal relationships in bone as observed in the electron microscope, III. Crystal and collagen morphology as a function of age. ANN. N.Y. ACAD. SCI., 60, 596 - 629.
56. WALLGREN, G., 1957. Biophysical analyses of the formation and structure of human foetal bone : a microradiographic and x-ray crystallographic study. ACTA. PAED., SUPPLEMENT 113.
57. CHATTERJI, S., Jeffery, J.W., 1968. Changes in structure of human bone with age. NATURE, 219, 482 - 484.
58. SCHERRER, P., 1918. GOTTINGER NACHRICHTEN, 2, 98.
59. PATTERSON, A.L., 1939. The diffraction of x-rays by small crystalline particles. PHYSICAL REVIEW, 56, 972 - 977.
60. PATTERSON, A.L., 1939. The Scherrer formula for x-ray particle size determination. PHYSICAL REVIEW, 56, 978 - 982.

61. BRAGG, W.L., 1919. In "The Crystalline State: A general survey", BELL & SONS LTD., LONDON, p. 189.
62. WILSON, A.J.C., 1950. Geiger counter x-ray spectrometer - influence of size and absorption coefficient of specimen on position and shape of powder diffraction maxima. J. SCI. INSTR., 27, 321 - 325.
63. SPENCER, R.C., 1931. Additional theory of the double x-ray spectrometer. PHYSICAL REVIEW, 38, 618 - 629.
64. SPENCER, R.C., 1939. The correction of experimental curves for the resolving power of the apparatus. PHYSICAL REVIEW, 55, p. 239.
65. SPENCER, R.C., 1949. Discussion of geometrical factors affecting x-ray spectrometer maxima. J. APPL. PHYS., 20, 413 - 414.
66. KLUG, H.P., Alexander L.E., 1954. In "X-ray Diffraction Procedures for Polycrystalline and Amorphous Materials", JOHN WILEY & SONS, NEW YORK, pp. 246 - 248 and pp. 491 - 538.
67. STOKES, A.R., 1948. A numerical Fourier analysis method for the correction of widths and shapes of lines on x-ray powder photographs. PROC. PHYS. SOC., 61, 382 - 391.
68. JONES, F.W., 1938. The measurement of particle size by the x-ray method. PROC. ROYAL SOC. LONDON, 166A, 16 - 43.
69. ALEXANDER, L., Klug, H.P., 1950. Determination of crystallite size with the x-ray spectrometer. J. APPL. PHYS., 21, 137 - 142.

70. RAU, R.C., 1963. Measurement of crystallite size by means of x-ray diffraction line broadening. NORELCO REPORTER, X, 114 - 120.
71. LUFT, J.H., 1961. Improvements in epoxy resin embedding methods. J. BIOPHYS. BIOCHEM. CYTOL., 9, 409 - 414.
72. CLARK, S.M., Iball, J., 1957. Structure of bone in relation to growth. NATURE, 179, 94 - 95.
73. VOSE, G.P., 1962. The relation of microscopic mineralisation to intrinsic bone strength. ANAT. REC., 144, 31 - 36.
74. WEAVER, J.K., Chalmers, J., 1966. Cancellous bone: its strength and changes with ageing and an evaluation of some methods for measuring its mineral content. J. BONE & JT. SURG., 48A, 289 - 308.
75. MATHER, B.S., 1968. The effect of variation in specific gravity and ash content on the mechanical properties of human compact bone. J. BIOMECHS., 1, 207 - 210.
76. CURREY, J.D., 1969. The mechanical consequences of variation in the mineral content of bone. J. BIOMECHS., 2, 1 - 11.
77. HIRSCH, C., da Silva, O., 1967. The effect of orientation on some mechanical properties of femoral cortical specimens. ACTA. ORTHOP. SCAND., 38, 45 - 56.
78. LINDAHL, O., Lindgren, A.G.H., 1967. Cortical bone in man, II. Variation in tensile strength with Age and Sex. ACTA. ORTHOP. SCAND., 38, 141 - 147.

79. BONFIELD, W., Li, C.H., 1968. The temperature dependence of the deformation of bone. J. BIOMECHS., 1, 323 - 329.
80. WOOD, J.L., 1971. Dynamic response of human cranial bone. J. BIOMECHS., 4, 1 - 12.
81. HIRSCH, C., Evans, F.G., 1965. Studies on some physical properties of infant compact bone. ACTA. ORTHOP. SCAND., 35, 300 - 313.
82. BURSTEIN, A.H., Currey, J.D., Frankel, V.H., Reilly, D.T., 1972. The ultimate properties of bone tissue: the effects of yielding. J. BIOMECHS., 5, 35 - 44.
83. DEMPSTER, W.T., Liddicoat, R.T., (1952). Compact bone as a non-isotropic material. AM. J. ANAT., 91, 331 - 362.
84. SEDLIN, E.D., Hirsch, C., 1966. Factors affecting the determination of the physical properties of femoral compact bone. ACTA. ORTHOP. SCAND. 37, 29 - 48.
85. SEDLIN, E.D., 1965. A rheologic model for cortical bone : a study of the physical properties of human femoral samples. ACTA. ORTHOP. SCAND., SUPPLEMENT 83.
86. DEMPSTER, W.T., Coleman, R.F., 1960. Tensile strength of bone along and across the grain. J. APPL. PHYSIOL., 16, 355 - 360.
87. EVANS, F.G., 1964. Significant differences in the tensile strength of adult human compact bone. In "Proceedings First European Bone and Tooth Symposium", PERGAMON PRESS, OXFORD, pp. 319 - 331.

88. BONFIELD, W., Li, C.H., 1966. Deformation and fracture in bone. J. APPL. PHYSICS, 37, 869 - 875.
89. EVANS, F.G., Lebow, M., 1951. Regional differences in some of the physical properties of the human femur. J. APPL. PHYSIOL., 3, 563 - 572.
90. PEDERSEN, H.E., Evans, F.G., Lissner, H.R., 1949. Deformation studies of the femur under various loadings and orientations. ANAT. REC., 103, 159 - 185.
91. EVANS, F.G., Pedersen, H.E., Lissner, H.R., 1951. The role of tensile stress in the mechanism of femoral fractures. J. BONE & JT. SURG., 33A, 485 - 501.
92. FRANKEL, V.H., Burstein, A.H., 1964. Load capacity of tubular bone. In "Biomechanics and Related Bioengineering Topics", PERGAMON PRESS, OXFORD, pp. 381 - 396.
93. VOSE, G.P., Kubala, A.L., 1959. Bone strength : its relationship to x-ray determined ash content. HUM. BIOL., 31, 262 - 270.
94. POPE, M.H., Outwater, J.O., 1972. The fracture characteristics of bone substance. J. BIOMECHS., 5, 457 - 465.
95. SAMMARCO, G.J., Burstein, A.H., Davis, W.L., Frankel, V.H., 1971. The biomechanics of torsional fractures : the effects of loading on ultimate properties. J. BIOMECHS., 4, 113 - 117.
96. BURSTEIN, A.H., Frankel, V.H., 1971. A standard test for laboratory animal bone. J. BIOMECHS., 4, 155 - 158.

97. BELL, G.H., Cuthbertson, D.P., Orr, J., 1941. Strength and size of bone in relation to calcium intake. J. PHYSIOL., 100, 299 - 317.
98. WOLINSKY, I., Simkin, A., Guggenheim, K., 1972. Effects of fluoride on metabolism and mechanical properties of rat bone. AM. J. PHYSIOL., 223, 46 - 50.
99. CLARKE, M.F., Bassin, A.L., Smith, A.H., 1936. Skeletal changes in the rat induced by a ration extremely poor in organic salts. AM. J. PHYSIOL., 115, 556 - 563.
100. BELL, G.H., Chambers, J.W., Dawson, I.M., 1947. The mechanical and structural properties of bone in rats on a rachitogenic diet. J. PHYSIOL., 106, 286 - 300.
101. WEIR, J.B., Bell, G.H., Chambers, J.W., 1949. The strength and elasticity of bones in rats on a rachitogenic diet. J. BONE & JT. SURG., 31B, 444 - 451.
102. SEMB, H., 1966. The breaking strength of normal and immobilised cortical bone from dogs. ACTA. ORTHOP. SCAND., 37, 131 - 140.
103. EICHLER, J., 1970. Inaktivitatsosteoporose. AKTUELLE ORTHOPADIE, 3, 1 - 80.
104. KAZARIAN, L.E., Von Gierke, H.E., 1969. Bone loss as a result of immobilisation and chelation: preliminary results in Macca Mulatta. CLIN. ORTHOP., 65, 67 - 75.
105. MELICK, R.A., Miller, D.R., 1966. Variations of tensile strength of human cortical bone with age. CLIN. SCI., 30, 243 - 248.

106. RAUBER, A.A., 1876. "Elasticitat und festigkeit der knochen", ENGELMAN, LEIPZIG.
107. SMITH, J.W., Walmsley, R., 1959. Factors affecting the elasticity of bone. J. ANAT., 93, 504 - 523.
108. FRANKEL, V.H., Burstein, A.H., "Orthopaedic Biomechanics : an introduction to the Engineering Fundamentals of Orthopaedic Surgery", LEA & FEBIGER, PENNSYLVANIA.
109. SHIMMINS, J., 1970. Mineral metabolism in bone studied with x-ray sources and radioactive isotopes. Ph.D. THESIS, UNIVERSITY OF GLASGOW.
110. HARPER, R.A., Posner, A.S., 1966. Measurement of non-crystalline calcium phosphate in bone mineral. PROC. SOC. EXP. BIOL. MED., 122, 137 - 142.

APPENDIX 1DERIVATION OF EXPRESSION YIELDING THE ANGULAR SEPARATION  
 $\delta\theta$  BETWEEN BRAGG ANGLES FOR WAVELENGTHS DIFFERING BY  $\delta\lambda$ 

Consider the Bragg equation

$$\lambda = 2.d. \sin \theta \quad (a)$$

Differentiate with respect to  $\theta$

$$\begin{aligned} \frac{\delta\lambda}{\delta\theta} &= 2.d.\cos \theta \\ \therefore \delta\theta &= \frac{\delta\lambda}{2.d.\cos \theta} \end{aligned} \quad (b)$$

Substituting for  $2d$  from equation (a)

$$\delta\theta = \frac{\delta\lambda.\tan \theta}{\lambda}$$


---



---

APPENDIX 2DIFFRACTION LINE BROADENING DUE TO CRYSTALLITES DAMAGED  
DURING GRINDING

The maximum dimension of any particle comprising the bone powder is 0.05 mm.

Thus, the minimum possible particle volume is that of a sphere of radius 0.025 mm. :-

$$V = \frac{4}{3} \cdot \pi \cdot (0.025)^3 \text{ mm}^3$$

But, the maximum size of crystallite capable of producing a significant pure broadening effect is about 0.0001 mm.

Therefore, the volume within which damaged crystallites might be small enough to contribute toward pure broadening is:-

$$v = \frac{4}{3} \cdot \pi \cdot (0.025^3 - 0.0249^3) \text{ mm}^3$$

Expressing  $v$  as a fraction  $f$  of the particle volume  $V$ ,

$$\underline{\underline{f = 1\%}}$$

APPENDIX 3REDUCTION OF VON LAUE LINE PROFILE EQUATIONS TO LINEAR FORM

$$(a) \quad I = I_{\max.} (1 + k^2 x^2)^{-1}$$

Rewriting this equation we obtain

$$I = \frac{I_{\max}}{k^2} \left( \frac{1}{k^2} + x^2 \right)^{-1}$$

Taking natural logarithms

$$\ln(I) = -\ln\left(\frac{1}{k^2} + x^2\right) + \ln\left[\frac{I_{\max}}{k^2}\right]$$

This can be rewritten as

$$Y = bX + c, \text{ where } Y = \ln(I),$$

$$X = \ln\left(\frac{1}{k^2} + x^2\right), \quad b = -1,$$

$$c = \ln\left[\frac{I_{\max}}{k^2}\right]$$

$$(b) \quad I = I_{\max.} e^{-K^2 x^2}$$

Taking natural logarithms

$$\ln(I) = -K^2 x^2 + \ln(I_{\max})$$

This can be rewritten as

$$Y = bX + c, \text{ where } Y = \ln(I), \quad X = x^2,$$

$$b = -K^2, \quad c = \ln(I_{\max}).$$

APPENDIX 4

CORRECTION OF OBSERVED BONE APATITE (002) REFLECTION  
INTENSITY FOR BACKGROUND VARIATION

X-ray photographic emulsions display a sensitive range within which photographic density is proportional to the logarithm of exposure,

$$D \propto \log E \quad (a)$$

Photographic density is defined as

$$D = \log (1/T) \quad (b)$$

where T is the fractional transmission of light through the film.

Now, around the circumference of the photographically recorded bone apatite (002) diffraction ring density results from exposure to (002) reflected x-rays, background exposure to diffusely scattered x-rays, and also film fogging,

$$E_{\text{total}} = E_{\text{002}} + E_{\text{BGD}} \quad (c)$$

From equations (a) and (b) we get

$$\log (E_{\text{total}}) = C \cdot \log (1/T_t) \quad (d)$$

$$\log (E_{\text{BGD}}) = C \cdot \log (1/T_B) \quad (e)$$

Where C is a constant,  $T_t$  is the fractional transmission at any point on the (002) ring, and  $T_B$  is the fractional transmission of the corresponding background region adjacent to the (002) ring.

Rewriting (d) and (e)

$$E_t = (1/T_t)^c \quad (f)$$

$$E_B = (1/T_B)^c \quad (g)$$

Substituting (f) and (g) into (c)

$$E_{OO2} = (1/T_t)^c - (1/T_B)^c \quad (h)$$

Now, background corrected density is,

$$D_{OO2} = C \cdot \log(E_{OO2}) \quad (i)$$

Substituting (h) into (i),

$$D_{OO2} = C^2 \cdot \log(T_B/T_t)$$

Thus, the ratio of background corrected maximum and minimum density is,

$$\frac{D_{OO2 \text{ max.}}}{D_{OO2 \text{ min.}}} = \frac{\log(T_{B \text{ max}}/T_{t \text{ max}})}{\log(T_{B \text{ min}}/T_{t \text{ min}})}$$

If  $T_{\text{max}}$  and  $T_{\text{min}}$  are each measured at diametrically opposite points of the (002) diffraction ring, then we can average the photographic densities to give,

$$\frac{\bar{D}_{OO2 \text{ max}}}{\bar{D}_{OO2 \text{ min}}} = \frac{\log(T_{B \text{ max } 1} \times T_{B \text{ max } 2}) - \log(T_{t \text{ max } 1} \times T_{t \text{ max } 2})}{\log(T_{B \text{ min } 1} \times T_{B \text{ min } 2}) - \log(T_{t \text{ min } 1} \times T_{t \text{ min } 2})}$$

APPENDIX 5STRAIN GAUGE INSTALLATION PROCEDURE

1. Specimen surface cleaned with degreasing solvent.
2. Surface prepared by wiping with an acid conditioner.
3. Acid neutralised with alkali wipe.
4. Strain gauge removed from packaging and placed, with bond side down, on clean glass plate. Three inch length of cellophane tape located over gauge.
5. Tape and gauge attached to specimen with gauge in desired position.
6. One end of tape held firmly while remainder of tape, and gauge, lifted clear of specimen surface.
7. Methacrylate catalyst applied to bond surface of gauge using fine brush.
8. After one minute, methacrylate adhesive applied to specimen surface: gauge brought into contact and held firmly with thumb pressure for one minute.
9. Polyurethane protective coat applied with fine brush.

APPENDIX 6

DERIVATION OF EXPRESSIONS RELATING TO RECORDER RESPONSE

If the recorder sensitivity is  $S$  volt/cm, then deflection of  $x$  cm. indicates a signal

$$\Delta V = x.S \quad (a)$$

Now, for a Wheatstone bridge circuit,

$$\Delta V \approx V. \frac{\Delta R}{4R} \quad (b)$$

where  $\Delta V$  is the imbalance voltage,  $V$  is the excitation voltage,  $R$  is the arm resistance, and  $\Delta R$  is the change in resistance giving rise to the imbalance voltage.

Substituting equation (a) into equation (b), and setting  $V = 2$  volts,

$$2.x.S = \frac{\Delta R}{R} \quad (c)$$

Now, each strain gauge is specified by a "GAUGE FACTOR"  $F$ , defined as the quotient of the fractional change in electrical resistance divided by fractional increase in length,

$$F = \frac{\Delta R/R}{\Delta L/L}$$

Thus, strain is given by,

$$\epsilon = \frac{\Delta L}{L} = \frac{\Delta R/R}{F} \quad (d)$$

Substituting from equation (c),

$$\epsilon = \frac{2.x.S}{F} \quad (e)$$

For, F-8 strain gauges,  $F = 2.16$ , and for Fb-2 strain gauges,  $F = 2.09$ , giving

$$\epsilon_{\text{long.}} = 0.923 \cdot x \cdot S \quad (\text{f})$$

$$\epsilon_{\text{lat}} = 0.957 \cdot x \cdot S \quad (\text{g})$$

APPENDIX 7ELASTIC INSTABILITY (BUCKLING) IN COMPRESSIVE TEST PIECES

Now, for an axially compressed rod, the load at which finite deflection occurs for no load increase is given by Euler's formula,

$$P_{\text{crit.}} = \frac{\pi^2 \cdot E \cdot I}{L^2}$$

The second moment of area of a circular cross-section about its centroid is,

$$I = \frac{\pi R^4}{2}$$

Thus, for a cylindrical rod,

$$P_{\text{crit.}} = \frac{\pi^3 E R^4}{2L^2}$$

At this load the stress is

$$\sigma_{\text{crit.}} = \frac{P_{\text{crit.}}}{A} = \frac{\pi^2 E}{8} \left[ \frac{D}{L} \right]^2$$

For bone tissue,  $E \approx 10^3 \text{ Kg/mm}^2$ ,

$$\therefore \sigma_{\text{crit.}} \approx \frac{10^4}{8} \cdot \left[ \frac{D}{L} \right]^2$$

Also, for bone tissue  $\sigma_{\text{ult}} \sim 10 \text{ Kg/mm}^2$ .

To avoid buckling, we require  $\sigma_{\text{ult}} < \sigma_{\text{crit.}}$

This condition is satisfied when  $\frac{L}{D} \lesssim 11$